

Functional Characterization of Human iPSC-Derived Neural Networks using MEA Systems for in vitro Modeling of Psychiatric Disorders

Areti Sfakianou

4736427

Functional Characterization of Human iPSC-Derived Neural Networks using
MEA Systems for in vitro Modeling of Psychiatric Disorders

By Areti Sfakianou

A Thesis in the Field of Neurobiological Psychiatry and Electrophysiology
for the Degree of Master of Biomedical Engineering



TU Delft supervisors:

dr. V. Valente

Erasmus MC supervisors

dr. Femke M.S. de Vrij

prof. dr. Steven A. Kushner

Committee of Defense

prof.dr.ir. W.A. Serdijn, TU Delft

dr. V. Valente, TU Delft

dr.ir. R.C. Hendriks, TU Delft

dr. Femke M.S. de Vrij, Erasmus MC

December 2019

...ἐς δὲ τὰ ἔσχατα νοσήματα αἱ ἔσχαται θεραπείαι ἐς ἀκριβείην,

κράτισται...

...Extreme remedies are the best for extreme diseases...

Ἱπποκράτης, Hippocrates (384-322 BC)

Abstract

Psychiatric disorders are associated with major societal, personal issues and comprise 13% of the global burden of disease. They are heritable and present a complex pathophysiology, characterized by hundreds of genetic variants which are cumulated together and provoke a specific psychiatric disorder. Although a considerable progress has been made in the identification of genetics variants, the way a cellular phenotype is related to a gene expression caused by biological pathways remains unclear.

Significant effort has been focused, over the last years, on psychiatric diseases modeling, to investigate the complex, polygenic neurobiological nature of these disorders. Human induced pluripotent stem cell (iPSC) technology has been widely used for in vitro disease modeling. Human iPSCs can be readily derived from patients and differentiated into any cell type including neurons.

The functional characterization of neurons constitutes a challenging procedure and different electrophysiological techniques can be applied. A hallmark of a non-invasive technique, in which the neuronal network dynamics can be observed, is the Microelectrode Array (MEA) measurements. The functional characterization of neuronal activity contributes to the cellular phenotype investigation of neuronal cultures, derived from patients who are affected by psychiatric disorders. The cellular phenotypes could be used as readouts for high-throughput pharmacological screenings and enhance the development of new drugs.

In the current thesis project, the combination of a long-term neural differentiation protocol with extracellular MEA measurements was implemented, to assess the spontaneous and synchronized network activity of human iPSC-derived neural cultures. This protocol generates both neurons and astrocytes from a common neural progenitor cell (NPC) into a control ratio (60:40). A commercial MEA system (Multiwell-MEA, Multi Channel Systems, GmbH, Germany) was used for extracellular recordings on the neural populations. Additionally, a spike sorting analysis was performed for spike waveform observation.

Experimental results presented a robust network activity derived from neural populations cultivated in neuronal medium (BrainPhys), for a period of ten weeks in vitro. Neuronal activity was characterized in terms of cumulative firing rate (CFR) per cell culture and mean firing rate (MFR) per electrode. Results showed a peak CFR of 1700 spikes/minute/culture (± 260 SEM) and a peak MFR of 215 spikes/minute/electrode (± 22.5 SEM). Additionally, a bursting activity was constantly detected on a scale of 270 burst/10 minutes/culture (± 31 SEM), during the period of ten weeks in vitro. A spike sorting analysis verified the successful monitoring of spikes' waveforms derived from the same unit of neurons in a two-week period. 88% of the detected waveform patterns presented a normalized cross-correlation higher than 0.9, which reinforced the argument that the electrodes detected electrical activity derived from the same unit of neurons in a constant way.

This project contributes to the creation of an optimized functional readout of human neural model in vitro, which, in a long-term vision, could be used as reference point for comparison between healthy and diseased cell lines derived from patients with psychiatric disorders.

Acknowledgements

A long trip has almost come to an end and I am grateful for what I have lived and for the people that I met. Although it seems like it was yesterday, when I left my job in Luxembourg in order to start the master in TU Delft, at the same time, I feel as it's been ages. These two years in TU Delft were full of extreme feelings and plenty of knowledge. And now, I have to admit that if I had the chance, I would do it all over again.

With the completion of this project, I would like to thank both of my supervisors, Femke de Vrij and Virgilio Valente for always being there to guide and support me. Both of you taught me how to think critical on a different way: Femke taught me how to be disciplined and accurate on writing sources from papers, while Virgilio how to be pragmatic on solving engineering challenges. Mark van der Kroeg, I deeply thank you for all the cell culturing knowledge that I gained from you. Borbala Hunyadi, thank you for the time you devoted in order to explain the principles on signal processing and spike sorting analysis to me, even if I was not your student. I would also like to thank Steven Kushner for providing me the opportunity to do both my internship and thesis in the Psychiatry lab at Erasmus Medical Center. Finally, Wouter Serdijn, a deep thank you for all your support, the conference opportunity and the amazing movie nights that we had. At the end of the day, we should all bear in mind that we are human beings. Thank you for your kind, unique, reminder.

Please let me thank my everyday heroes, my beloved persons. They know who they are and just mentioning them in a piece of paper is not enough. I would like to finish my acknowledgments by devoting this thesis project to a little girl that will never fade from my memory. A girl who struggled to read and write as the letters were jumping and the lines were fluctuating. A girl who still thinks in pictures instead of words. And as all adults still have an inner child inside them, let me finish with some "magic words":

In every job that must be done,
there is an element of fun.
And every task you undertake,
becomes a piece of cake.

Areti Sfakianou,

11/12/2019

CONTENTS

Introduction	4
1.1 Psychiatric disorders	5
1.2 Modeling psychiatric disorders in vitro	6
1.3 Problem Statement	7
1.4 Project Overview	9
Chapter 2.....	10
Background	10
2.1 The need of early brain development observation	11
2.2 Establishment of in vitro cultures	12
2.3 Directed differentiation of neurons from human iPSCs	13
2.4 The road to modeling psychiatric disorders in a dish	14
2.5 MEAs in vitro: extracellular recording of neuronal activity	15
2.5.1 Electrodes on MEAs	16
2.5.2 Electrode-Neuron interface	17
2.5.3 Extracellular action potentials	18
2.5.4 MEAs and neural cell cultures.....	19
2.6 Quantitative assessment of neuronal network development	20
Chapter 3.....	22
Materials and Methods.....	22
3.1 Neural differentiation protocol on the Multiwell-MEA plate	23
3.2 Multiwell-MEA System.....	24
3.3 Algorithms for spike, burst and network burst detection	26
3.4 Wave_clus: fully automatic spike-sorting implementation	28
3.4.1 Spike sorting implementation on Multiwell-MEA System	30
3.4.2 Formation of mean waveform patterns	30
3.5 Data and statistical analysis	31
Chapter 4.....	33
Experimental Measurements.....	33
4.1 Experimental strategy and settings	34
4.2 Evaluation of different NPC densities on Multiwell-MEA plate	35
4.3 Evaluation of BrainPhys and Neurobasal medium on neural cultures	38
4.4 Spike sorting implementation on a single cell culture	52
4.4.1 Clusters derived from Wave_clus algorithm.....	52
4.4.2 Assessment of mean waveform patterns	55

Chapter 5.....	58
Discussion and Prospects.....	58
5.1 Discussion.....	59
5.2 Conclusions and future prospects.....	61
REFERENCES.....	63
APPENDIX A.....	67
APPENDIX B.....	69
APPENDIX C.....	79

List of ABBREVIATIONS

ALPHABETICALLY ORGANIZED

AP	:	Action Potential
ASD	:	Autism Spectrum Disorder
AZT	:	telomerase inhibitor azidothymidine
CFR	:	Cumulative Firing Rate
CP	:	Cortical Plate
ESC	:	Embryonic Stem Cells
EAP	:	Extracellular Action Potentials
iPSC	:	induced Pluripotent Stem Cell
ICM	:	inner cell mass
iSVZ	:	Inner Ventricular Zone
IZ	:	Intermediate Zone
MEA	:	Microelectrode Array
MFR	:	Mean Firing Rate
NDDs	:	Neurodevelopmental Disorders
NPC	:	Neural Progenitor Cell
oSVZ	:	Outer Ventricular Zones
PGD	:	pre-implantation genetic diagnosis
SCZ	:	Schizophrenia
SVZ	:	Subventricular zone
VZ	:	Ventricular Zone

CHAPTER 1

Introduction

Psychiatric disorders comprise 13% of the global burden of disease and they are characterized as polygenic, meaning that several genetical factors are implicated on a specific psychiatric disorder. The advent of human induced Pluripotent Stem Cell (iPSC) technology promises the creation of neural models which recapitulate the neurodevelopmental procedure in accuracy and can be utilized as powerful platforms for understanding their complex pathogenesis in a cellular level. The electrophysiological functionality of neuros is examined with intracellular or extracellular methods. A widely used extracellular recording method is Microelectrode Array (MEA) system, which allows the observation of neurons' network dynamics. In the current thesis project, the combination of a long-term neural differentiation protocol with the use of MEA recordings was implemented for the functional characterization of human iPSC derived neurons in the level of neuronal network connectivity.

1.1 Psychiatric disorders

Psychiatric disorders are associated with the major societal and personal issues and comprise 13% of the global burden of disease. The stigma of mental illness constitutes a significant barrier that limits the research and negatively affects patients as individuals, their families, and the society. Schizophrenia (SCZ), Autism Spectrum Disorder (ASD), bipolar disorder, anorexia nervosa and major depressive disorders are some of the most serious psychiatric disorders. Psychiatric disorders are presented as overlapping nosological entities with the broad field of Neurodevelopmental Disorders (NDDs), resulting in deficiencies on motor and learning skills, cognition and communication [1], [2]. Based on family/twins' evidence, psychiatric disorders are heritable, and present a complex pathophysiology, characterized as polygenic [3], [4]. The term polygenic refers to a combination of hundreds of genetic variants which are cumulated together and provoke a specific psychiatric disorder. It has been observed that most of these genetic variants individually present a low impact on a specific neuropsychiatric disease, while genetic variants with high impact, rarely appear [5].

The progress in understanding psychiatric disorders from a psychological to a biological perspective has been achieved after several years of research. Despite the widespread heterogeneity among these disorders, genetic studies have shown cellular and synaptic malfunctions as their major effect [5]. Cellular and synaptic malfunctions involve imbalances in membrane excitation, dysfunction of ion-conducting channels and abnormal synaptic transmission [6]. Animal models have also significantly contributed on comprehending psychiatric disorders' pathophysiology. Especially rodent models appear as tractable and accessible platforms in which several well-established behavioral and physiological tests have been successfully performed. Additionally, the technology of transgenic mice provides the opportunity of observing the effects of genetical manipulations. Transgenic mouse technology has brought an uprising in the field of biology, as it is possible to model a human disease in an animal model by modifying the mouse genome [5].

Although genetics and rodent models have played a crucial role on understanding the complexity of psychiatric disorders, the way a cellular phenotype is related to a gene expression caused by biological pathways remains unclear. Very few of the current findings provide a strong link between an individual gene and a discriminative phenotype. This pitfall might be a reflection of the polygenic nature of psychiatric disorders. Indeed, the study of only one gene with low impact on disease risk is unlikely to reveal a specific cellular phenotype [5]. Additionally, animal models cannot recapitulate complex psychiatric phenomena and by extension human phenotype, i.e. the phenomenon of psychosis. Moreover, drug screening on rodent models might not be effective, as two species differ and therefore, preclinical studies might reveal misleading information [7].

The creation of a disease model *in vitro* which would be able to recapitulate the complex genetic background of psychiatric disorders is essential. The model should exhibit either the cumulative effect of several genetic variants with low impact on a specific disease, or the effect of a single genetic variant with high impact, based on which a phenotype screening could be applied [5]. The aim is to shed a light on the biological pathways leading to gene expression and, to the strong relation between a gene expression and a cellular phenotype which manifests a psychiatric disorder.

1.2 Modeling psychiatric disorders in vitro

The advent of human induced Pluripotent Stem Cell (iPSC) technology has revolutionized human disease modeling in vitro, invented by Yamanaka and Takahashi in 2007 [8]. The technology of human iPSCs is based on reprogramming human somatic cells. Fibroblasts (skin cells), nowadays also blood cells, are taken from donors (healthy or diseased) and are induced back to their very early pluripotency state (stem cells) by transduction of four transcription factors (OCT4, SOX2, KLF4 and cMYC). Human iPSCs can be differentiated into any cell type and therefore, appear as a promising tool for differentiation of iPSCs into neurons which combines both structural and functional characteristics of donor's neurons. Moreover, neuronal models made directly by patients' cells offer useful information about molecular and cellular features which can be used for the investigation of the deficits in a single cell unit or in a cellular population in which a gene mutation is hidden [7].

The major advantage of iPSCs derived neuronal culture, which also constitutes the biggest challenge, is to create a model that mimics the neurodevelopmental procedure by generating authentic cell types, also mimics cell to cell interactions, as well as neuronal connectivity [9]. The neurodevelopment in vitro allows the precise observation of neuronal cultures in order to interrogate the phenotypes correlated with gene mutations. The phenotype investigation constitutes a challenging procedure and its assessment is implemented in various ways. The electrophysiological assessment of neurons for phenotype determination is always implemented with intracellular or extracellular recording methods [5].

The gold standard of electrophysiology is the whole cell patch-clamp recording, a single-cell intracellular measurement method, in which electrical activity of a single excitable neuron is observed. In case of psychiatric disorders, as one of the major neuronal issues appears on synaptic connectivity, neuronal network dynamics could also provide valuable information in addition to monitoring single neuron activity. Therefore, the cellular pathology in psychiatric disorders may point to the need of an electrophysiological method which allows the observation of neuronal activity in a higher network level with the use of an extracellular recording approach [5].

Microelectrode Array (MEA) system is an effective tool for extracellular measurements on neuronal models. It is a device used for the recording of the electrical activity of neuronal cultures and consequently, the cellular phenotype determination is based on processing of signal waveforms, firing and bursting rate of neurons. MEA application presents a significant advantage on observing neuronal network dynamics for diseases, in which the genetic deficit might be expressed on neuronal connectivity. Moreover, MEA systems in vitro appear as high throughput neurotoxicity testing platforms as they have been built specifically for pharmacological and toxicological analysis. They provide the advantage of screening chemical compounds by measuring the electrical activity of neurons as an effect of inserting drugs into cultures [10].

The neuronal models in vitro derived by human iPSCs can be utilized as powerful platforms for understanding disease pathogenesis. Although, cellular morphology, single-cell gene expression, neurotransmitter identity of human iPSC derived neurons have been mainly studied with biochemical method, the electrophysiological properties of neurons in vitro have been analyzed with electrophysiological techniques which constitute reliable methods for profiling neurons based on their activity. The quantitative evaluation of neuronal firing patterns from electrophysiological recordings, i.e. MEA measurements, enhance the investigation of cellular phenotypes related to specific gene mutations by observing abnormalities on neuronal functions. The long-term vision of these models is the ability to run large scale drug screening, in which the reversion of cellular impairments might be achieved. Several studies have shown that drug responses vary among different psychiatric conditions

and patients. Therefore, this observation led to another application of iPSC derived neurons, the prediction of the way drugs respond to individuals. If a reliable prediction of drug response to neurons derived from individuals is achieved, patients would heal from severe symptoms with the use of pharmacological treatment that has already been tested on neural cultures derived by them. This procedure is known as “personalized medicine” (Figure 1.1) [11].

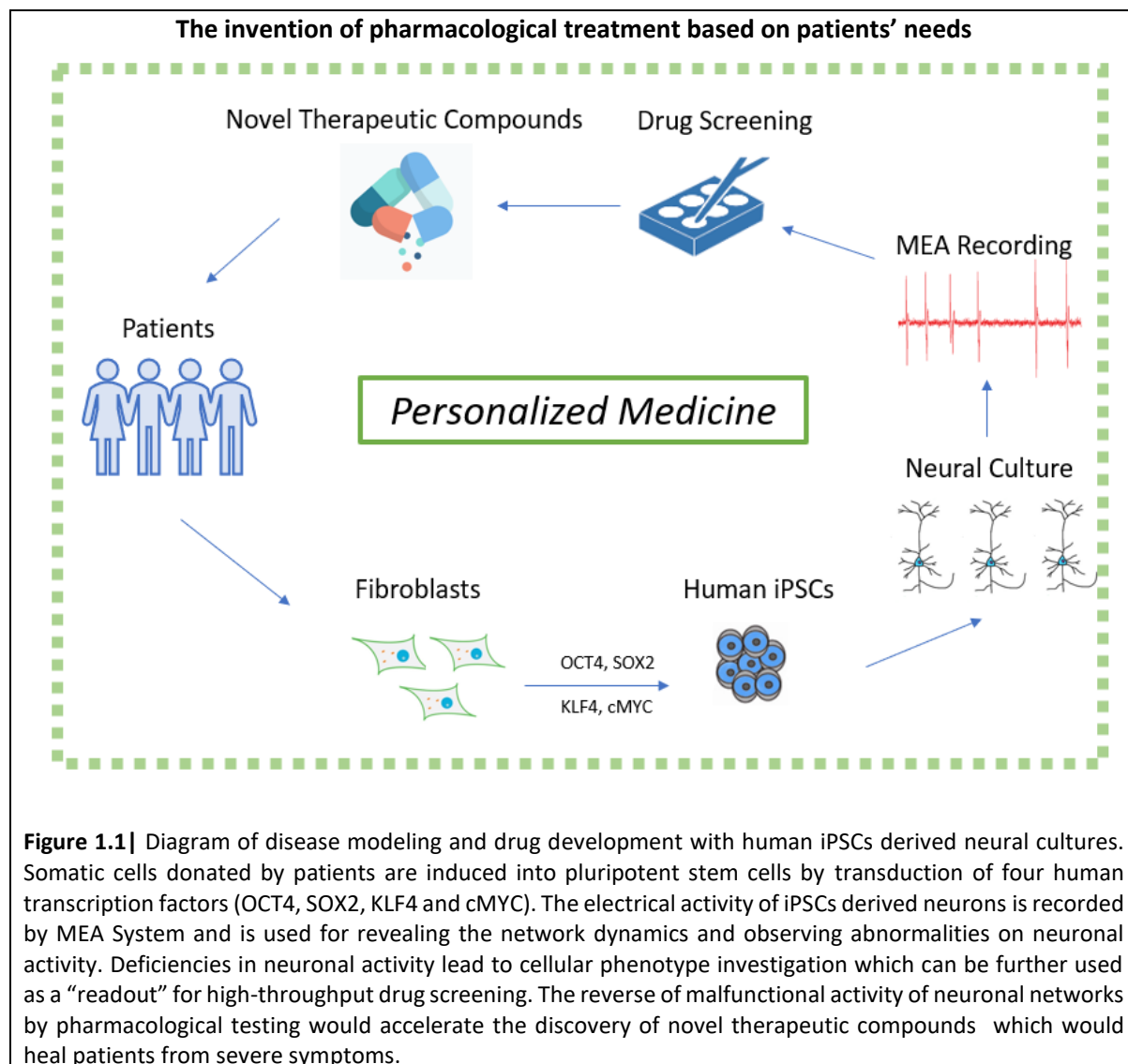


Figure 1.1| Diagram of disease modeling and drug development with human iPSCs derived neural cultures. Somatic cells donated by patients are induced into pluripotent stem cells by transduction of four human transcription factors (OCT4, SOX2, KLF4 and cMYC). The electrical activity of iPSCs derived neurons is recorded by MEA System and is used for revealing the network dynamics and observing abnormalities on neuronal activity. Deficiencies in neuronal activity lead to cellular phenotype investigation which can be further used as a “readout” for high-throughput drug screening. The reverse of malfunctioning activity of neuronal networks by pharmacological testing would accelerate the discovery of novel therapeutic compounds which would heal patients from severe symptoms.

1.3 Problem Statement

The process of modeling psychiatric disorders in vitro at a cellular level exhibits several potential risk sources. Firstly, the genetic variations observed on different iPSC lines should be derived from the different genetical background of donors and not due to inconsistency in iPSC reprogramming protocols. Reprogramming protocols should guarantee the successful inducement of somatic cells into a pluripotent state similar to the inner cell mass of an early human embryo where stem cells are derived [5]. Additionally, cell culturing techniques should also provide a stable cellular environment, in which, differentiation protocols can achieve the successful differentiation of iPSCs into specific neuronal subtypes. Neurons in vitro should demonstrate all the neuronal features appearing on in vivo observations and constituting the neuronal identity [7].

Several differentiation protocols have been used to obtain iPSCs derived neuron subtypes, networks or whole brain organoids in a short or long-term culturing period. The long-term culture protocols present a significant advantage compared to short term culture protocols, as they can recapitulate stages of early neurodevelopment procedure in a more precise way. Additionally, the generation of glial cells (astrocytes and oligodendrocytes) after the main wave of neurogenesis, is another important developmental step that the differentiation protocols need to mimic. Glial cells play a crucial role on neuronal functionality and their existence in a neuronal culture might suggest an increase of neuronal maturation [9].

In the current thesis project, a neural differentiation protocol was used, in which the differentiation of human iPSCs into neurons and glia was derived from a common neural progenitor cell (NPC). NPCs were differentiated into functional neural network cultures of neurons and astrocytes in a controlled ratio. The authors of this protocol, published in 2018, have already proved the electrophysiological maturity of nearby neurons at 8 to 10 weeks of neural differentiation in vitro with the use of intracellular measurements, whole cell patch-clamp recording [12]. However, the maturity of neural network on a larger scale, looking at the entire activity and synchronicity of neural population had not been studied yet. Consequently, the combination of this neural differentiation protocol with extracellular MEA measurements was implemented for the thesis scope in order to assess the electrophysiological characteristic of neurons in a higher level, the level of neuronal network connectivity.

The main goal of the thesis was the creation of a neural model derived from a healthy individual which would be able to recapitulate the electrophysiological maturity of neurons in a similar way as it is observed in the early embryonic neurodevelopment in vivo. The main challenge was the creation of stable cell culturing conditions which would allow the electrophysiological maturity of neurons, in parallel with the effective detection of neuronal network activity by the MEAs. The outcomes of the current project would contribute to the creation of an optimal neural cell culture model which would ensure the physiologically functional development of neural cell cultures as it is observed in vivo assessments. In a long-term vision, this model can be used for comparison of neural cultures derived from disease and healthy cell lines. By verifying that this cell culture model enhances the physiological neural development, significant differences on the neuronal functionality between disease and control (healthy) cell lines might reveal the exact electrophysiological malfunction on the neural cultures derived from patients, and consequently, a cellular phenotype related to a gene expression.

The main research questions were formulated as follows:

- i. *Could a neural culture derived by this differentiation protocol remain on the MEA system for a long period of time, 8 to 10 weeks in vitro?*
- ii. *Which are the optimal cell culturing conditions on a MEA system based on cell density and cultivation medium?*
- iii. *Could a neuronal activity be detected by MEA system in a constant way during the whole experimental period?*
 - a. *If yes, in which terms could the neuronal network activity be characterized (spontaneous or synchronized activity of neurons)?*
 - b. *Is the classification of neuronal waveforms into clusters possible? Is the monitoring of the same clusters of neuronal waveforms over the time possible?*

1.4 Project Overview

The thesis project was accomplished in cooperation with the Psychiatry lab at Erasmus Medical Center and the Technical University of Delft. At the beginning of this project, a literature review was performed in order to examine the technology of human iPSCs, the neural culture modeling, as well as the MEA systems. An overview of the findings covering the theoretical background needed for the thesis project is cited on Chapter 2. In the following Chapters the methods, experimental procedure, the results and the outcomes of the project are presented. The long-term neural differentiation protocol, the commercial Multiwell-MEA system as well as the data and statistical analysis are described explicitly in the Chapter 3. The data analysis included the calculation of the active electrodes per well, Mean Firing Rate (MFR) per electrode, Cumulative Firing Rate (CFR) per well and the number of detected bursts per well. Additionally, a spike sorting analysis was applied on some of the extracted data, in order to classify the spike waveforms into clusters, and for this purpose, the optimized version of Wave_clus algorithm by Fernando J. Chaure et. al was used. The similarity of waveform clusters derived on different recording performances from the same electrode were evaluated with the use of a cross correlation function. Chapter 4 includes the results from experimental process and Chapter 5 includes the outcomes, conclusions and important suggestions for future work. Appendices A, B and C can be found at the end of the thesis report in which additional information about the experimental process, results and waveforms' clusters derived from spike sorting analysis are presented.

CHAPTER 2

Background

The development of human brain occurs during the embryonic and fetal period, in which neurogenesis (neurons' development) and synaptogenesis (synapses' formation) are the two main events. It has been observed that for psychiatric disorders, malfunctional neuronal activity is derived from abnormal embryonic neurodevelopment. Considering the limited access of human brain tissue from diseased individuals, a model in vitro derived from human cells would allow the precise observation of neurodevelopmental stages to understand the circuit-level abnormalities and cell-cell interactions. After 113 year of cell culture progress, the invention of human iPSCs promises the recapitulation of the complexity of psychiatric disorders in vitro for phenotype screening. Several neural (both neurons and glial cells) differentiation protocols have been published the last years, promoting the creation of 2D (monolayer) or 3D cultures (organoids). A plethora of studies have shown the successful achievement of 2D culture formation for psychiatric disease modeling. A high-throughput system for both extracellular recording and drug screening is the MEA system. The extracellular action potentials, spikes, are detected on the top of background noise of the recorded signal by the electrodes. The spike trains can provide a variety of additional information about the firing patterns and synchronicity of neuronal networks. A spike sorting analysis provides further information about a specific unit of neurons, i.e. neuronal type determination.

2.1 The need of early brain development observation

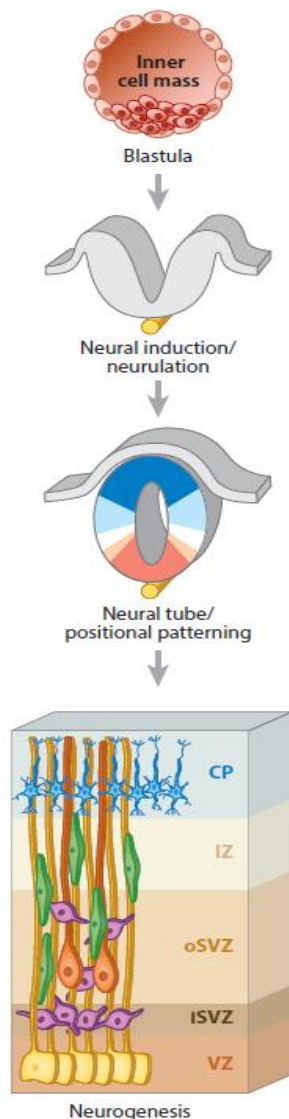


Figure 2.1| Neurogenesis in vivo. Blastula transformed into gastrula promoted the neural induction with the formation of the neural tube. Neurogenesis starts after the extensive proliferation of neural progenitor cells into the ventricular (SV) and subventricular zone. Abbreviations: Cortical Plate (CP), Intermediate Zone (IZ), Outer Ventricular Zones (oSVZ), Inner Ventricular Zone (iSVZ) Ventricular Zone (VZ) Figure taken from [7].

Human brain represents one of the most complex organs in human body, and its development mainly occurs during the embryonic and fetal period [13]. During the third week of pregnancy, the embryo is converted from blastula into gastrula. As depicted in Figure 2.1, blastula is a fluid filled hollow sphere in which a small cluster of 20 to 30 rounded cells exists at one side, called the inner cell mass (ICM) [14]. The inner cell mass is the source of human Embryonic Stem Cells (ESC) that can be differentiated into any other type of cell [15]. Gastrula is composed of three primary germ layers (ectoderm, mesoderm and endoderm), each layer being responsible for a different type of organ formation (organogenesis). Ectoderm, which is the outer layer of gastrula, is responsible for neurulation, brain and spinal cord development [14].

The neural induction starts with the formation of neural tube by the inward folding of ectoderm (Figure 2.1). The neural tube encloses a fluid filled cavity that later develops the brain ventricles. The development of human brain starts with neurogenesis, during which neurons start to develop. Neural progenitor cells (NPCs) derived from neural tube proliferate extensively into the ventricular (VZ) and subventricular zones (SVZ), lining the developing ventricles (Figure 2.1). This proliferation event enhances the differentiation of NPCs into intermediate progenitor cells (IPCs) and neurons. After the main wave of neurogenesis, glial cells such as astrocytes and oligodendrocytes, are generated and their existence is highly related to neuronal maturation. One of the last events occurring in the mature fetus by the end of pregnancy, is synaptogenesis, synapse formation, in which the neurons are connected [7], [9], [13].

Abnormalities in neurons' or synapses' development and functions appear as the main cause of psychiatrist disorders. Differences during the neurodevelopment altering the time or the cell differentiation of NPCs have been noticed in these disorders, for instance in SCZ. Additionally, impairments in glial cells affecting the neuronal functionality might also arise during brain development [5]. Additionally, postmortem histological analysis on patients with neuropsychiatric diseases has shown a variety of neuroanatomical changes [9]. Ideally, the direct assessment of human brain would provide a valuable chance for understanding the disease pathology on a cellular and network level. However, the access of brain tissue from a diseased individual is limited. Therefore, a diseased in vitro model derived by human cells, being able to recapitulate all the stages of neurodevelopmental procedure, constitutes a powerful tool for understanding the circuit-level abnormalities and cell-cell interactions. Additionally, considering psychiatric disorders which affect several cell types across different brain regions, an ideal in vitro model should present enough cellular and regional diversity for valid observations and conclusions.

2.2 Establishment of in vitro cultures

The first approach of cell culture in vitro was performed 113 years ago by the seminal work of Harrison. Harrison observed neurons extracted from a frog embryo and cultured them in a lymph medium as graft. The experiment shed a light on what was later called in vitro conditions and is considered as the establishment of cell cultures in vitro. For several years, researchers optimized the culturing methods of maintaining whole tissue grafts in vitro for a prolonged period of time, in order to observe the physiological and cell-biological processes [13]. At a later time, the invention of immortal cell lines eliminated the need of repeated tissue acquisition and set the foundation of a new cell-biological research [16].

In the field of neuroscience, adult and embryonic neurons had been used for characterization of the diverse neuronal functions. The most significant drawback of this approach was their problematic maintenance under in vitro conditions and their inability to proliferate. A solution to those issues was the establishment of a clonal neuronal line derived from a mouse neuroblastoma (cancer cell line) which provided a controlled manner of neuronal production [17]. However, even rodent cell cultures models presented serious limitations on recapitulating specific neurodevelopmental events, such as the time of human neurogenesis [13].

A breakthrough of in vitro culture establishment was the invention of ESCs. Human ESCs are derived from preimplantation embryos during the clinical oriented pre-implantation genetic diagnosis (PGD), a process required for in vitro fertilization. Human ESCs are isolated from the inner cell mass (ICM) of human blastocyst and are cultured under pluripotency-supporting conditions. Human ESCs approach presents significant advantages compared to the alternative of culturing methods. The most important is the ability of human ESCs to be differentiated into any cell type of the three germ layers and remain pluripotent in culture for long periods of time. However, human ESC models are limited due to the availability of PGD and ethical concerns [15].

The advent of human iPSCs technology constitutes a milestone on cell culture models. Human iPSCs are produced by an optimized transduction method. Somatic cells are induced into their very early pluripotency state (stem cells) with the use of the four human transcription factors OCT4, SOX2, KLF4 and cMYC [8]. Takahashi and Yamanaka's protocol guarantees a pluripotency state similar to the ICM of an early embryo. The basic characteristic of iPSCs concerns their ability to form a stem cell line from almost any type of tissue and present the fundamental properties of ESCs. The innovation of human iPSCs allows the creation of cell cultures in vitro derived from living human patients.

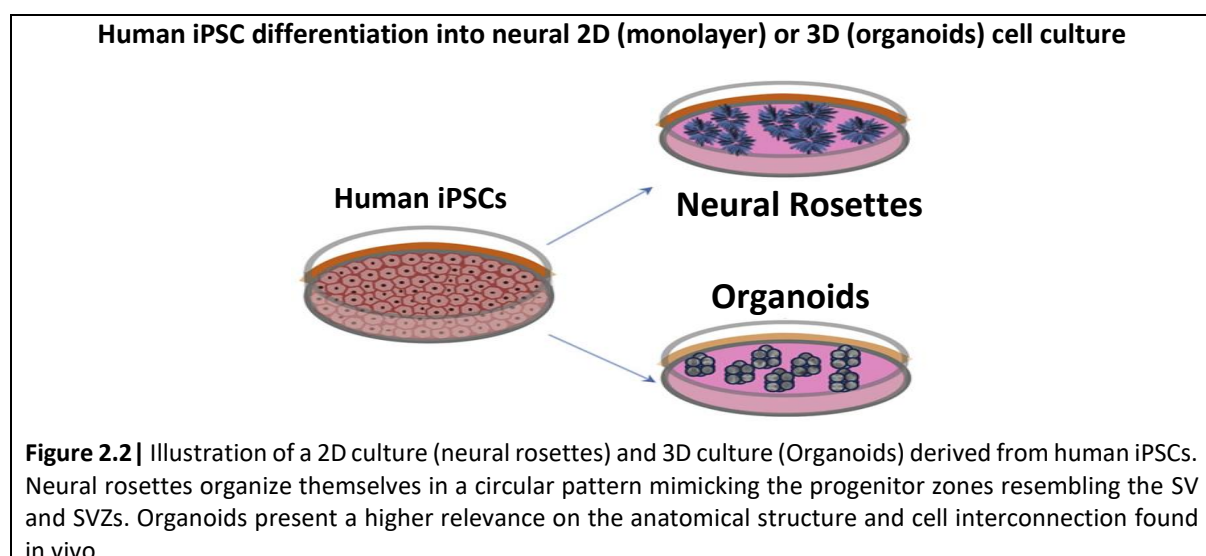
There is an increasing number of research studies in which iPSCs technology has been reported as a means of capturing in vitro specific pathophysiology of diseases, such as cardiovascular, cancer, ocular, diabetes mellitus and neurological disorders. Especially for psychiatric disorders, human iPSCs appear as a valuable tool in order to recapitulate the complexity of those disorder in vitro and be used as cellular "readouts" for phenotype screening [5]. Since their establishment, several protocols have been devised for neuronal differentiation. Most of them induce the directed differentiation of specific neural cell types, including neurons from both centrals and peripheral nervous system. Additionally, there is an ongoing effort of mimicking the neurodevelopmental stages with the use of controlled protocols of administering supplements. Although significant effort has been noticed on modeling neuropsychiatric disorders in a dish, the whole approach is still at the dawn of a new era. The brain presents an incredibly huge complexity and the replication of human brain tissue in vitro is a huge challenge [13].

2.3 Directed differentiation of neurons from human iPSCs

A variety of neural or neuronal¹ differentiation protocols, published in the last years, promotes the directed differentiation of human iPSCs into specific types of neurons, while the complexity of the generated tissue differs from method to method. The selection of the differentiation procedure is always related to the research question and the specific brain area which is targeted to be reproduced in vitro.

The majority of methods differentiating human iPSCs derived neurons produce brain cells into 2D cultures, monolayer. 2D culture models enhance a relatively homogenous cell population. Neural rosettes (Figure 2.2), mainly grow in monolayer, organize themselves into structures similar to progenitor zones resembling the SV and SVZs with the presence of radial glia, NPCs responsible for generation of neurons in cerebral cortex [18], [19]. Several neuronal cell types have been cultured in vitro with the use of 2D models, such as lower motor neurons, midbrain dopaminergic neurons, cortical excitatory and inhibitory neurons. The significant advantage of 2D culture models is their easy implementation, the production of pure neuronal cell type and their scalable nature. However, the 2D culture models lack an endogenous tissue architecture in three dimensions, which hampers the complex cell interactions in 3D structure and fosters the cellular maturation in vivo. Additionally, 2D models present a significant limitation on developing an extensive cellular diversity on the same cell culture [9], [13].

3D culture models, a recent innovation on the cell culturing techniques, appear as a promising tool to overcome the barriers presenting in 2D cultures. Compared to 2D models, 3D brain tissue models in the form of brain organoids present a higher relevance on the anatomical structure and cell interconnection found in vivo (Figure 2.2) [20], [21]. In the context of neuropsychiatric disorders, the reproduction of the 3D structure of a brain region promised the optimization of the conditions of modeling these diseases in vitro, as their major impairment appears on a neural network level which affects multiple cell lines across different brain regions. However, until now, 3D models are mainly able to recapitulate specific brain regions, while they are limited to exhibit exogenous morphogenic and fate-specific cues which allow the generation of multiple brain regions and diverse cell populations [9], [13].



¹ The term neural refers to cell cultures existing both neurons and glia cells, while the term neuronal refers to cell cultures with neurons .

Except from the anatomical structure of brain tissue models, another important factor that neural models should exhibit is the accurate recapitulation of the neurodevelopmental stages in the same time period with prenatal and postnatal events. Both 2D and 3D culture models mimic the stages of in vivo early brain development in high accuracy, while they are incapable of reaching a further neurodevelopmental stage of late embryonic or early fetal stage [9]. Very few protocols, promoting the organoid generation, reach the neurodevelopmental stage of up to late mid-fetal period in vivo [20], [22]. Additionally, glial cells and myelination² are features that should exist in cell culture models in which their aim is to reach a developmental phase to late fetal and postnatal events. Several protocols for both 2D and 3D culture have been invented to generate neurons and astrocytes on the same culture model or to allow the later deposition of astrocyte co-culture on the neuronal model [12], [23], [24], [25]. Another aspect is the inability of vascularization which constitutes the most significant obstacle on neural culture modeling, as it is difficult to deliver signaling molecules deep inside the tissue, which enhance neuronal maturity. Especially for organoids, the lack of vascularization deteriorates the oxygen penetration to their center [13].

2.4 The road to modeling psychiatric disorders in a dish

Modeling psychiatric disorders in a cellular level is a challenging procedure, as many factors are implicated on this process. It is crucial the cellular and functional variances observed in different human iPSCs lines derived neurons to reflect the different genetic background of individuals. Therefore, these variances shouldn't be an outcome of iPSC reprogramming, neural differentiation or cell culturing deficiency. Nowadays, the reprogramming method has been further optimized since its invention from Yamanaka and Takahashi, and a consistent procedure of reprogramming somatic cells into iPSCs with reducing the intra-line variation has been ensured [26], [27], [28].

One of the big challenged of iPSCs technology is the selection and therefore, the precise comparison of control (healthy) and diseased cell lines, as the donors might present considerable differences in genetic background, age, sex and ancestry. Therefore, the selection of the optimal control and disease cell line plays a crucial role on the outcome of the research [5]. Many studies were performed in family context, healthy and diseased family members with a similar genetic background donated skin samples for disease modeling in vitro and this approach guarantees the less variation between distinct cell lines [5]. However, the ideal approach which has recently been established, is the generation of isogenic iPSC lines. In cases of a common genetic mutation, there is always the possibility of making isogenic iPSC lines with the aid of genome editing techniques by introducing the mutation to the healthy cell line or correcting the mutation to the disease cell line. Consequently, two identical cell lines are produced and the comparison of cellular network activity between the healthy and the diseased cell line is a useful tool for phenotype screening [29].

Neuropsychiatric disorders have mainly been modeled by 2D neural cultures and the main target was the assessment of gene expression, cell morphology, neuronal excitability and synapses formation [9]. In 2011, Brennan K. J. et al. observed human iPSCs derived neuronal cultures from patients with SCZ. They noticed that neurons exhibited a variety of abnormalities such as decreased neurite number, limitation on the expression of glutamate receptors and synaptic scaffolding protein PSD95. In parallel with these observations, neuronal cultures presented a reduction on synaptic connectivity, an impairment which appears on most psychiatric disorders [30]. In 2016, Mertens, J. et al. proved that

² Myelination is a postnatal event in which neuronal axons are coated with myelin, a fatty sheath for protection and electrical insulation [14].

hyperexcitability and mitochondrial abnormalities presented in putative hippocampal neurons from patients with bipolar disorder, can be reversed with the application of lithium. However, not all neuronal cultures had the same performance after the lithium deposition. This observation led to the conclusion that some patients were resistive to lithium as a pharmacological treatment [31].

Several studies on modeling monogenic disorders, such as Rett syndrome (RTT) and Timothy syndrome (TS) which present comorbidity with ASD, have presented important results that may assist in revealing the molecular and cellular complexity of other ASDs [32]. For instance, Insulin-like growth factor 1 (IGF1) has been successfully used for relieving RTT malfunctions to human iPSCs derived neural cultures. Subsequently, IGF1 has been proposed as a potential medication for patients suffering from ASD [33], [34]. Moreover, human iPSC-based models for ASDs have shown that synaptic regulators neurexin and neuroligin appear as potential ASD candidates. Mutation on gene NRXN1 causes a dysfunction on neurexin-1 (protein), resulting in reduced glial differentiation, malfunctions on cell adhesion and on neuron differentiation [35].

From a handful studies, there is a clear indication that differentiation protocols generating 2D culture formation can be successfully used for psychiatric disease modeling, although these cultures are lacking the 3D structure responsible for complex cell to cell interactions and cellular maturity. Additionally, there is also some valuable evidence of organoid models which positively achieved to provide important results from specific psychiatric disorders. For instance, in 2015, Mariani et al. compared wild type control organoids with ASD-derived organoids and they noticed that diseased organoids presented a decreased cell cycle length, resulting to their over-proliferation. Additionally, the ASD-derived organoids appeared an increase production of GABAergic inhibitory neurons due to over expression of FOXP1 gene [36].

Impressive is also the increasing effort of neural differentiation protocols' improvement and the rapid development of the next-generation in vitro models, which are the 3D cultures, organoids [9], [13]. Although there is much work to be done in order to recapitulate all the brain complexity into 3D models in vitro, the research evidence derived from the current studies is considerably encouraging for understanding the impairments of psychiatric disorders in a cellular level. There is a tremendous need for advanced technology to assess the neuronal networks based on their genetical expression, shape, morphology and electrophysiology. Especially, on the electrophysiology sector, optical-electrophysiology, calcium imaging and high density, micro-electrode array recording would provide in depth information about the cell to cell interaction and functional maturity derived from the complex 3D arrangement of neurons.

2.5 MEAs in vitro: extracellular recording of neuronal activity

During the last decades, advanced technologies of genetic markers, immunostaining, optical and electro-optical methods, electrophysiological recording have been used for identifying neuronal types, explaining molecular machinery, as well as, characterizing the functional activity of neurons. Electrophysiology presents significant advantages compared to other methods, as it allows the analysis of neuronal activity by capturing a wide range of neuronal phenomena, from the spiking activity of individual neurons to the slower network oscillations of small neuronal populations. The excitable nature of neurons, propagating electrical signals among them, permit the activity to be detected by electrodes either in a direct contact or in a relate distance by the source.

Electrophysiological methods are separated into three levels: microscale, mesoscale and macroscale. In microscale level, the intracellular activity of single neurons is measured. The golden standard of intracellular measurement is the whole cell patch-clamp recording. Mesoscale level concerned

methods in which neuronal network activity is observed with extracellular measurements. It appears as a well-suited method for neural cultures *in vitro*, in which the functionality of network activity and the maturity of neurons, due to their interconnective structure, is assessed [37]. Additionally, in case of modeling psychiatric disorders *in vitro* where the genetic deficit might be expressed on synapse functionality, extracellular methods seem suitable tools to evaluate the functional role of neurons in a network cellular level [5]. The macroscale level contains all methods of indirect measurement of large areas of the brain's activity, such as functional magnetic resonance imaging (fMRI), positron emission tomography (PET), and electroencephalography (EEG) [37].

The mesoscale-extracellular recordings are mainly composed by metal electrodes integrated into large arrays, so-called microelectrode arrays (MEAs). Nowadays, there is an effort on replacing metal electrodes with active components such as open-gate field-effect transistors (OGFETs) or oxide-semiconductor FET (OSFET). The reason of integrating active electronic components on MEAs is their size, which allows higher electrode number and density. Moreover, this approach overcomes the connectivity limitation of metal electrodes, while active components allow the data transfer from a high number of channels with the use of active switches to time multiplex signals [37], [38].

Over the years, several subtypes of MEA have developed and they are categorized based on the basic features they present, i.e. emphasizing the type of the transducers used (multi-transistor array, microelectrode array, multielectrode array, micro-nail array, capacitive-coupled array, 3D MEA), also on the type of substrate (active array, passive array), the shape of the device (needle-type probe, polytrode, neuro dish), the channel count (multichannel array), the electrode density (HDMEA) or the application (implantable array, *in vivo* MEA, *in vitro* MEA) [37].

2.5.1 Electrodes on MEAs

In vitro MEAs, applicable for cell culture recordings, generally include a cell culture dish, where the substrate is made by a glass or silicon wafers in which an integrated array of electrodes has been photoetched [10]. The most common MEA substrate is the glass wafer, which allows an easy observation of the cell culture under a light microscope. *In vitro* MEAs are composed by a few up to 10.000 electrodes, in a micrometer scale [39]. Typically, electrodes are made of metallic conductors, such as gold (Au), titanium nitride (TiN), platinum (Pt), stainless steel, aluminum (Al) and alloys like iridium oxide (IrOx). The opposite end of electrodes extends to the periphery of the chip which is connected to an amplifier. The amplifier conveys the electrical signal towards the analog-to-digital converter and then a computer is used for signal analysis and data storage [37].

The general issue that appears on MEAs is the high impedance due to micrometer scale of the electrodes, ranging from 10 to 100 μ m [40]. The strategy of coating the tip of electrodes with porous conductive materials increases the effective surface area and reduces the electrode's impedance significantly. Examples of such coating materials are Pt-black, Au nanostructures, carbon nanotubes (CNTs), and conductive polymers like poly(3,4-ethylenedioxythiophene) (PEDOT). Additionally, these materials have been tested for toxicity in prolonged periods of time and are considered as biocompatible [37], [40].

Electrodes on MEAs *in vitro* can perform recordings for a long period of time and they sense Extracellular Action Potentials (EAP), known as spikes, from a population of neurons close by the recording site. The maximum distance that a microelectrode can detect activity is approximately 100 μ m to 150 μ m. Furthermore, in most of the cases, electrodes can disturb neuronal activity with the use of current or voltage stimulation [37], [41].

2.5.2 Electrode-Neuron interface

In the volume conduction theory, electrical signals, Action Potentials (APs), generated by neurons, create a localized change in ionic concentration due to ions' movement across the cell membrane. This movement is propagated via an electrolyte to an electrode. The relationship between a recorded potential at an electrode (V) (located at x, y, z) and the transmembrane current source (I) (AP located at x', y', z') in an infinite volume conductor, also with homogenous extracellular electrical conductivity (σ) is described with the following equation [42].

$$V(x, y, z) = \frac{I}{4\pi\sigma\sqrt{(x - x')^2 + (y - y')^2 + (z - z')^2}} \quad (1)$$

Based on Equation 1, the amplitude of the recorded signal is mainly influenced by the relative position of the electrode compared to the neuron. Tightly coupled neurons with electrodes enhance the recording accuracy and the amplitude of field potentials. However, the fact that neurons migrate or die, can be the cause that no electrical activity is recorded. Moreover, sodium and potassium maturation leads to different AP generation and consequently, neurons might fire less or be silent [43].

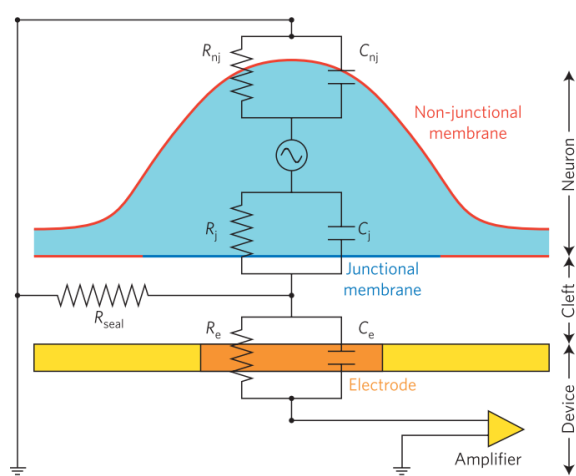


Figure 2.3] Spatial relationship between neuron and electrode with the equivalent passive electrical circuit. Neuron's plasma membrane is defined by the junctional membrane (in contact with the electrode) and the non-junctional membrane (facing the bath solution and the MEA substrate). Electrical signal generated by the neuron passes via the non-junctional and junctional membranes to the cleft containing ionic solution. The voltage created over the R_{seal} charges the electrode connected with the MEA amplifier. Figure taken from [39].

of the plasma membrane, the non-junctional membrane (red color) is represented by the non-junctional membrane resistance (R_{nj}) and the non-junctional membrane capacitance (C_{nj}) and is in direct contact only with the cellular medium and the MEA substrate [39].

APs or synaptic potentials producing complex extracellular currents propagate via the non-junctional and the junctional membranes and reach the cleft. The ionic solution in the cleft generates a resistive environment (R_{seal}). Subsequently, the voltage formed on the R_{seal} , modify the charge dispersal across the passive metal electrode. Finally, the electrode (orange color) represented by a resistance (R_e) and a capacitance (C_e) propagates the sensed signal to the amplifier of the MEA system [39].

Moreover, sodium and potassium maturation leads to different AP generation and consequently, neurons might fire less or be silent [43].

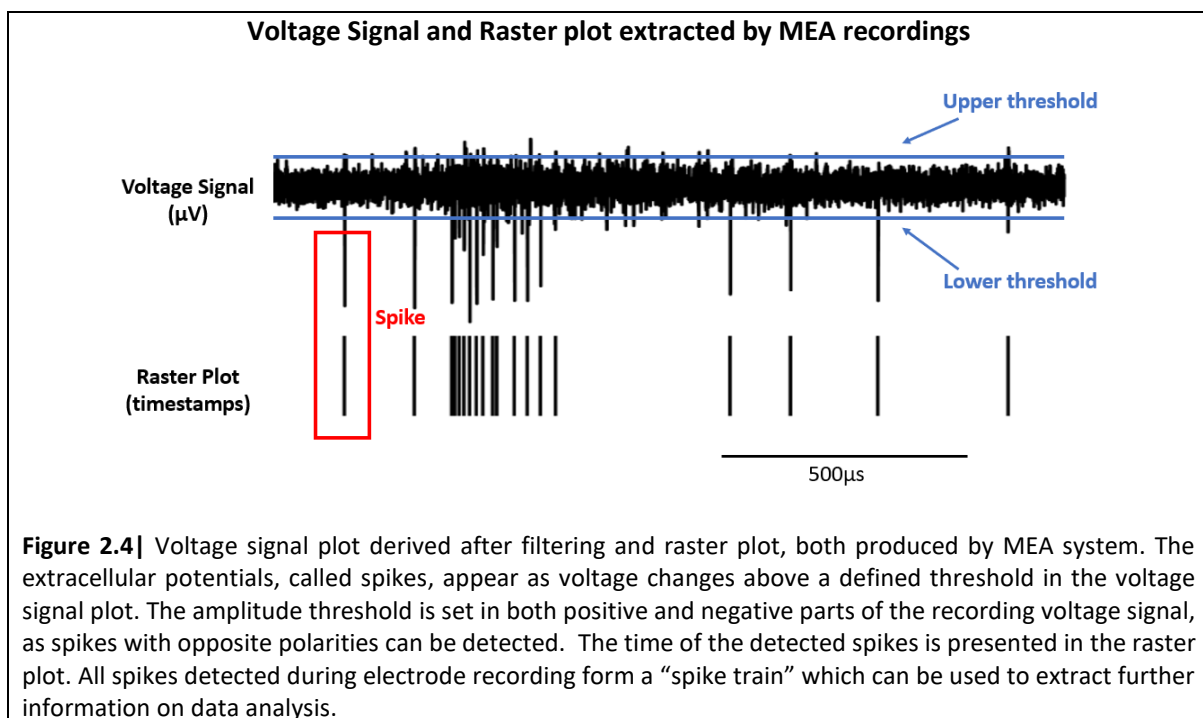
The spatial relationship between a neuron and a substrate-integrated planar electrode with the equivalent analogue passive electrical circuit is schematically illustrated in Figure 2.3. However, in real time, several neurons are in direct contact with a single electrode.

The neuroelectronic structure is composed by the cell body of a neuron (light blue), a cleft (the area between the neuron and the substrate) which contains the ionic solution and the electrode (orange colored part). The junctional membrane (blue color) which is a part of neuron plasma membrane, adhere to the electrode surface by electrochemical molecules derived from both neurons and experimentalists' coating. The junctional membrane is represented by the junctional membrane resistance (R_j) and junctional membrane capacitance (C_j). The rest

2.5.3 Extracellular action potentials


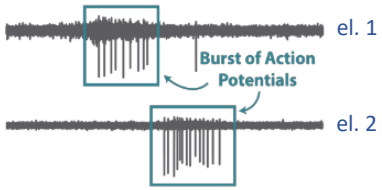
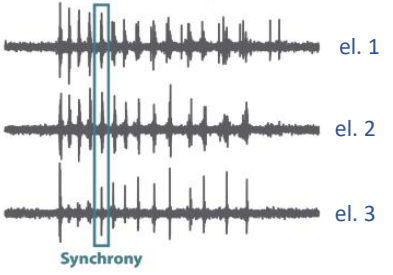
The EAPs are mainly caused by ionic currents from the closest neurons. During an AP of a neuron, the initial rapid Na^+ ion influx creates a sink, which results in a large negative spike in the extracellular space. Subsequently, the slow K^+ efflux produces a source resulting in a small positive spike [37]. EAPs, spikes, constitute the high frequency components of the recorded signal and are detected with the use of bandpass filter which ranges from 300 to 3000 Hz.

Spikes are identified as voltage signals on the top of the background noisy activity, when they overpass a predefined threshold. The threshold is usually set as “n” multiple times of the baseline noise level, calculated as the root mean square of the signals with a mean value of zero. However, in presence of many spikes detected, it is suggested that the threshold is calculated based on the median, which eliminates the effect of outliers on the noise level. All the spikes detected by an electrode constitute a spike train. One of the most important information is the timestamp of spikes. A raster plot contains only the timestamps of spikes and they are illustrated in the raster plot as vertical columns, “ticks”, indicating that neuronal activity took place at that specific moment (Figure 2.4) [10].



The extracellular activity of neurons is characterized based on functionality, connectivity and synchronicity (Table 2.1). The term functionality refers to the ability of neurons to fire, which is represented in the voltage signal or raster plot as single spikes. Bursts (connectivity) indicate the periodical activity of neurons to fire multiple APs within a short time of some milliseconds (burst) and then to be silent until the next burst starts. In the voltage signal or raster plot, a burst appears as multiple spikes in a time interval of a few milliseconds. Synchronicity is characterized by the synchronized bursts between different populations of neurons sensed by different electrodes on the same time [10].

Table 2.1 | Criteria for neuronal characterization

<p><u>Functionality:</u> Neurons start firing APs which appear as single voltage changes (spikes) above a defined threshold in the voltage signal plot derived from each electrode.</p>	
<p><u>Connectivity:</u> Bursting activity, neurons fire multiple action potentials in some milli seconds. A lag period occurs before the next burst starts. MEA systems contain advanced algorithms for burst detection</p>	
<p><u>Synchronicity:</u> Synaptic connectivity is observed based on synchronized bursts generated on different neuronal populations on the same culture and detected by the electrodes existing on these neuronal population areas.</p>	

For in vitro MEAs, the shape of spikes is an additional feature of neuronal characterization influenced by the morphology and the size of neurons, as well as by external factors, such as the level of coupling and the distance between electrode and neurons, the electrode impedance and the conductivity of cellular medium. Additionally, it has been noticed that glial cells have a considerable impact on the shape of the recording signals, as the paths around them are less resistive than the paths through them. Consequently, extracellular currents flow around glial cell and thus different neuronal structures can significantly change the shape of the detected spikes. Moreover, based on in vivo observations, somatic spikes are usually wider (0.7- 1ms) compared to axon spikes (0.4-0.5ms) and therefore, a relatively similar detection is expected from in vitro measurements [37], [42].

2.5.4 MEAs and neural cell cultures

MEAs have mainly used as a method for investigation of neuronal growth and connectivity at a basic level, and thereafter for pharmacological and diagnostic tests. In general, MEAs are specialized as high-throughput systems as they provide high-throughput platforms (multiple wells on the same plate), which allow simultaneous screening of chemical compounds on multiple neuronal cultures. Additionally, variability in network function measured by MEA technology is reduced with the use of a high-throughput platform, as neural cultures are seeded at the same time and they are kept under the same conditions. Moreover, the simultaneous observation of neural networks recapitulating different brain regions is also possible on such multiwell MEA platforms [10]. Nowadays, MEA approach is combined with other advanced technologies, such as immunostaining or fluorescence microscopy, in order to correlate the neuronal activity with specific neuronal cell types or synapses. Moreover, stained neurons in a low density cultures on MEA substrate allows not only the visual observation, but also the estimation of the cellularly functional maps derived from the connections of neurons [37].

In parallel with combining advanced methods with MEA systems, new MEA systems are optimized under the condition that more of the processes should be automated in order to provide stable conditions for neural cultures, eliminate the human error and enhance the neuronal activity detection. For instance, liquid handle robots are preferred for cultivation medium refresh and chemical compound deposition [10]. Another considerable limitation of the conventional MEA systems is the neuronal growth in a multidirectional way around the electrodes, which creates issues on the signal detection by the electrodes. Pre-patterned MEA substrates have been designed for guiding the growth of neuron in a unidirectional path in order to enhance recording performance in vitro. The double chamber MEA (DCMEA) is composed of two chambers, the “emitting” and “receiving” chambers, which are connected to each other with channels. The channels include barbs which allow axons to extend from the emitting to the receiving chamber and impede the axon growth in the opposite direction [44]. Another example is a microtunnel MEA system, providing MEA platforms made of microtunnels, in which the neuronal axons grow. Each microtunnel contains one recording and one stimulation electrode placed at the bottom. Microtunnel MEA increases the signal-to-noise ratio and the spike amplitude, as it maintains the position of axons inside the microtunnel on the top of the electrode, even if the cell soma incorporates into an aggregation of multiple neurons or detaches from the MEA substrate [45].

2.6 Quantitative assessment of neuronal network development

The analysis of the spike trains can provide a plethora of additional information that can be elicited from these trains. An initial analysis includes the calculation of the spike rate (spikes/time) and the bursting rate (bursts/time) per electrode, as well as the whole network rate of spikes and bursts. The burst detection along with the analysis, constitute a challenging procedure. Although bursting activity is a fundamental characteristic in the central nervous system (CNS), an established pattern of bursting activity is lacking due to the variability between neuronal cultures. Different software applications have been used for bursting detection and classification providing pre-defined or adaptive parameters. Algorithms for burst classification are useful tools for MEA platforms that include a significant number of electrodes, i.e. 60 up to 4000 [10], [37], [46].

Measures considering the network function such as synchronicity and oscillation require a more complex analysis, which includes autocorrelograms, cross-correlograms and probabilistic models for network connectivity [10]. A statistical analysis with several mathematical tools, such as n-dimensional embedding, correlation integrals and non-linear prediction methods have been used to prove that a low-dimensional deterministic process drives the synchronized bursts [40]. For instance, cross-correlation analysis has been used to identify the relation between the recorded electrical activity of a representative channel, compared to the electrical activities detected by all the other channels, on 2D and 3D cultures. The findings showed that 2D and 3D cultures exhibit high synchronicity during bursting activity. However, 3D cultures present significantly higher spontaneous activity compared to 2D cultures [47].

An analysis method oriented in spike-waveforms classification is the spike sorting technique. The importance of this analysis method is based on the fact that nearby neurons are triggered by different stimuli and consequently, this kind of information might be useful for neuronal characterization and neuronal type determination [41]. For example, spike sorting analysis on waveforms derived from cortical neurons related to memory function is essential for the determination of their firing patterns [48], [49].

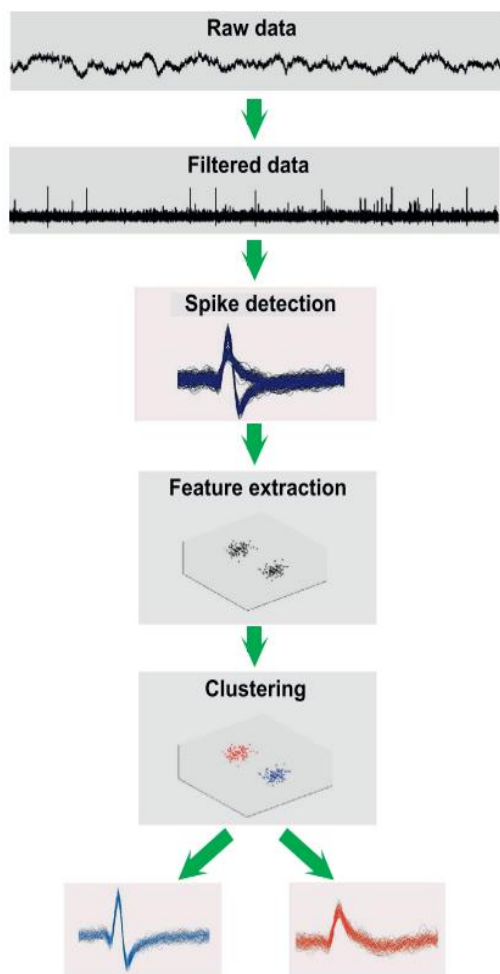


Figure 2.5 | Spike Sorting Method. Spikes are detected on filtered raw data, above a pre-defined threshold. Relevant features of spike waveforms are extracted and assigned into units. Clustering algorithms classify the features into clusters. Each cluster provides a distinct waveform. Figure taken from [41].

Novice algorithms classified spikes based on their amplitude, but this approach was missing the important information of the spikes' waveform. Current algorithms are focusing on categorizing spikes based on their waveform. Some spike sorting methods categorize the spike waveforms using "window discriminators" or "template matching" techniques. These techniques have the significant limitations of electrode number dependence, manual intervention and readjustment [41].

The most effective way of spike sorting based on discriminative feature extraction and spike clustering is depicted in Figure 2.5. The raw data extracted by MEA recording are filtered with a bandpass filter and the spike detection is based on a predefined threshold. The features extracted by each waveform are represented as points in a M-dimensional space, where M is the number of samples of each waveform. Subsequently, clustering algorithms such as Gaussian Mixture Models, hierarchical or non-parametric clustering methods group the points into clusters. It is obvious that when the features are distinct, clustering algorithms perform accurate classification of features into clusters. Each cluster contains features which form a different type of waveforms. The mean waveforms of the clusters indicate a spike shape associated with a specific unit of neurons [41].

The major issue of the spike sorting technique is the overlapping waveforms. Nearby neurons can fire synchronously in the same amplitude, producing the same waveforms. The discrimination of these two identical waveforms is hard and most of the times leads to incorrect clustering. Additionally, as the spike waveforms change during bursting activity, the spike sorting methods eliminate the bursting information. Moreover, neuronal maturation and instability of conductivity medium influence the spike-waveforms which might alter during time. Therefore, during a long-term recording period, the spike sorting analysis might create different waveform clusters which are all derived from the same type of neurons [41].

Through all these different techniques of data analysis, neuronal activity derived from in vitro models is characterized. Moreover, some analysis methods validate the correct usage of some other methods. For instance, cross-correlation function for synchronicity detections verify the correct detection and analysis of bursting activity. In order to confirm the investigation of a cellular phenotype, the same data analysis methods can be applied on both control and disease cell lines. The comparison of results might present a neurodevelopmental delay on the disease cell lines. As MEA system is a high-throughput system for toxicological analysis, the above methods for data analysis can be also used for comparison between data extracted before and after the deposition of chemical compounds which would reveal, or not, a significant reversed activity due to drug deposition.

CHAPTER 3

Materials and Methods

For the experimental procedure, a long-term neural differentiation protocol was used for the cell culturing process. The protocol promotes the differentiation of human iPSCs into functional neurons in a monolayer. The differentiation procedure is based on firstly differentiating iPSCs into NPCs and continuously, gives rise to both neurons and astrocytes, in a controlled ratio of 60:40. A Wild Type Control iPSC (WTC-11) line from a healthy individual was obtained from the Gladstone Institute (original line Coriell GM25256) for neural cell cultures. The commercial Multiwell-MEA system from Multi Channel Systems MCS GmbH Germany was selected for extracellular measurements. Algorithms embedded on the commercial software packages provided by Multi Channel Systems were used for spike, burst and network burst detection. The optimized Wave_clus algorithm by Fernando J. Chaure et al. was selected for spike sorting analysis on the extracted data. The data analysis included the calculation of active electrodes per well, Cumulative Firing Rate per well and Mean Firing Rate per electrode, as wells as the total number of bursts detected per well/recording performance. The unpaired student's t-test or ANOVA analysis for repeated measurements were applied where comparison between different data set was needed.

3.1 Neural differentiation protocol on the Multiwell-MEA plate

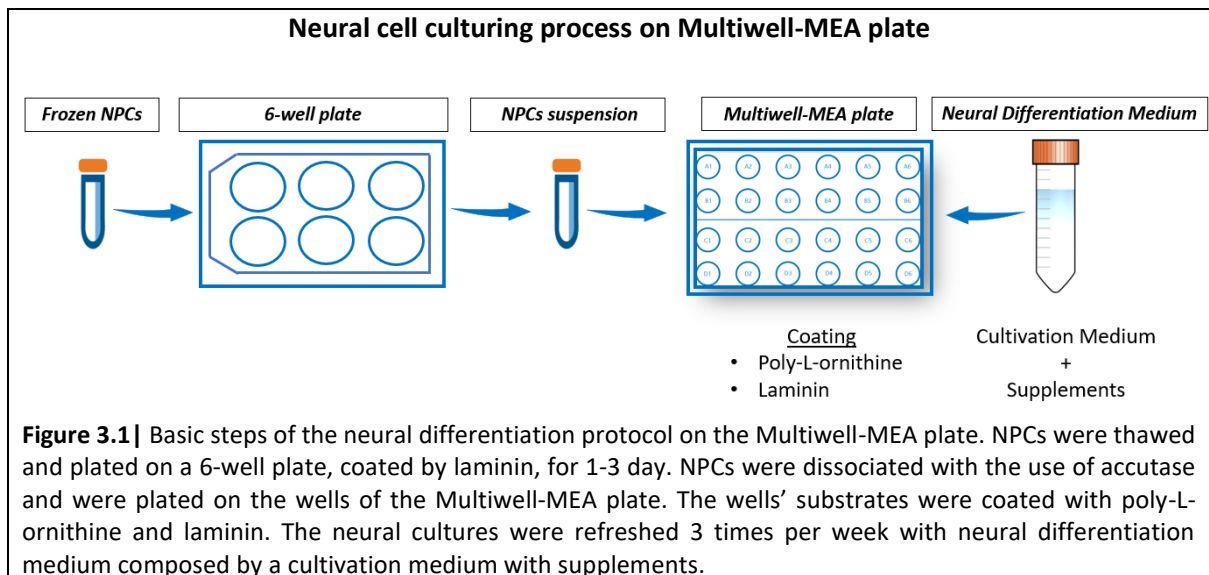
A Wild Type Control iPSC (WTC-11) line from a healthy individual was obtained from the Gladstone Institute (original line Coriell GM25256). The iPSC line was derived by reprogramming of human skin fibroblast into iPSCs. The neural differentiation protocol published in 2018 by N. Gunhanlar et al. [12] was selected for the neural cell culturing process which promotes the differentiation of human iPSCs into functional neurons in a monolayer. The differentiation procedure is based on firstly differentiating iPSCs into NPCs and continuously, gives rise to both neurons and astrocytes, in a controlled ratio of 60:40. The procedure of iPSCs differentiation into NPCs was not part of the thesis project and consequently, frozen stocks of NPCs that were kept into a liquid nitrogen freezer were used for the experimental procedure. NPCs were thawed and seeded on the Multiwell-MEA plates of Multiwell-MEA system, launched by Multichannel Systems MCS GmbH Germany, for extracellular recordings.

NPCs were thawed and grew in the 6-well plate, coated by laminin (Sigma-Aldrich), for 1-3 days. Laminin is an extracellular matrix protein which enhances the attachment, proliferation and differentiation of NPCs. The Multiwell-MEA plate of Multiwell-MEA system, launched by Multi Channel Systems MCS GmbH Germany, were used for neural cell culturing. The substrate of each well of the Multiwell-MEA plate was coated with 0.5 ml of poly-L-ornithine (Sigma-Aldrich) for 1h, at room temperature. Poly-L-ornithine helps NPCs to attach on the substrate. The coated MEA substrates were washed 3 times with sterile water and air-dried for 30 min. Continuously, a drop³ (7.5-50 μ l) of laminin (Sigma-Aldrich) solution, 50 μ g ml⁻¹ in DMEM/F12 advanced medium (Thermo Fisher Scientific), was placed in the middle of each MEA substrate, incubated for at least 30 min at 37°C / 5% CO₂ and removed just before adding the NPCs. Both Laminin and poly-L-ornithine are used as a cell culture substratum.

NPCs were dissociated with the use of accutase and resuspended in neural differentiation medium (cultivation medium, 1% N2 supplement (Thermo Fisher Scientific), 2% B27-RA supplement (Thermo Fisher Scientific), 1% minimum essential medium/non-essential amino acid (Thermo Fisher Scientific), 20 ng ml⁻¹ brain-derived neurotrophic factor (ProSpec Bio, Rehovot, Israel), 20 ng ml⁻¹ glial cell-derived neurotrophic factor (ProSpec Bio), 1 μ M dibutyl cyclic adenosine monophosphate (Sigma-Aldrich), 200 μ M ascorbic acid (Sigma-Aldrich), 2 μ g ml⁻¹ laminin (Sigma-Aldrich) and 1% penicillin/streptomycin (Thermo Fisher Scientific). A drop⁴ of NPC suspension was plated on the laminin coated spot of each well for 1h to allow the attachment of the NPCs on the MEA substrate in neural differentiation medium. After 1h, 0.5 ml of neural differentiation medium was added on each well. The neural cultures were refreshed with neural differentiation medium 3 times per week. During the first 4 weeks, the medium was fully refreshed, 0.5 ml. From the 5th week until the end of the experimental procedure, only half of the volume of the medium was refreshed, 0.25ml. The following figure illustrates the basic steps of the cell culturing technique. The Multiwell-MEA plate with neural cell cultures were kept in an incubator at 37°C and 5% CO₂.

³ During the experimental process different volumes of laminin were selected. The laminin volumes were always the same with the selected volume of NPC suspension for plating on MEA substrate (refer to Chapter 4).

⁴ Different volumes of NPC suspension were plated on the Multiwell-MEA plates used for the experimental process (refer to Chapter 4).



During the experimental process two different cultivation medium were used for neural cell culturing: Neurobasal medium (Thermo Fisher Scientific) and BrainPhys medium (StemCell Technologies). Neurobasal medium was used as a cultivation medium according to the neural differentiation protocol published in 2018 [12]. BrainPhys medium is a recent invention, in 2015, by C. Bardy et al. and presents a significant advantage compared to classical basal media, as its osmolarity ranges in the same level with human cerebrospinal fluid ($300 \text{ mOsmol L}^{-1}$) [50]. By readjusting the concentrations of inorganic salts, neuroactive amino acids and energetic substrates, BrainPhys medium enhances the neuronal activity and allows the survival of human neurons in cultures. Additionally, in long-term usage, BrainPhys improves the proportion of neurons that are synaptically active. All in all, BrainPhys provides a neural cell culturing environment similar to brain physiological conditions in vivo and thus, support the development of neurophysiological activity.

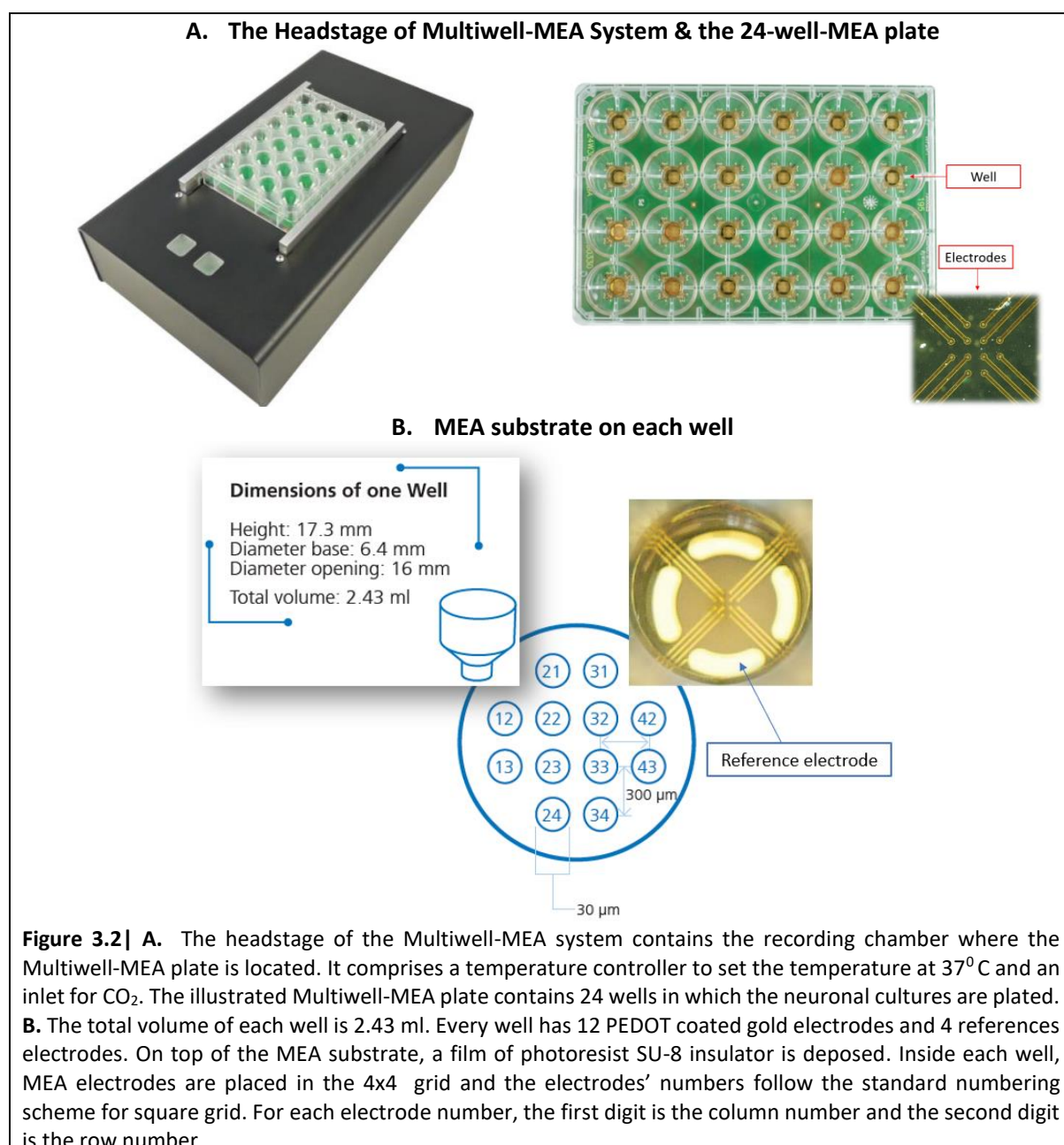
Additionally, during some experiments, laminin which was used as a coating, was replaced by matrigel (Corning Life Sciences). Matrigel is a gelatinous protein mixture secreted by Engelbreth-Holm-Swarm (EHS) mouse sarcoma cells. The deposition of telomerase inhibitor azidothymidine (AZT) was also inserted in some neural cultures during the procedure of medium refreshing (dilution factor: $4\mu\text{l}$ AZT per 1ml of cultivation medium). AZT reduces the number of dividing progenitors without inducing cell death by promoting the differentiation of NPCs into neurons [51].

3.2 Multiwell-MEA System

The Multiwell-MEA System consists of four main components: the Multiwell-MEA plates, a headstage, an interface board and two commercial software packages, the Multiwell-Screen and the Multiwell-Analyzer for data visualization during the recording performance and data analysis respectively. The system is considered as a perfect tool for medium or high throughput electrophysiology, as it provides plates with 24 or 96 wells per plate which allows the simultaneous observations of several cultures. The data can be sampled up to 50kHz per channels (simultaneously in all channels) while the data resolution is 24 bits. The system provides both recording and stimulation performances and is applicable for both neuronal and cardiac samples.

The headstage is the core element of the system (Figure 3.2 A). In the headstage, there is a designed area called recording chamber where MEA plates are placed on. This area also includes a temperature controller which keeps the plate in a constant temperature of 37°C and an air inlet in order to provide

a gas mixture containing 5% concentration of CO₂. The 24-well-MEA plate contains 4 rows of 6 wells, with a total volume of 2.43 ml per well (Figure 3.2 A, B). Every well has 12 PEDOT coated gold electrodes at a 4x4 grid, on a glass base which allows the visual monitoring of cell culture (Figure 3.2 B). The PEDOT coating on the top of the electrodes is a conductive biocompatible polymer which reduces the electrode's impedance by two or three orders and maintains the high quality of the recording signal [52]. The electrode's diameter is 30 μm while the distance between two neighbor electrodes, center to center, is 300 μm. A layer of photoresist SU-8 insulator is deposited on top of the MEA substrate by leaving open the recording sites. SU-8 is a biocompatible, non-toxic for cell cultures material which produces a thin, uniform and pinhole-free layer [53]. Additionally, four reference electrodes exhibit in each well, as depicted in (Figure 3.2 B). MEA-electrodes had an impedance of 15-25 kOhm according to the specifications of the manufacturer (Multi Channel Systems).



3.3 Algorithms for spike, burst and network burst detection

In order to detect the spikes on the top of the background noisy activity, an amplitude threshold was set which was 5 times the standard deviation of the recording signal. The standard deviation was calculated in a time window of 1 second. The value of the amplitude threshold was selected based on previous empirical observations [54], [55], [56]. Based on these studies, extracellular recording had performed on neural cultures with the same MEA system or another commercial or in-house system in which it was investigated that an amplitude threshold of 5 times the standard deviation of the recording signal allowed the accurate detection of spikes without considering background noise. When the signal crossed the amplitude threshold, considered as a spike, a signal waveform of 3 ms was extracted (1 ms before the spike event and 2 ms after the spike event).

After each spike detection, a dead time window of 3 ms was applied, in which any other voltage signal overpassing the amplitude threshold was considered as a part of the previously detected spike. The value of the dead time window was suggested by the Multichannel System; however, it was possible to be changed based on the user's preference. The suggestion of the value of 3ms on the dead time window is based on the concept that an AP of a single neuron last at about 3 ms (from the beginning of depolarization until the end of hyperpolarization) [14]. Therefore, the time duration of a spike derived from the simultaneously contribution several APs lasts the same. A carefully selection of the value is suggested as by decreasing or increasing the dead time window, there is a possibility to lose spike activity or to merge more than one spikes together. The limitation on this strategy is the complex issue of overlapping spikes which can happen independently of the value of the dead time window [41].

The bursting activity was detected with the use of the Max Interval Method algorithm [57]. As presented in the flow chart of Figure 3.3, the bursting algorithm started by scanning the spike train in order to find two consecutive spikes whose interval was equal or less than the "maximum interspike interval at the start of a burst". Continuously, following interspike intervals which were equal or less than "maximum interspike interval in a burst" were merged with the first pair of spikes. The burst was terminated on the interspike interval, which was greater than "maximum interspike interval in a burst". Finally, the detected bursts with less than the defined "minimum burst duration" or "minimum number of spikes in a burst" were omitted. The sequential bursts whose interburst intervals were less than the "minimum interval between two bursts" were merged. The selection of these specific values was chosen based on empirical observations of previous studies [56], [55] where a nice bursting activity derived from iPSCs derived neurons was detected.

Flow chart of the Max Interval Method algorithm

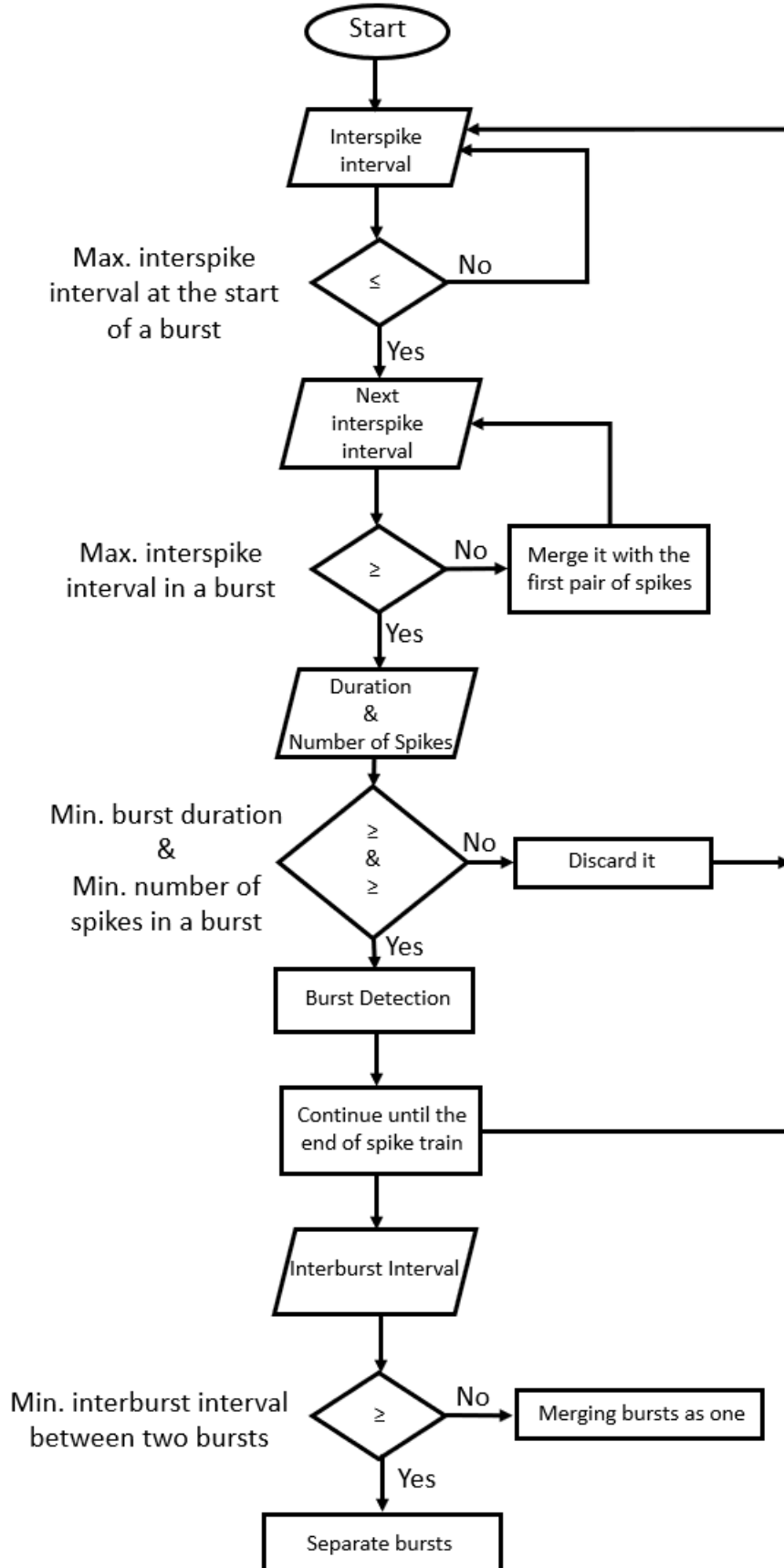
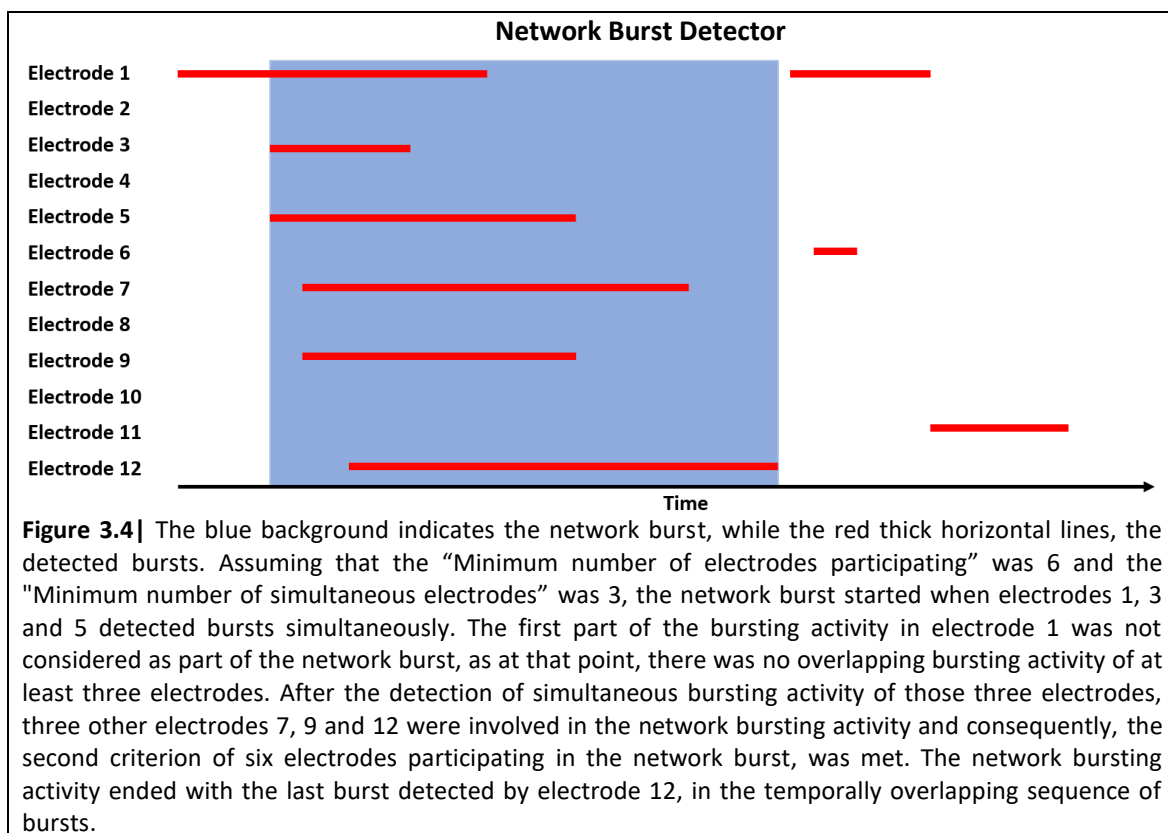


Figure 3.3 | Max Interval Method algorithm was used by the Multiwell-MEA system for bursting detection [57]. The algorithm scanned the spike train and detected the bursts which obeyed on the parameters of burst detection. Based on the flow chart, the algorithm searched the interspike intervals one by one until finding the first interspike interval which is equal or less than the “maximum interspike interval at the start of a burst”. Consecutive spikes with interspike interval equal or less than the “maximum interspike interval in a burst”, were merged with the first pair of spikes. In order to consider a sequence of a spikes as a burst, their number and their duration should be equal or greater than “minimum burst duration” and “minimum number of spikes in a burst” respectively. The algorithm continued the burst detection process until it reached the end of the spike train. Consecutive bursts with intervals less than the “minimum interval between two bursts” were merged as one burst.

Additionally, the temporal overlapping bursting activity among different electrodes was detected with the use of the Network Burst Detector [58], [59]. To qualify a network burst, two parameters should be met simultaneously: the “Minimum number of electrodes participating” in the network burst and the “Minimum number of simultaneous electrodes” detecting a bursting activity. An example of network burst detection is given in Figure 3.4.



3.4 Wave_clus: fully automatic spike-sorting implementation

The optimized Wave_clus algorithm by Fernando J. Chaure et al. was selected for spike sorting analysis on the extracted data from Multiwell-MEA system [60]. Wave_clus algorithm is characterized as a non-parametric, meaning that there is no need of a priori knowledge about data structure. The cornerstone of this implementation is the wavelet decomposition, in which the representative features are extracted from the detected waveforms, and also the Superparamagnetic Clustering (SPC), which is a relatively new clustering method developed in the context of statistical mechanics and especially for magnetic models.

The Wave_clus algorithm is composed by four main steps: signal filtering, spike detection, feature extraction and clustering. The first two steps had already been implemented by Multiwell-MEA system and therefore, the last two steps were only used. Feature extraction is implemented by a four-level decomposition with a Haar wavelet, resulting in 76 wavelet coefficients for each spike waveform. Wavelet decomposition is defined as the convolution of the signal and the dilated or contracted shifted version of a unique wavelet function. The significant advantage of wavelet transform is the optimal resolution in both time and frequency domain. The Haar wavelet is suitable for cases in which there is no theoretical knowledge of the waveforms' shapes. Additionally, the Lilliefors test is used, based on the Kolmogorov-Smirnov test, in order to select the most significant wavelet coefficients and consequently, enhance the algorithm efficiency and the computing time. The Lilliefors test is a normality test in which data that deviate from normality are selected. Based on this test, only a few coefficients per spike, the most significant ones, are selected as the representative features for spike sorting. In order to avoid outliers, only the coefficients with three times the standard deviation were selected [61].

Subsequently, SPC is used for spike clustering in a feature space and groups data points based on the nearest-neighbor interactions. Proportionally to the methodology of statistical mechanics on magnetic models, SPC demonstrates three phases: ferromagnetic, superparamagnetic and paramagnetic. A Potts spin is assigned on every data point and consequently, the clusters appear naturally in Potts model as regions of aligned spins. The methodology starts with the assumption that at a low temperature all spins are aligned, and they belong to the same cluster (ferromagnetic phase). As the temperature increases, the spins belonging to the same high density region are aligned, while different regions remain uncorrelated (superparamagnetic phase). In that phase, natural clusters appear, which means that the data points are separated into clusters based on their substantial differences. In the last paramagnetic phase, the whole system is disordered, as even minor differences in the data points play a crucial role and therefore the system has reached the level in which each data point represents a single cluster [62].

A simplified example in order to understand the superparamagnetic clustering is the unsupervised learning of a young child. Assuming that a child has never seen a giraffe and an elephant before, and it is exposed to a significant number of pictures containing giraffes and elephants. At the beginning, the child will categorize all the pictures together, as all of them illustrate animals (ferromagnetic phase). After some time, the child might realize that these pictures show two different creatures and consequently, it will classify these pictures into two groups, elephants and giraffes. This is the phase of a superparamagnetic stage and the appearance of natural clusters. It is highly possible the child will continue to categorize further the pictures of these two groups based on the animals' size, shape, color, whether it is an animation or not. The classification will start being meaningless as too much minor information is taken as important. This is the paramagnetic phase where the system is completely disordered.

The key parameter in the SPC is the temperature. Wave_clus algorithm uses a temperature parameter which ranged from 0 to 0.25 in increments of 0.01, labeled as T_i with $i=\{0..0.25\}$. At each temperature the detected clusters appear in a descending order with respect to their size, i.e. for a temperature T_n the largest cluster is denoted as $C_1^{T_n}$, the second as $C_2^{T_n}$ etc. The clusters are identified by the Wave_clus algorithm with a predefined threshold in which, as it is described in the following equation, the size of the n cluster on the temperature T_n should have been increased by 20 spikes compared to the previous temperature T_{n-1} .

$$|C_i^{T_n}| - |C_i^{T_{n-1}}| \geq 20, \text{ with } C_i^{T_{n-1}} = 0 \quad (2)$$

After finishing the extraction of clusters for each temperature, the Wave_clus algorithm defines the end of the superparamagnetic regime and the beginning of the paramagnetic regime at the highest temperature that at least one cluster obeys to equation 2. All the detected clusters from different temperatures are considered as putative clusters. Subsequently, the Wave_clus algorithm selects the final clusters among different temperatures with the use of inclusion criterion. Based on this criterion the overlapping coefficient $O_{ij}^{T_n T_m}$ is calculated, as described in equation 3, which ranges from 0, if clusters on different temperatures ($C_i^{T_n}$ $C_i^{T_m}$) are completely unrelated, until 1, if clusters are the same. In the algorithm, only clusters which present a correlation equal or higher than 0.9 are omitted from the final cluster selection.

$$O_{ij}^{T_n T_m} = \frac{|C_i^{T_n} \cap C_i^{T_m}|}{\min(|C_i^{T_n}|, |C_i^{T_m}|)} \quad (3)$$

Finally, the remaining unclassified spike waveforms are assigned to the selected clusters with the use of a template matching procedure. For each cluster the centroid (mean waveform) and the variance of the waveforms are calculated. Every unclassified waveform is then assigned to a cluster with the smallest Euclidian distance from cluster's centroid, as long as this distance is smaller than 3 times the cluster's variance. If there are still unclassified waveforms, they are considered as background noise.

3.4.1 Spike sorting implementation on Multiwell-MEA System

The spike sorting analysis was applied on the detected waveforms of each electrode separately. The distance of neighbor electrodes, from center to center, was 300 μ m and consequently, it was not feasible that two nearby electrodes could record an activity derived from the same unit of neurons. The approach of merging the detected activity of two or more electrodes together is applied in tetrodes in vivo where the distance of neighbor electrodes, from center to center, is maximum 40 μ m [60]. Additionally, the spike sorting analysis applied on consecutive recording with a maximum time internal of seven days for a period of two weeks. The efficiency of Wave_clus algorithm has been tested in real and simulated set of data with a sampling frequency of 28 KHz and 30 KHz, respectively. It was decided to select such sampling frequency in order to assurance the efficiency of Wave_clus algorithm. The provided options by Multiwell-MEA system close to 28 KHz and 30 KHz were 20, 25 and 40 KHz. The selected sampling frequency was 25 KHz.

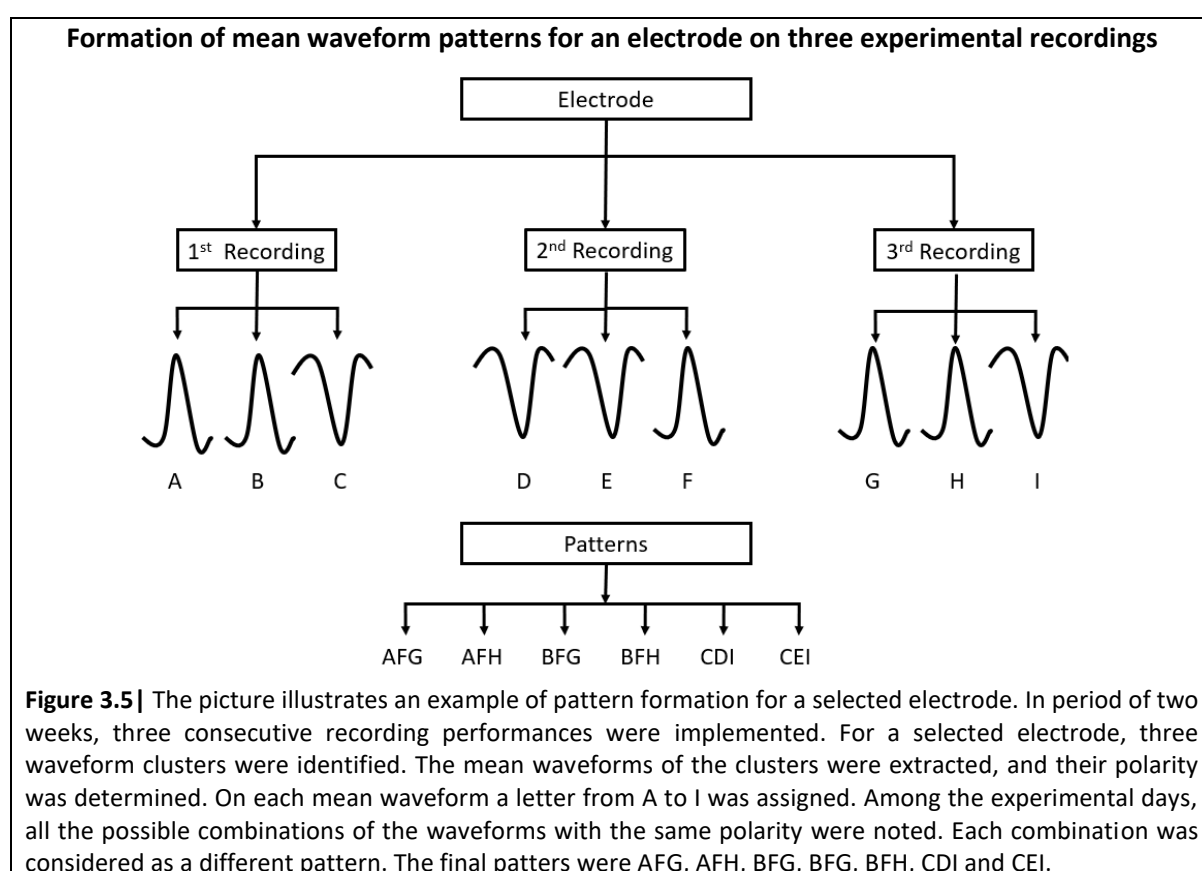
The two weeks period was selected due to uncertainty whether it would be feasible to record the activity of the same unit of neurons for a longer period of time, as neurons migrate or undergo cell lysis. The duration of spike waveforms extracted by the Multiwell-MEA system was 3 ms and each spike waveform was composed by 76 samples. Continuously, the detected spike waveforms for each electrode were aligned to their maximum at data point 26th.

3.4.2 Formation of mean waveform patterns

Following the spike sorting analysis on each electrode per recording performance, the mean waveform (centroids) of each cluster was extracted, which provided a representative shape of the spikes belonging to the cluster. The main goal was to compare the mean waveforms among different recordings in order to investigate whether mean waveforms from different experimental days of the same electrode could present high correlation, which would reveal the possibility these waveforms deriving from the same unit of neurons. As it has been mentioned on Chapter 2.3, spikes with opposite polarities can be detected. Consequently, for each recording day, the mean waveforms with a positive

and negative polarity were identified per electrode. Then, all possible combinations of mean waveforms with the same polarity per electrode were noted among the recordings and consequently, each combination had so many mean waveforms, as the number of recordings. Every different combination constituted a pattern, so, “n” patterns were formed for each electrode. The illustration of pattern formation is depicted in Figure 3.5.

The next step was to estimate the similarity among the waveforms of each pattern and for this purpose, the normalized cross-correlation function of MATLAB was used. The cross-correlation is useful in aligning two time series, one of which is delayed compared to the other. The results of the normalized cross correlation function are coefficients ranging from -1 to 1 and demonstrate the degree of correlation. Value -1 represents a direct negative correlation, 0 represents no correlation, and +1 represents a direct positive correlation. Value 0.9 was considered the threshold so as for a pattern to be accepted as highly correlated and therefore all waveforms of the pattern should exhibit a correlation value greater than 0.9.



3.5 Data and statistical analysis

The extracted data from the Multiwell-MEA system were analyzed with the help of the free available software Multiwell-Analyzer, the MATLAB toolbox McsMatlabDataTools from Multichannel Systems and custom-build MATLAB software. Additionally, the Multichannel Data Manager software by Multi Channel System was used for exporting the recorded data into a compatible format for MATLAB. Every set of data derived from each Multiwell-MEA plate was treated separately, based on the activity that neuronal cultures displayed. However, the main steps of data analysis were the same.

The basic analysis was the estimation of the average number of the active electrodes per well, which gave an indication of the overall activity in the MEA plate. Continuously, the Mean Firing Rate (MFR)

per active electrode was calculated by averaging all the spikes detected by the total number of active electrodes. The MFR was expressed on spikes per minute and provided information about the average activity of neurons per electrode. Additionally, the Cumulative Firing Rate (CFR) was estimated by averaging the total number of spikes detected by the active electrodes per well. In the same way as CFR, the bursting activity was estimated, the total number of detected bursts per well for the whole recording duration. Finally, the mean amplitude of spikes per well was estimated. As previously explained in Chapter 2, the polarity of a spike is either positive or negative appearing with a peak. For this reason, on each well, the mean peak-to-peak amplitude was calculated by averaging all the peak-to-peak amplitude of spikes detected by active electrodes per well. Spikes that detected by non-active electrodes were ignored.

All presented data show mean value \pm Standard Error of Mean (SEM). The unpaired student's t-test or repeated measurements ANOVA were applied where comparison between different data set was needed, under the assumption that the data followed a normal distribution. Asterisks indicate significant values (* $p < 0.05$, ** $p < 0.01$, *** $p < 0.001$).

CHAPTER 4

Experimental Measurements

During the experimental process, two main aspects were studied: the investigation of an optimal NPC density plated on the MEA wells and the comparison of two cultivation media, Neurobasal and BrainPhys mediums. The investigation of an optimal NPC density was not conclusive based on the low activity detected on neural cell cultures derived from different NPC densities ranging 1000 to 5000 cells. On the other hand, BrainPhys appeared as the most suitable cultivation medium for neuronal functionality enhancement, either applied from the first day of plating NPC on MEAs or at a later time, after 30 experimental days of neural cultures existing on MEA plate. Finally, a spike sorting analysis demonstrated the successful observation of spike waveforms derived from the same units of neurons through an experimental period of two weeks.

4.1 Experimental strategy and settings

The strategy of the experimental procedure was to investigate the optimal conditions on MEA plate that would enhance the proliferation and differentiation of NPCs into electrophysiological mature neurons and thus the electrophysiological maturing of a whole neural network. The experimental procedure was separated into two main phases. The aim of the first phase was the investigation of an optimal NPC density plated on the MEAs which would potentially promote the homogenous expansion of NPCs around the electrodes and would enhance the detected activity by the electrodes. Neurobasal medium was used as a cultivation medium. In the second phase, Neurobasal and BrainPhys media were applied on different neural cultures in order to assess which one offered a better cell culturing condition for neural differentiation and maturation and consequently, enhanced the neuronal activity. Additionally, the spike sorting algorithm Wave_clus was applied on a specific neural cell culture in order to assess the detected spike waveforms over a specific experimental period of two weeks. In total, four Multiwell-MEA plates were used for the experimental procedure. The first experimental day for the neural cultures was considered the day of the NPC plating on the Multiwell-MEA plate.

The whole system was turned on half hour before the recording performances for the temperature to be stabilized in the recording chamber. The setting values for MEA recording are summarized in Table 4.1. The Multiwell-MEA plate was placed in the recording chamber and the recording performance started after 10 minutes for the neural cultures to get used to the new environment. The recording performances lasted for 10 minutes. After finishing the recording procedure, the plate was returned to the incubator. Each measurement resulted in 7.5GB of recorded data from 288 channels recording simultaneously for 10 minutes. Finally, an electrode was considered active when it had detected at least 6 spikes per minute. Additionally, a well was considered as active, when at least 6 active electrodes were observed in this well.

Table 4.1 | Settings of the Multiwell-MEA system

Settings	Parameters	Values
Data Source	Sampling Frequency	10.000 Hz
Filtering	High-Pass Filter	100 Hz
	Low-Pass Filter	3500 Hz
Burst Detector	Maximum interspike interval at the start of a burst	50 ms
	Maximum interspike interval in a burst	100 ms
	Minimum burst duration	50 ms
	Minimum interval between two bursts	100 ms
	Minimum number of spikes in a burst	4
Network Burst Detector	Minimum number of simultaneous electrodes	3
	Minimum number of electrodes participating	6

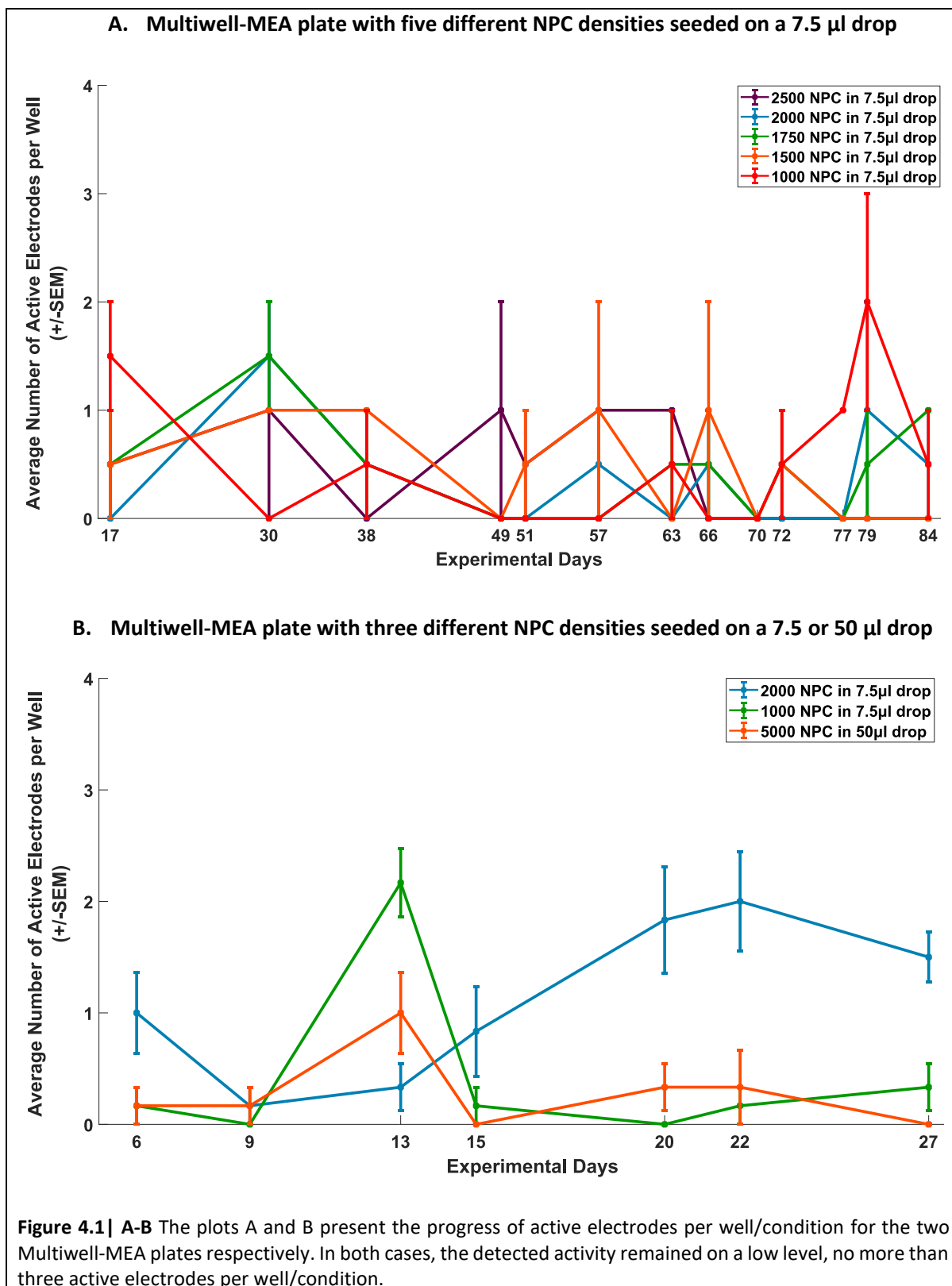
4.2 Evaluation of different NPC densities on Multiwell-MEA plate

During the first part of the experimental procedure, different NPC densities, ranging from 1000 to 5000 NPCs, were selected to be seeded in two Multiwell-MEA plates (Table 4.2). In the first experimental trial, five different cell densities (2500,2000,1750,1500 and 1000) of NPCs were seeded on the Multiwell-MEA plate suspended in a drop of 7.5 μ l. Each condition contained two wells with the same number of NPCs. In the second experimental trial, only three NPC densities were selected for the MEA plate, 1000 and 2000 cells in a drop of 7.5 μ l while 5000 cells in a drop of 50 μ l. The number of wells per condition was 6. In both Multiwell-MEA plates, the substrate of the wells was coated with laminin. The configuration of NPC densities on the two Multiwell-MEA plates is illustrated in Appendix A.

Table 4.2 | Multiwell-MEA plates with different NPC densities

First Experimental Trial (Multiwell-MEA plate A)				
Conditions	NPC Density	Drop	Coating	Wells
1	2500 cells/well	7.5 μ l	Laminin	2
2	2000 cells/well	7.5 μ l	Laminin	2
3	1750 cells/well	7.5 μ l	Laminin	2
4	1500 cells/well	7.5 μ l	Laminin	2
5	1000 cells/well	7.5 μ l	Laminin	2
Second Experimental Trial (Multiwell-MEA plate B)				
Conditions	NPC Density	Drop	Coating	Wells
1	1000 cells/well	7.5 μ l	Laminin	6
2	2000 cells/well	7.5 μ l	Laminin	6
3	5000 cells/well	50 μ l	Laminin	6

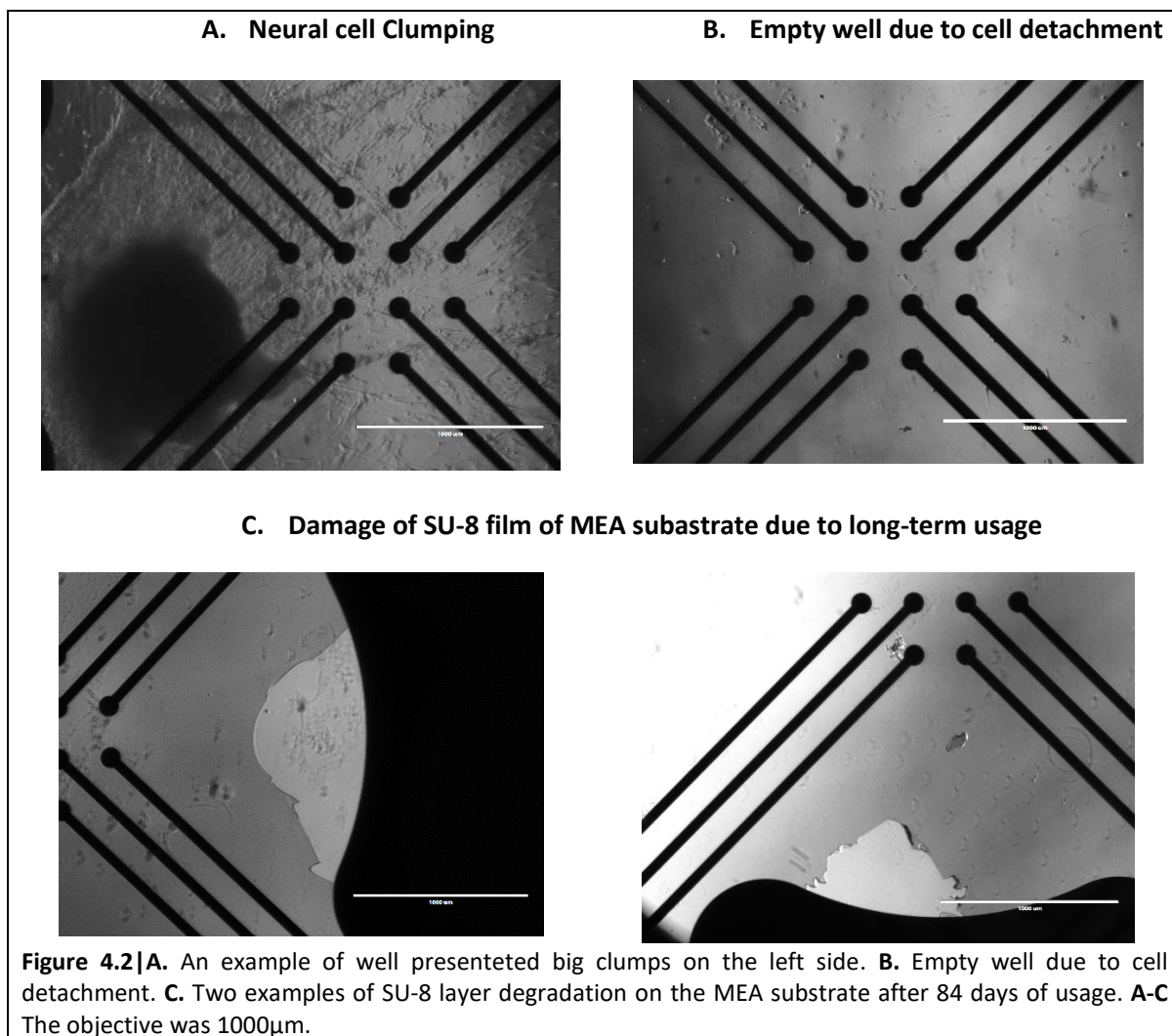
In both experimental trials, the neuronal activity presented significant low, not overpassing the 3 active electrode per well/condition. It was obvious that the different NPC densities did not aid to increase the detected activity by the electrodes. As shown in figure 4.1 A, all the conditions of Multiwell-MEA plate with five NPC densities presented an extremely low number of active electrodes per well, and none overpassed the two active electrodes per well. Remarkable was the fact that on experimental day 70, there was no active electrode in the whole plate. The same detected activity was presented by the Multiwell-MEA plate with the three NPC density conditions for the first 27 experimental days.



Overall, in both plates, the Mean Firing Rate (MFR) fluctuated between 8 to 30 spikes per minute/electrode and it was low compared to other studies [55], [56] (Appendix A). Moreover, due to low neuronal firing rate, bursting activity was absent.

Considering the morphology of the neural cultures, in both plates, neurons aggregated together and created relatively big clumps. The last experimental days of the Multiwell-MEA plate with five different

NPC densities, the cell clumping had deteriorated as several neural cultures demonstrated huge dark clumps and they had migrated far away from the center of the electrodes. Moreover, in the same plate, it was observed the detachment of some of the neural cultures and lost during the refreshing process of medium (Figure 4.2 A, B). Another important observation was the delamination of the SU-8 insulator film of the MEA substrate. This might be a matter related to the long-term usage of the plate (84 experimental days) or due to the use of pipettes in order to refresh the cultivation medium (Figure 4.2 C).



4.3 Evaluation of BrainPhys and Neurobasal medium on neural cultures

In the second phase of the experimental procedure, it was investigated whether BrainPhys could enhance the electrophysiological maturity of neurons, compared to the Neurobasal Medium and this was based in three concepts: the effect of its later insertion in neural cultures growing on Neurobasal medium; the effect of Neurobasal and BrainPhys medium when both applied from the beginning of NPCs seeded on MEA plate; the functional development of neural culture when only BrainPhys is applied.

- Assessment of later insertion of BrainPhys medium on neural cultures

The Multiwell-MEA plate with the three different NPC densities (1000, 2000 and 5000) from the previous experiment was used in order to evaluate the later usage of BrainPhys medium on neural cultures already growing in Neurobasal medium. As depicted in Table 4.3, on each condition, four wells remained with Neurobasal medium while BrainPhys medium was applied on one well of each condition. In Appendix B, the configuration of the MEA plate after the insertion of BrainPhys medium is illustrated. The change of cultivation medium from Neurobasal to BrainPhys medium was implemented after the recording performance of the experimental day 27. The next recording was performed three days after cultivation medium change, on the experimental day 30, and other eight were followed.

Table 4.3 | Multiwell-MEA plate with different cultivation media and NPC densities

Neurobasal Medium				
Conditions	NPC Density	Drop	Coating	Wells
1	1000 cells/well	7.5µl	Laminin	4
2	2000 cells/well	7.5µl	Laminin	4
3	5000 cells/well	7.5µl	Laminin	4
BrainPhys Medium				
Conditions	NPC Density	Drop	Coating	Wells
1	1000 cells/well	7.5µl	Laminin	1
2	2000 cells/well	7.5µl	Laminin	1
3	5000 cells/well	50µl	Laminin	1

After changing the cultivation medium, there was an obvious difference on the neuronal activity between wells with BrainPhys and Neurobasal medium. During the recording performances, the activity of the cultures with Neurobasal Medium stayed on the same low level, no more than 2 active electrodes per well and per condition, while cultures with the BrainPhys, presented a fluctuation on their activity and all the wells reached the pick of 8 active electrodes on different recording days (Appendix B). The most outstanding result derived from the assessment of the MFR of all active electrodes on the wells with Neurobasal Medium and BrainPhys respectively, for each recording performance. As the plot in Figure 4.3 shows, the MFR of active electrodes in BrainPhys medium remained significantly higher compared to the MFR of active electrodes in Neurobasal medium. The highest difference appeared on the last recording day, where the electrodes in BrainPhys medium exhibited a MFR of 110 spikes/minute, while the electrodes in Neurobasal medium had an activity of less than 20 spikes/minute.

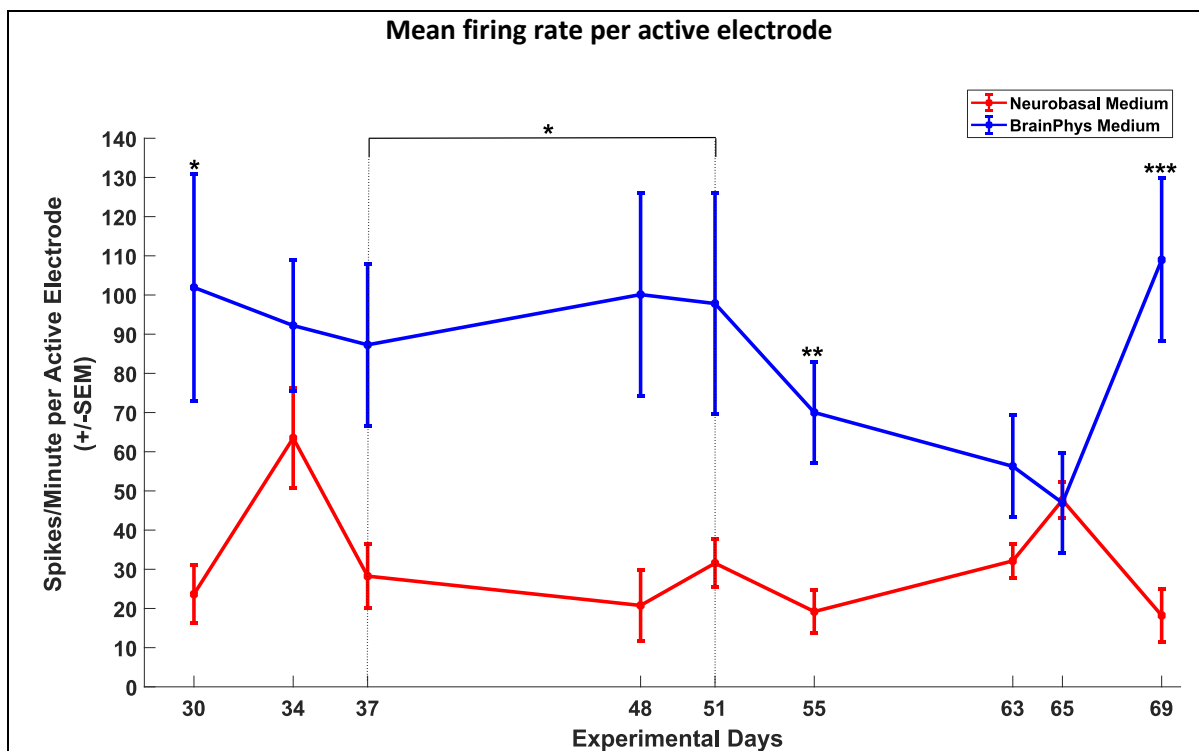


Figure 4.3 | The red and blue lines display the MFR per active electrode for each of the two cultivation media, for every experimental day where a recording was performed. By ignoring the different cell densities existing in the wells, the MFR per active electrode in Neurobasal medium was calculated by averaging the firing rates of all active electrodes in the twelve wells, while the MFR per active electrode in BrainPhys medium was calculated by averaging the firing rates of all active electrodes in the three wells. Asterisks indicate the significant value of the unpaired Student's t-test between the MFRs of Neurobasal and BrainPhys Medium (* $p < 0.05$, ** $p < 0.01$ and *** $p < 0.001$).

In the wells where the medium was changed from Neurobasal to BrainPhys, a bursting activity appeared sporadically, without being significant, so deeper investigation was not necessary. Multiwell-MEA plate was terminated on experimental day 69 as all neural cell cultures had gradually started to present big clumps. As an overall conclusion, the BrainPhys medium, when applied at a later stage, indeed achieved to enhance the electrophysiological functionality on neurons.

➤ Assessment of BrainPhys and Neurobasal medium application

The main goal of this experimental concept was the evaluation of the functionality of neurons growing on BrainPhys or Neurobasal medium from the beginning until the end of the experimental period. In parallel with this, it was tested whether a different coating, matrigel, or AZT on the neural cultures can also positively contribute to the electrophysiological maturity of neurons. The idea behind the usage of two different coatings (laminin and matrigel) was the investigation of which coating could offer a better cell culture substratum and reduce the big clumps of cells that might impede the recording, while AZT application aimed to increase the number of differentiated neurons and therefore, the recorded activity. Additionally, AZT might prevent the aggregation of cells which create cell clumps and consequently, cells remain homogenous spread on the culturing substrate.

As depicted in Table 4.4, the Multiwell-MEA plate was divided into two groups: Neurobasal and BrainPhys medium and subdividing in laminin and matrigel coating conditions and +/-AZT, resulting in eight different conditions in three wells each. On each well, 2000 NPCs were seeded in a drop of 10 μ l. In Appendix B, the configuration of different conditions applied on the wells of the MEA plate is illustrated. The Multiwell-MEA plate was kept for sixty-five experimental days in the incubator. MEA

recordings were performed two or three times per week. The first recording was performed on day 7 of the experiment and the last on day 65. The total number of MEA recordings was twenty.

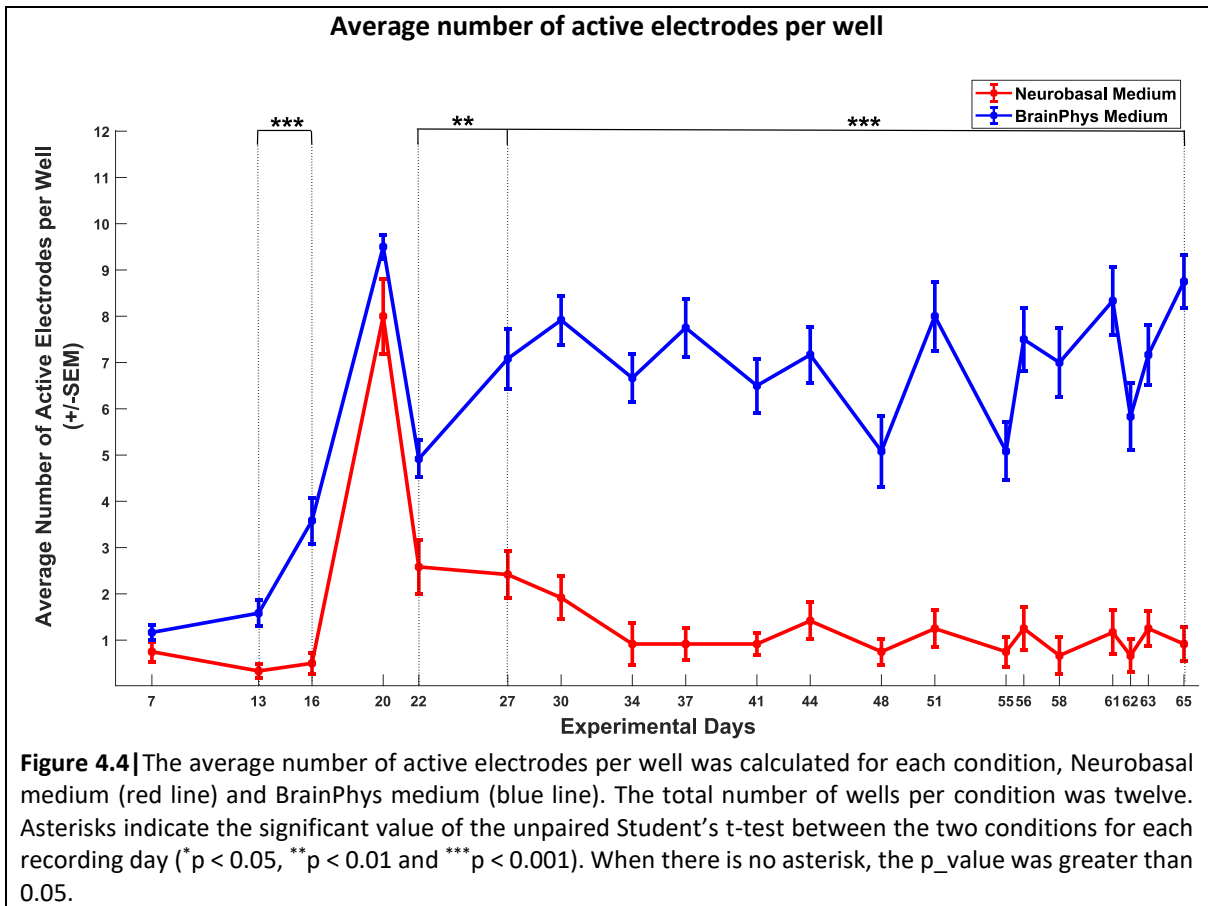
Table 4.4| Multiwell MEA plate exhibiting eight different condition

Conditions	Neurobasal Medium				BrainPhys Medium				
	Laminin	Matrigel	AZT	Wells	Laminin	Matrigel	AZT	Wells	
1	✓			3					
2		✓		3					
3	✓		✓	3					
4		✓	✓	3					
5						✓			3
6							✓		3
7						✓		✓	3
8							✓	✓	3
Total Wells	12				12				

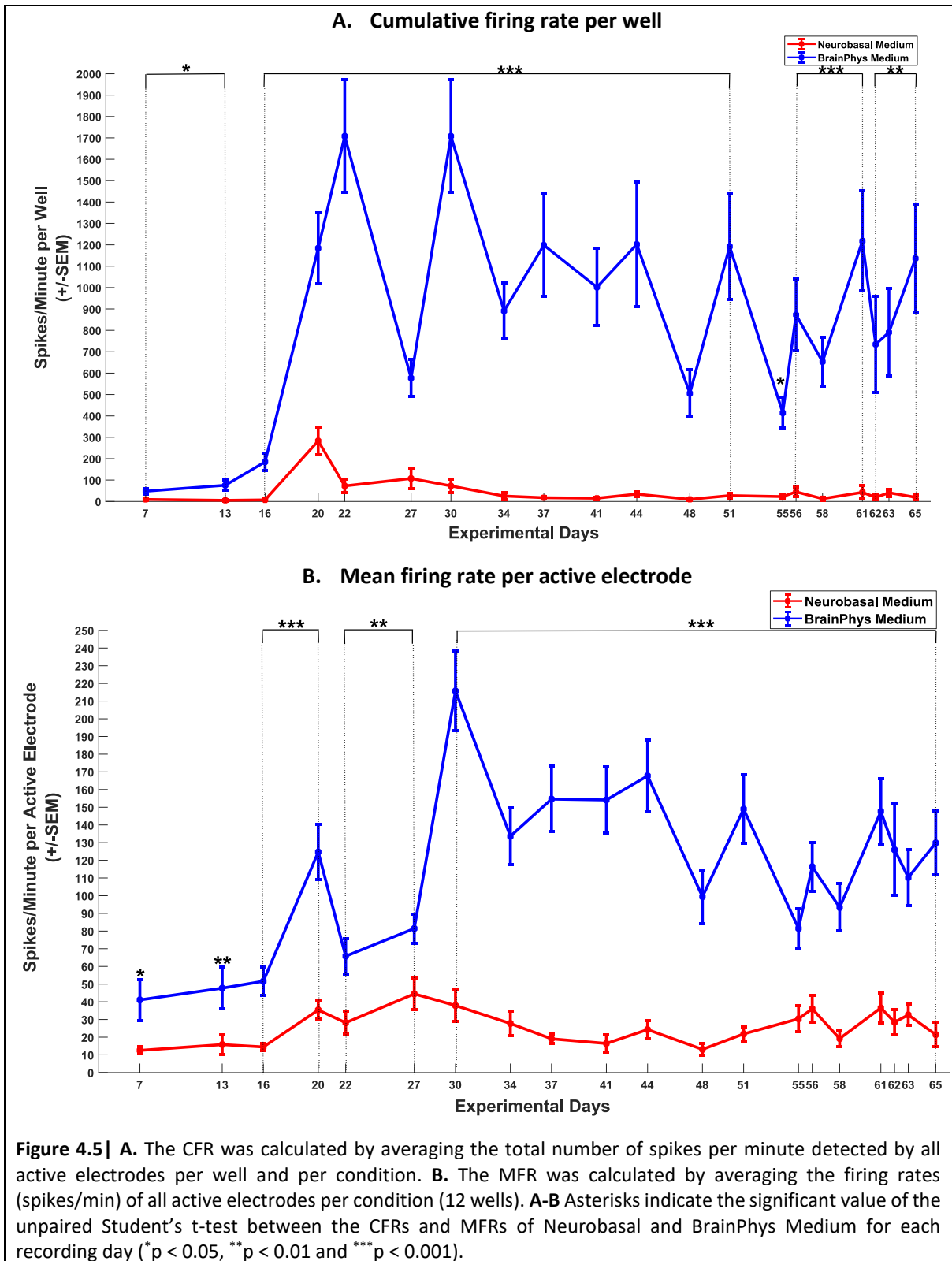
Due to the fact that several conditions overlapping among different wells on the Multiwell-MEA plate, the analysis was separated into two steps, principal analysis and secondary Analysis (Appendix B). The main target of the principal analysis was to compare the functionality of neurons in the wells with Neurobasal medium, against the neurons in the wells with BrainPhys medium, over time, by ignoring the different coating or the existence of AZT into these wells. In the secondary analysis, it was investigated whether neuronal activity on the wells with the same differentiation medium presented a significant difference between the coatings, laminin and matrigel, or whether the existence of AZT promoted higher or less neuronal excitation.

The principal analysis verified the null hypothesis, that BrainPhys medium provided a better cell environment for neurons and thus, promoted the functional maturity of neurons. The neurons in the wells with BrainPhys medium presented a dramatically higher activity compared to neurons in Neurobasal medium. On the other hand, the secondary analysis did not provide a clear answer whether one of the two coatings or AZT could enhance the electrophysiological activity of neurons. For this reason, only the plots from principal analysis are presented and discussed, while plots of second analysis can be found in Appendix B.

As shown in Figure 4.4, the average number of active electrodes per well for BrainPhys medium was three times higher in almost all MEA recordings expect from the days 7 and 20. In general, BrainPhys medium trend showed an increase from starting day, reaching a peak of 10 active electrodes on day 20. Then, the number of active electrodes fluctuated around 7 per well. On the other hand, Neurobasal medium remained in a low number of active electrodes, 1 or 2 active electrodes per well, except from day 20 when a peak of 8 active electrodes was observed. Most probably, this unexpected increase was an artifact.



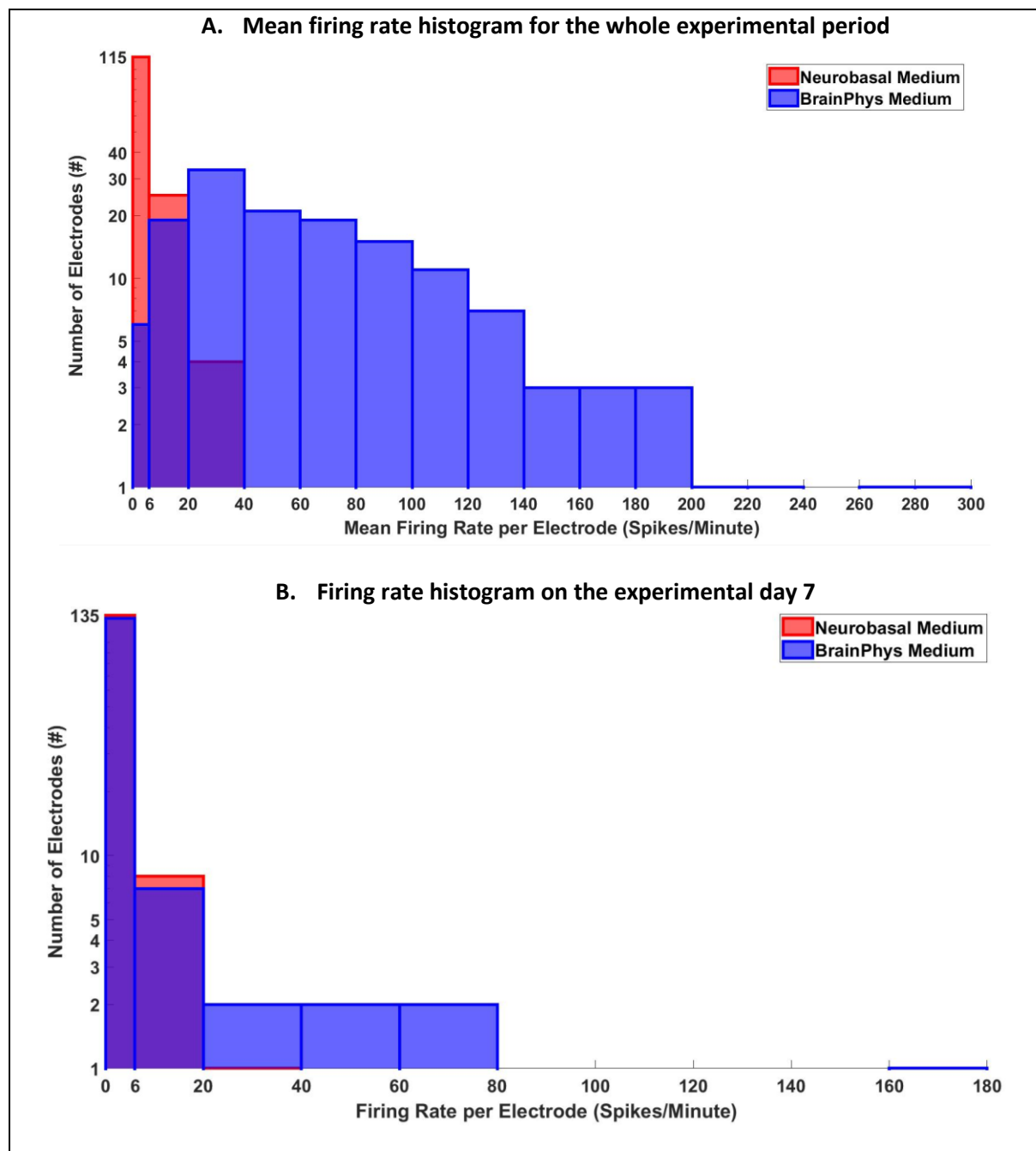
Both the CFR and MFR appeared twenty times higher in the wells with BrainPhys medium compared to the wells with Neurobasal medium during the whole recording period from the first recording day 7 until the last day 65 (Figure 4.5). During the experimental period, CFR values of BrainPhys was fluctuating at around 1000 spikes per min per well, presenting twice a peak of 1700 spikes/min/well. On the other hand, Neurobasal medium presented a low CFR, being during most experimental days, less than 100 spikes/min/well. On the same pattern, MFR followed a similar trend, for BrainPhys fluctuating around 140 spikes/min/active electrode, while for Neurobasal the activity was around 20-30 spikes/min/active electrode.

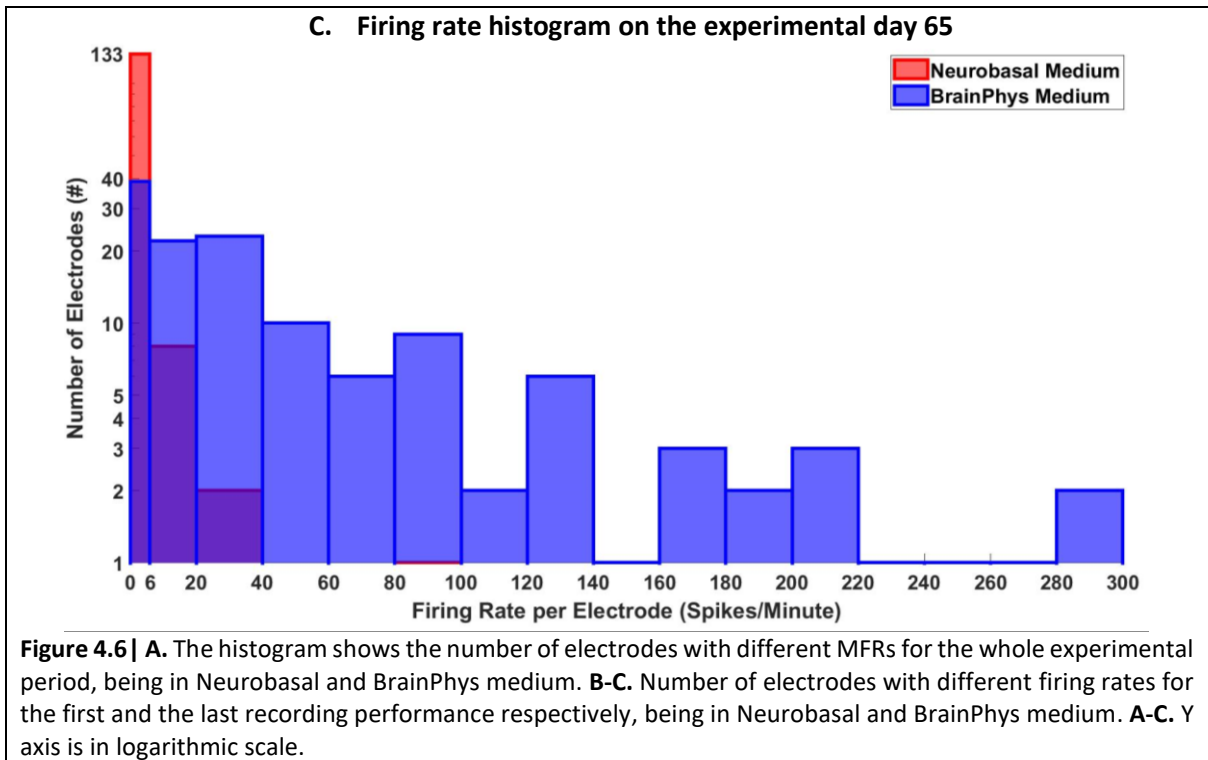


The CFR per well and the MFR per electrode were calculated based on the detection of active electrodes per recording day. Inactive electrodes had also detected little activity, less than 6 spikes/minute, not enough though to overpass the threshold. Additionally, it was observed that electrodes which were active in one recording day, were inactive in the following recording day. In order to assess which was the overall performance of the electrodes in Neurobasal and BrainPhys medium, the MFR of each electrode during the whole experimental period was calculated irrespective

of being active or not (Figure 4.6 A). The total number of electrodes for each medium was 144 (12 electrodes per well, 12 wells per condition). Furthermore, the firing rates of electrodes for the experimental days 7 and 65 were calculated for each cultivation medium (Figure 4.6 B, C).

As illustrated in the histogram of Figure 4.6 A, the majority of electrodes in BrainPhys (138 electrodes), presented a MFR higher than 6 spikes/minute and consequently, remained active during the whole experimental period. On the other hand, 115 electrodes, out of the 144 total number of electrodes existed in Neurobasal medium, remained inactive as they presented a MFR less than 6 spikes/minute. During the first recording performance, electrodes on both media showed a similar firing rate, which is normal, as it was the beginning of the long-term culture period. However, during the last recording performance, 105 electrodes in BrainPhys were active, an indication that BrainPhys enhanced the neuronal activity, while the electrodes in Neurobasal medium presented the same level of detected activity compared to the first recording performance.





The calculation of active electrodes per well and the CFR, MFR provided robust information about the functionality of neurons on these two cultivation media, Neurobasal and BrainPhys. Another important factor needed to be examined was how strong the detected signals were, in other words what was the amplitude of spikes. For each condition the mean peak-to-peak amplitude per well was determined. The interesting information provided after this estimation was that mean amplitude per well did not seem to differ significantly on these two cultivation media. As shown in Figure 4.7, in most recording performances, the mean amplitude per well for each condition appeared to be on the same level. The only difference on spike amplitude between Neurobasal and BrainPhys was observed during the consecutive recordings 34, 37, 41 and 44. On those days, the mean amplitude of spikes per well in BrainPhys ranged on 40 μ V while the mean amplitude of spikes per well in Neurobasal medium appeared lower on 20 μ V to 25 μ V.

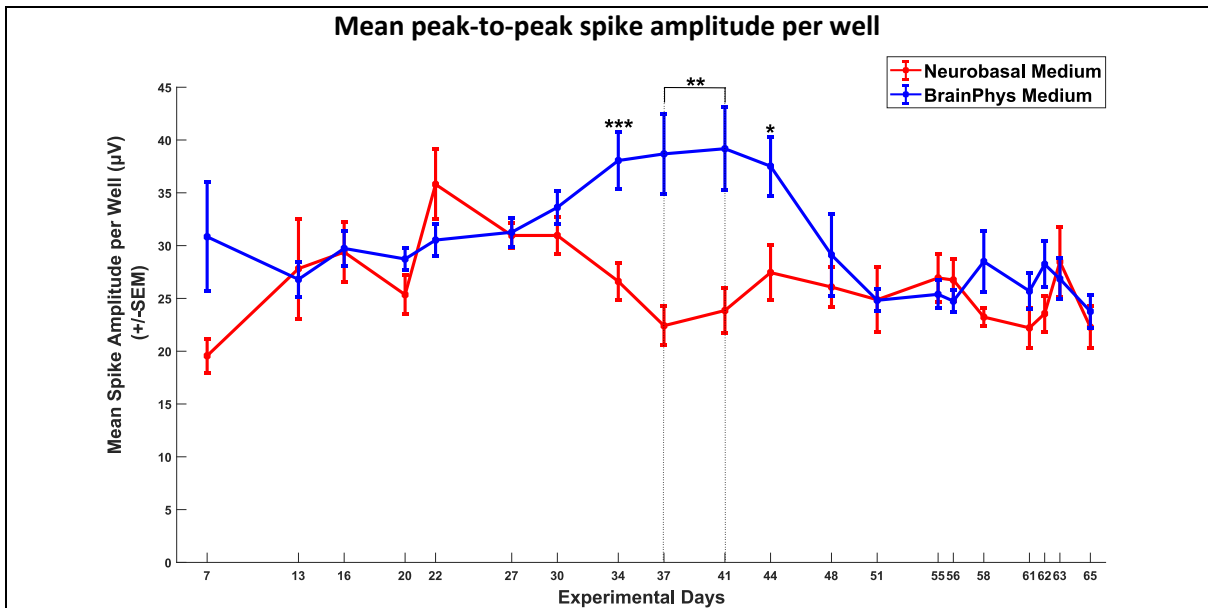


Figure 4.7 | For each recording day, the mean peak-to-peak amplitude of the detected spikes by active electrodes per well was estimated and continuously, mean amplitude per well for each condition was estimated. Asterisks indicate the significant value of the unpaired Student's t-test between the mean amplitude per well of Neurobasal and BrainPhys Medium for each recording day (* $p < 0.05$, ** $p < 0.01$ and *** $p < 0.001$). When there is no asterisk, the p_{value} was greater than 0.05

In order to evaluate the connectivity of neurons on the two cultivation media, the bursting activity per well and per condition was assessed. Figure 4.8 displays the average number of detected bursts per well for each condition, for the whole recording period (10 minutes recording) on each experimental day. The neural cultures in the wells with BrainPhys medium presented a high bursting activity during all the experimental period, reaching a peak of 800 bursts per well for 10 minutes recording. On the other hand, the bursting activity in the wells with Neurobasal medium was dramatically low, no more than 60 bursts per well, and intermittent between consecutive recording performances.

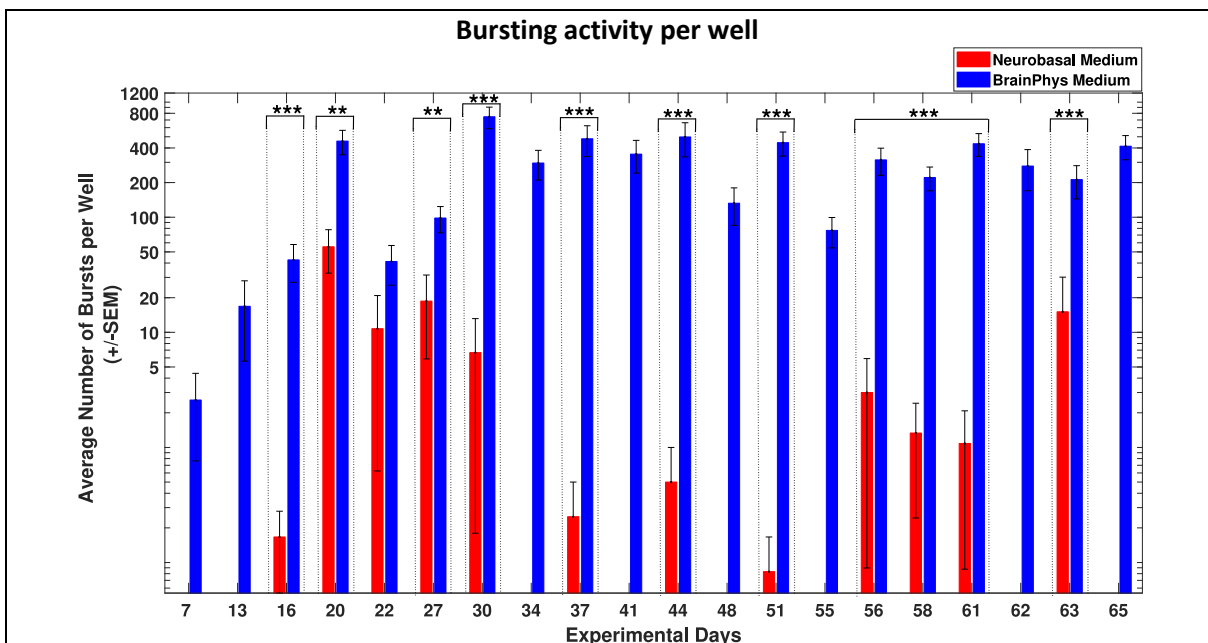
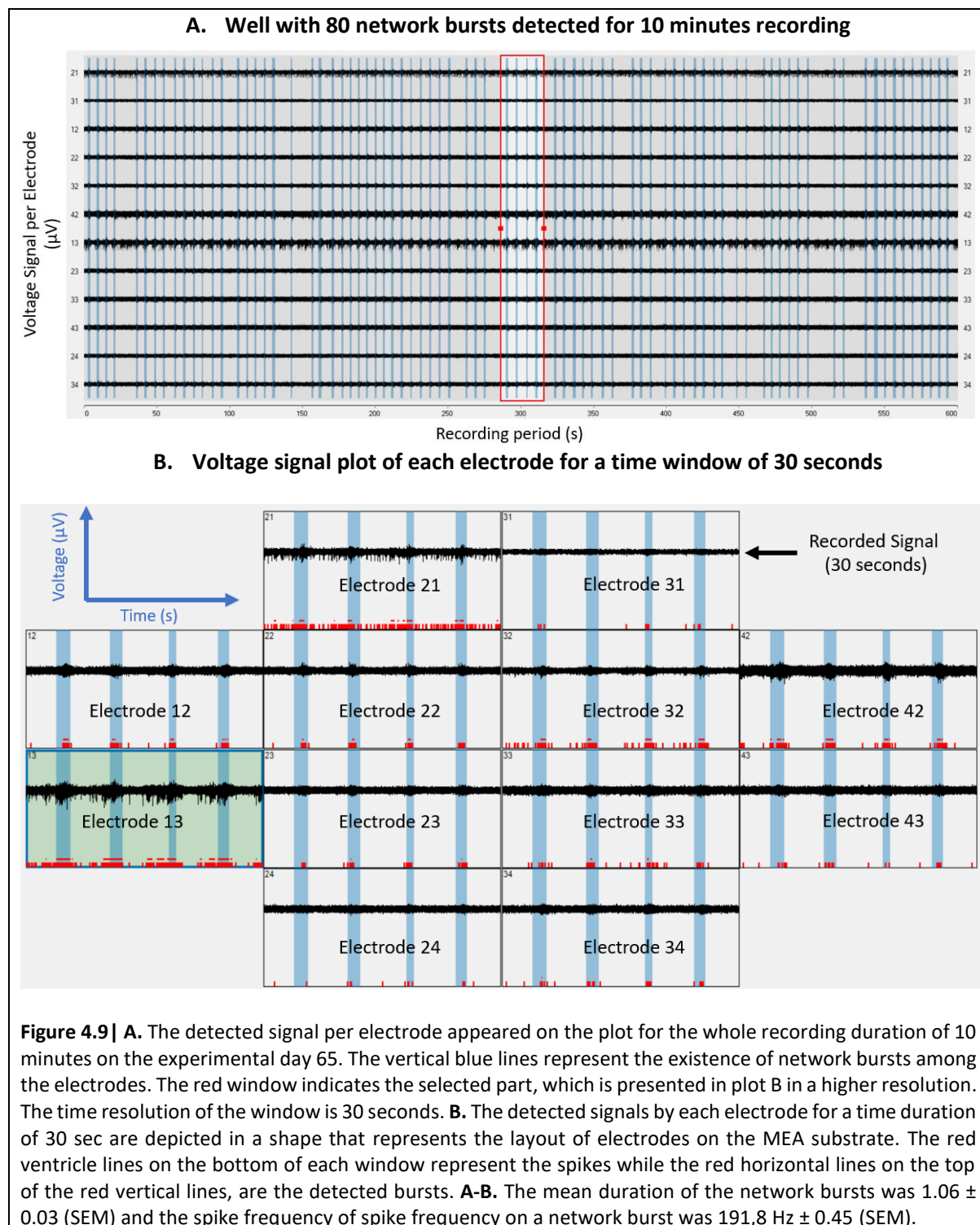
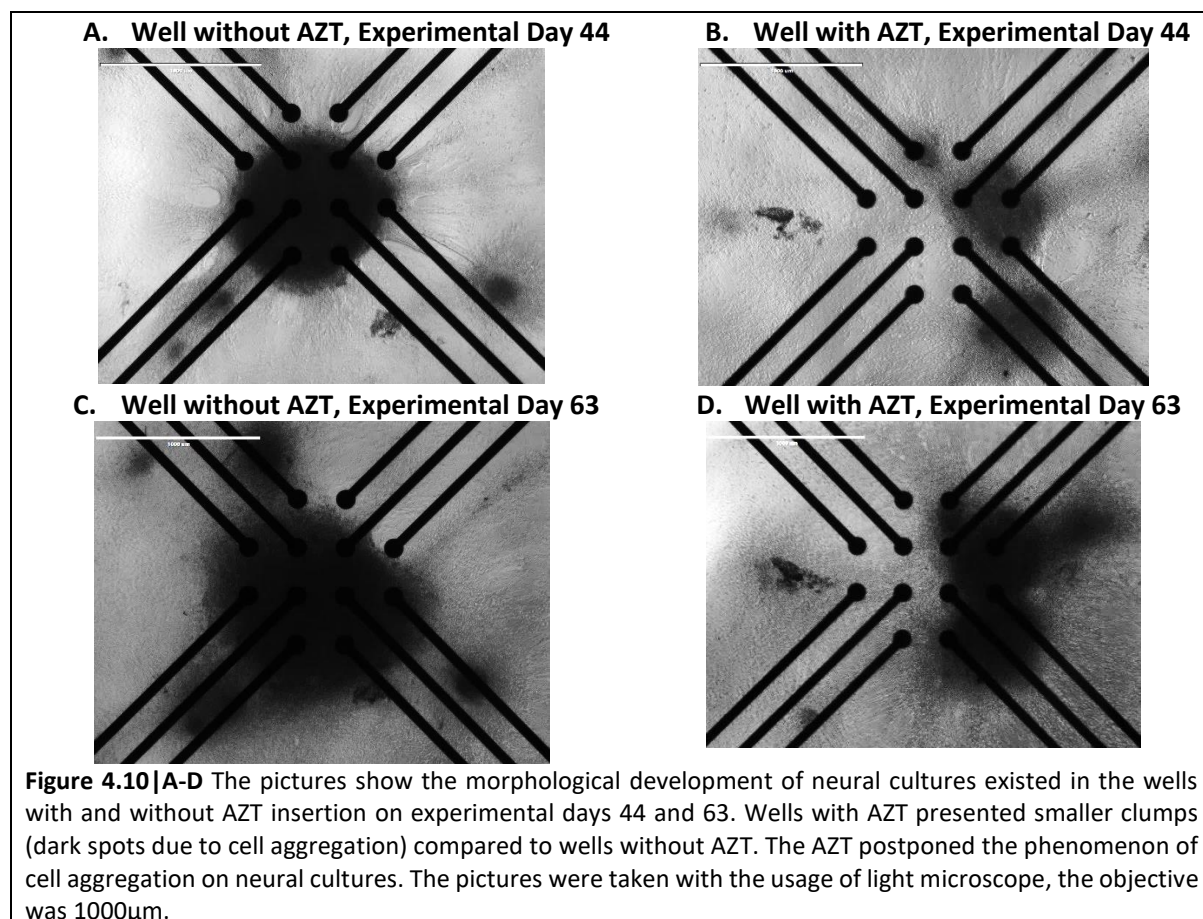


Figure 4.8 | For each recording day, the number of bursts detected on the wells with the same cultivation medium for the whole recording performance (10 minutes) was averaged per well. Y axis is in logarithmic scale. Asterisks indicate the significant value of the unpaired Student's t-test between the two conditions for each recording day (* $p < 0.05$, ** $p < 0.01$ and *** $p < 0.001$).

The synchronicity on neuronal cultures was evaluated by the presence of network bursting activity which was detected only on the wells with BrainPhys medium. The network bursting activity appeared sporadically among the wells with BrainPhys medium and not in a constant way during the experimental period (Appendix B). The highest number of network bursts that had ever detected in a single recording performance per well, 80 network burst for 10 minutes recording, appeared on a well with BrainPhys Medium, matrigel as a coating and without the deposition of AZT on the experimental day 65 (Figure 4.9). Additionally, experimental day 61 was characterized as a recording day with most wells presenting network bursting activity (7 wells out of 12 with BrainPhys medium).



During the whole experimental period, the morphological development of neural cell cultures existed in Neurobasal or BrainPhys medium was observed on a weekly basis. The cell clumping remained as a general characteristic in all the neural cultures either in Neurobasal or in BrainPhys medium. Especially, neural cultures in Neurobasal medium presented after the first 20 days, relatively big cell aggregations on the MEA substrate. However, the wells with BrainPhys and AZT appeared an intensive cell clumping on a later time compared to neurons on wells without AZT on the same medium. An example of these morphological observations is illustrated in Figure 4.10 A and B. At the last ten days of the experimental period, all the neural cultures, even those existed in the wells with BrainPhys and AZT formed clumps (Figure 4.10 C and D).

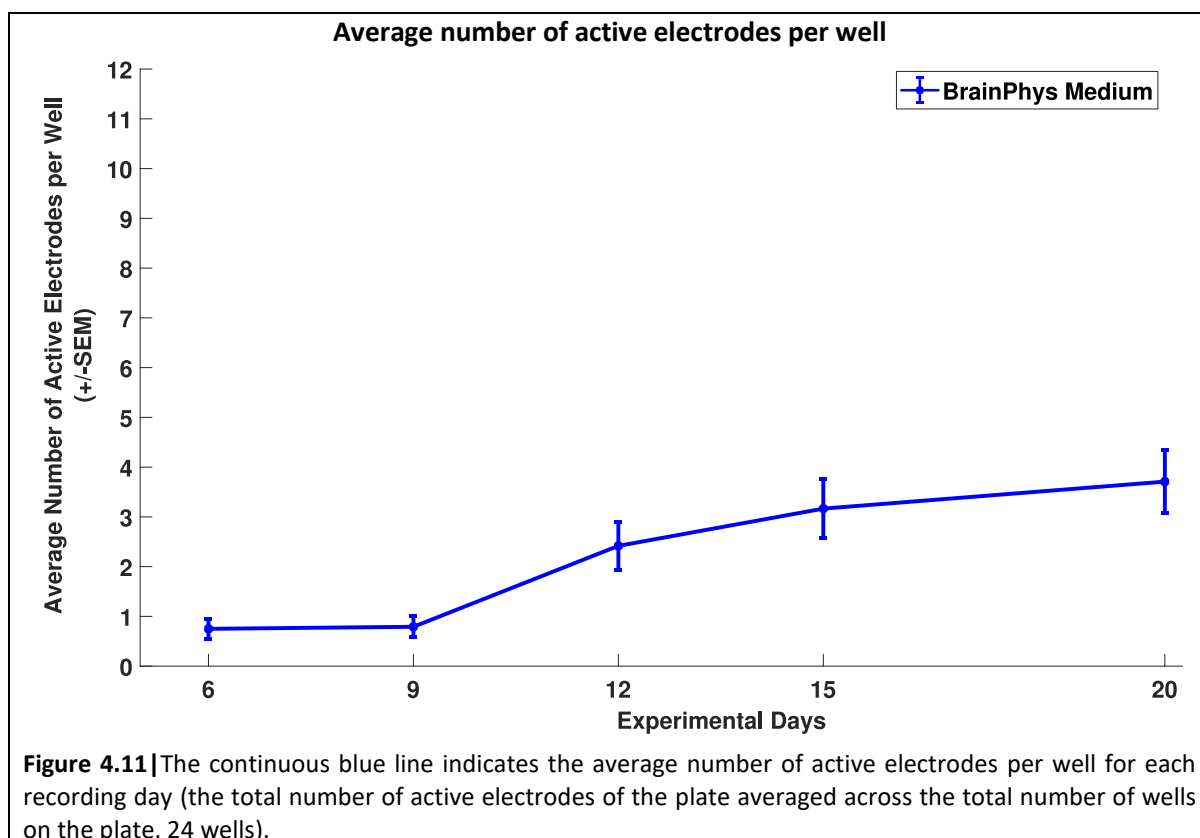


➤ Assessment of neural culture development progress with BrainPhys medium

The last part of the second phase of the experimental procedure was the validation of BrainPhys medium efficiency. For that, it was decided to apply BrainPhys at the whole Multiwell MEA plate, containing 24 wells (and 24 cultures), and observe the functional maturity of the neural cultures. Additionally, it was observed whether a later use of AZT, applied on half of the plate's cell cultures, would enhance the differentiation of NPCs into neurons and therefore, the detected activity. On each well, 2000 NPCs were seeded in a drop of 10 μ l and matrigel was selected as a cell culture substratum. The MEA plate was kept for 54 experimental days and the AZT insertion started after the recording performance of the experimental day 20. The Multiwell-MEA plate configuration is depicted in Appendix B.

During the first five recording performances, before AZT insertion, the average number of active electrodes per well increased gradually from 1 active electrode to 3 active electrodes per well on the

last recording day (Figure 4.11). During this experimental period, it was observed a big variation among the active electrodes per well. The big variation on detected activity among wells might derive from the fact that the NPC plating on almost half of the wells did not succeed on seeding the cells on the middle, where the electrodes reside.



After insertion of AZT on half of the MEA plate, the average number of active electrodes per well as well as CFR and MFR were calculated for the wells with and without AZT. As depicted in Figure 4.12, both conditions presented a similar activity, while in all three diagrams, the wells with AZT presented a slightly lower activity compared to the wells without AZT, although this difference is not statistically important. For instance, during day 42, while the average number of active electrodes per well without AZT appears to be significantly higher than wells with AZT, the CFR and MFR are not significantly different between these two conditions. Generally, the later insertion of AZT does not enhance the functionality of neurons.

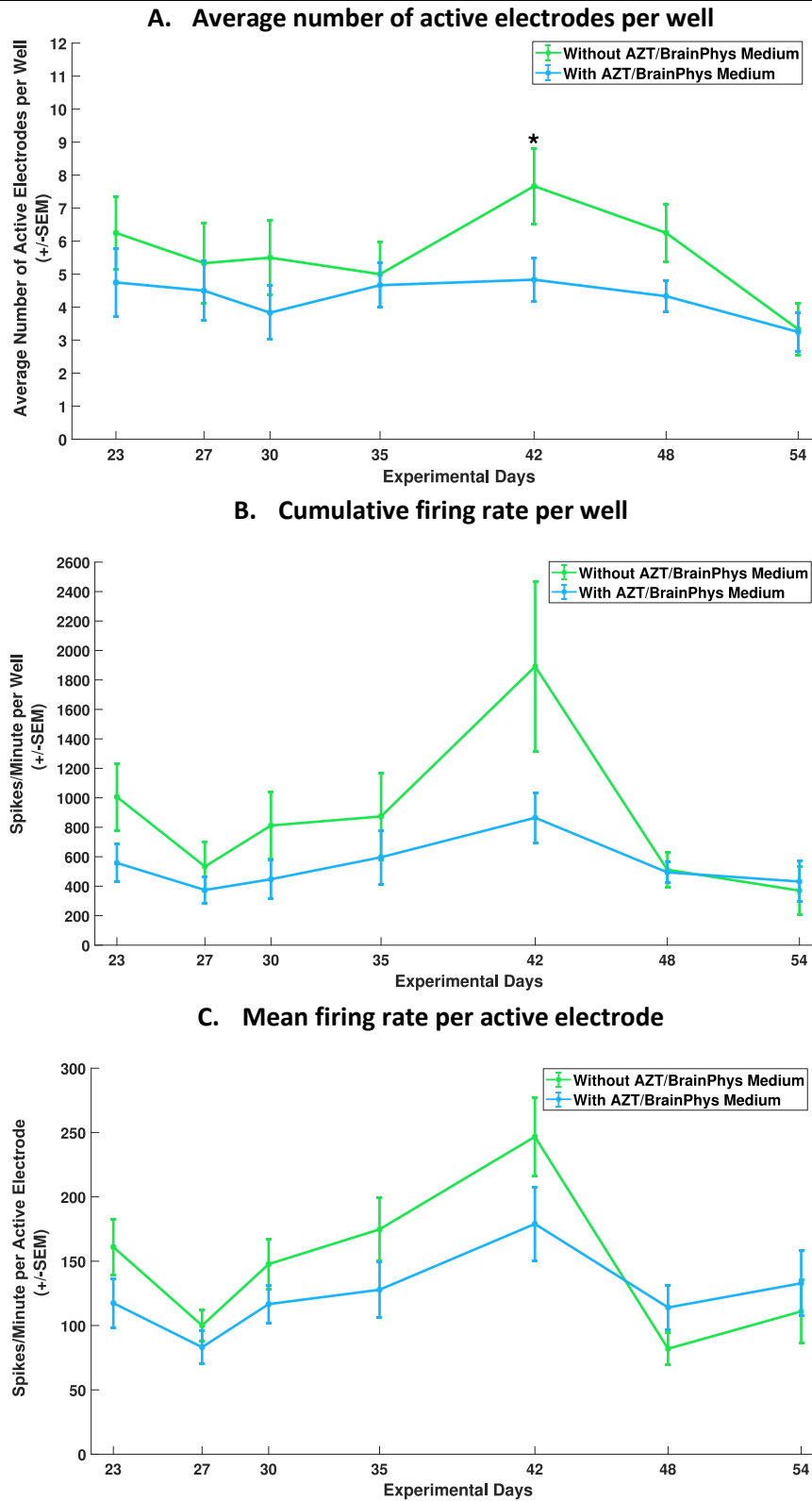


Figure 4.12 | **A.** The average number of active electrodes per well was estimated for the 12 wells without AZT and the 12 wells with AZT. **B.** The CFR per condition was calculated by averaging the number of all spikes detected by active electrodes in all the wells of the condition across the number of the wells. **C.** The MFR per condition was calculated by averaging the number of firing rates of active electrodes on the wells of the condition, across the number of active electrodes. **A-C** Asterisks indicate the value of the unpaired Student's t-test between the two conditions for each recording day (* $p < 0.05$). When there is no asterisk the p_{value} was greater than 0.05.

The neural cultures of the two conditions, except for the similar activity, appeared almost the same peak-to-peak amplitude, a degree of similarity of 95% (Figure 4.13). Both conditions displayed a mean amplitude range between 25 μ V to 30 μ V.

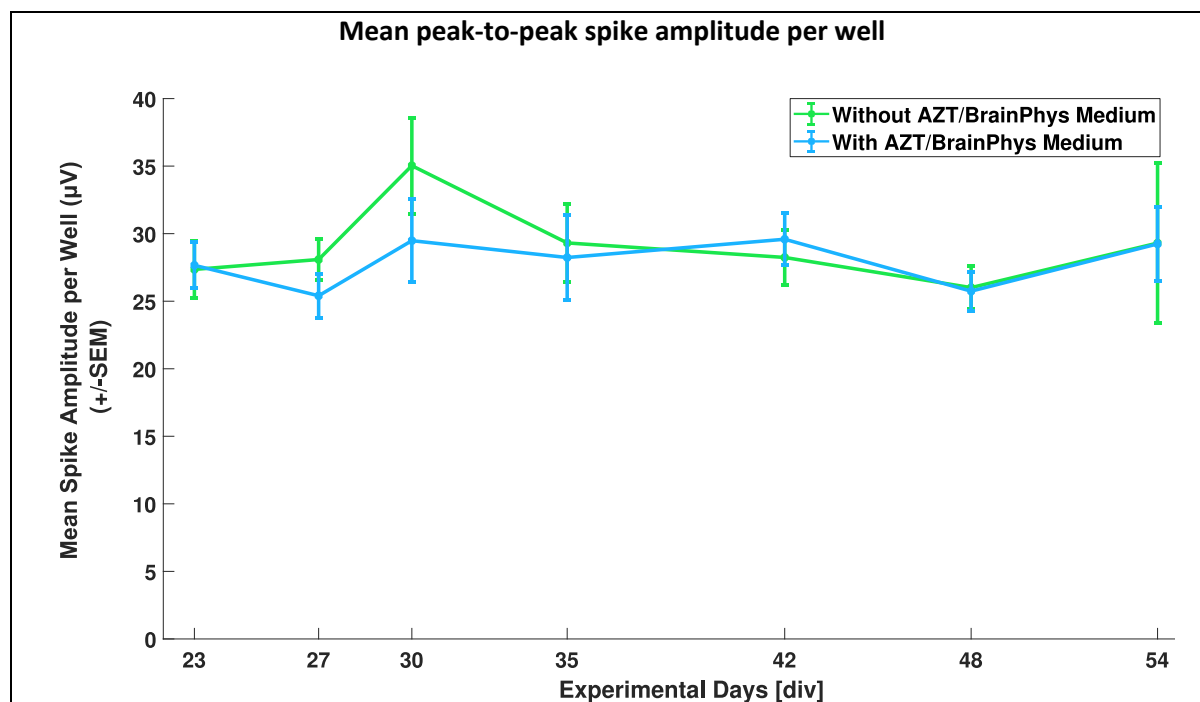
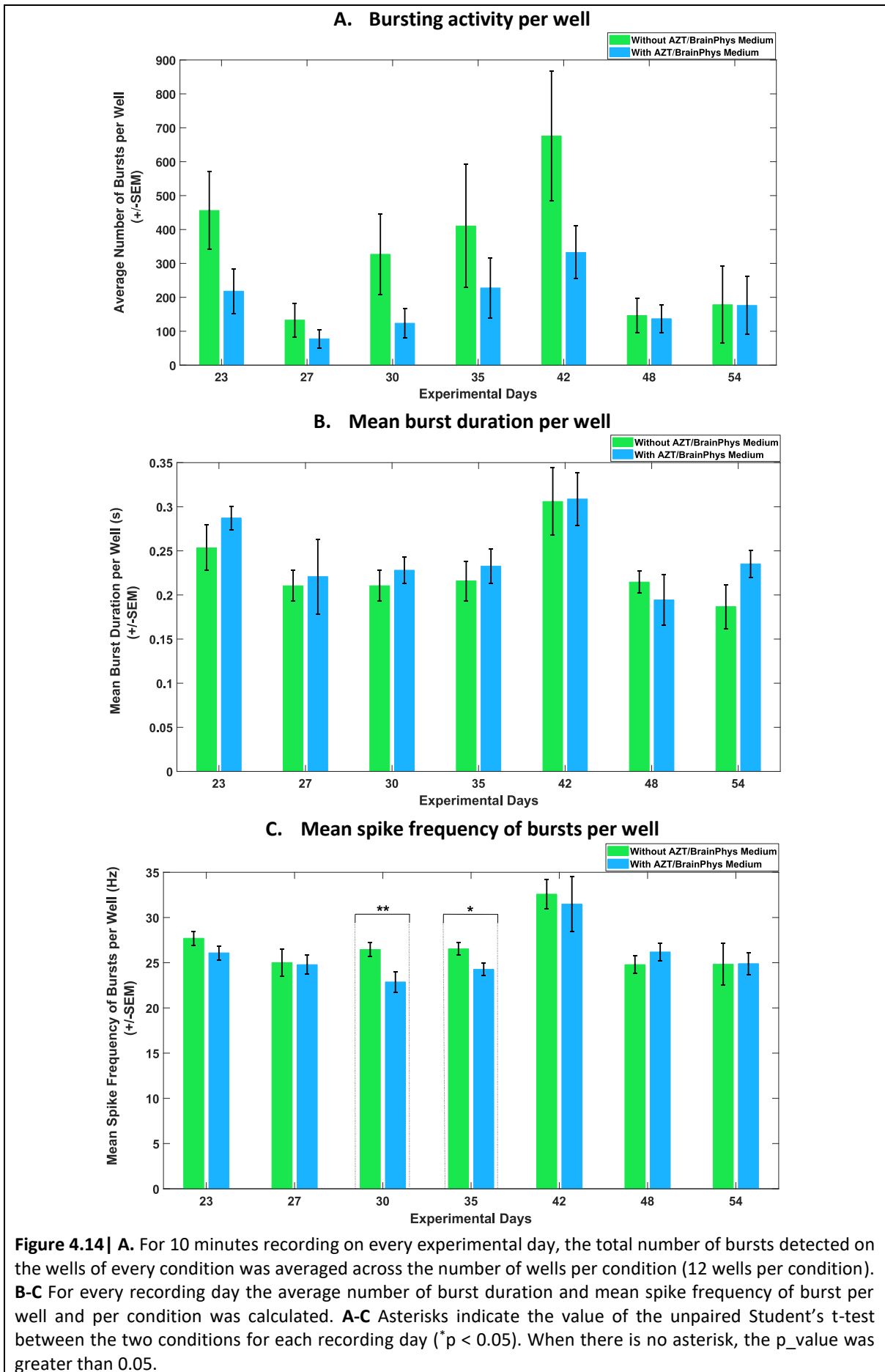


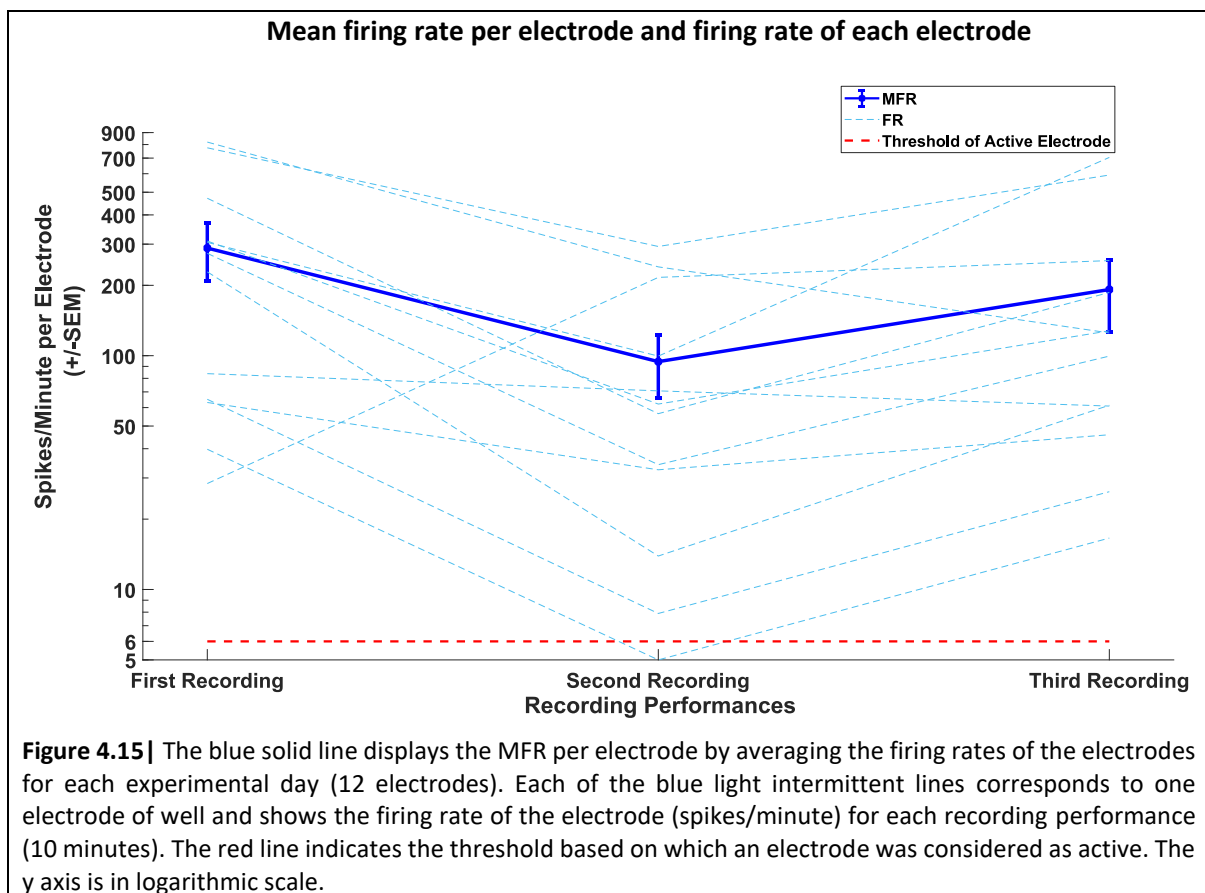
Figure 4.13 | The mean peak-to-peak amplitude was calculated by averaging all the peak-to-peak amplitudes detected by active electrodes of each well across the number of the wells per condition (12 wells with and without AZT respectively). The unpaired Student's t-test provided a p_value greater than 0.05 for each recording and thus, this indicated that the two conditions did not present any significant difference during the experimental period.

The detected bursting activity on both conditions did not show any significant difference (Figure 4.14 A). Generally, both conditions presented a high bursting activity, with more than 150 bursts per well for 10 minutes recording. The wells without AZT appeared to have a higher bursting activity compared to wells with AZT until the experimental day 42. During the last two recording performances, the bursting activity remained the same on both conditions. Additionally, the mean burst duration per well and the mean spike frequency of bursts per well was assessed per condition, showing that the fired bursts were similar (Figure 4.14 B, C). Although both conditions presented a considerable bursting activity, it was not adequate to cause a network bursting activity. This was a clear sign that even though neurons presented good connectivity, they were still functional immature considering their synchronized activity, which would be an indication of a network connectivity among neurons. A network bursting activity was detected at seven wells during the two last experimental days. The highest number of detected network bursts appeared on a well without AZT on the last experimental day, 129 network bursts for 10 minutes recording.



4.4 Spike sorting implementation on a single cell culture

Low activity in wells with Neurobasal medium, created unstable cell culturing conditions which did not allow the systematic spike sorting analysis. One neural culture was selected for spike sorting analysis, growing in BrainPhys medium. Three consecutive recordings were performed, and their time intervals were exactly 7 days. The neural culture existed between the 7th to 8th differentiation week in vitro. The MFR per electrode as well as the firing rate of each electrode for those three recording performances is presented in Figure 4.15. The firing rates and consequently the MFR presented a fluctuation over the three recording performances. As shown in Figure 4.15, the electrodes detected a high activity during the first recording, while this activity decreased in the second recording performance and again was increased on the third recording at the same level with the first recording.



4.4.1 Clusters derived from Wave_clus algorithm

The Wave_clus algorithm was used separately for every electrode and the waveforms of detected spikes were classified into clusters. The identified clusters per electrode for the three recording performances are presented in Table 4.5. Overall, on the first recording performance, the Wave_clus algorithm classified the waveforms of each electrode into clusters ranging from 2 until 6, while in the following recordings, the majority of electrodes exhibited only two clusters. A positive sign of successful clustering derived from the number of unclassified waveforms, which remained 0 in the majority of electrodes on the recording performances (Table 4.6). Additionally, a few false positives (mismatched waveforms) were detected on the clusters of each electrode per recording. The only important false positives were detected on electrode “33”, on the second recording performance,

when due to low number of waveforms (50 spikes), waveforms with opposite polarities were assigned to the same cluster. For this reason, the clustering of this electrode was omitted.

Table 4.5 | Number of clusters per electrode for the three recording performances

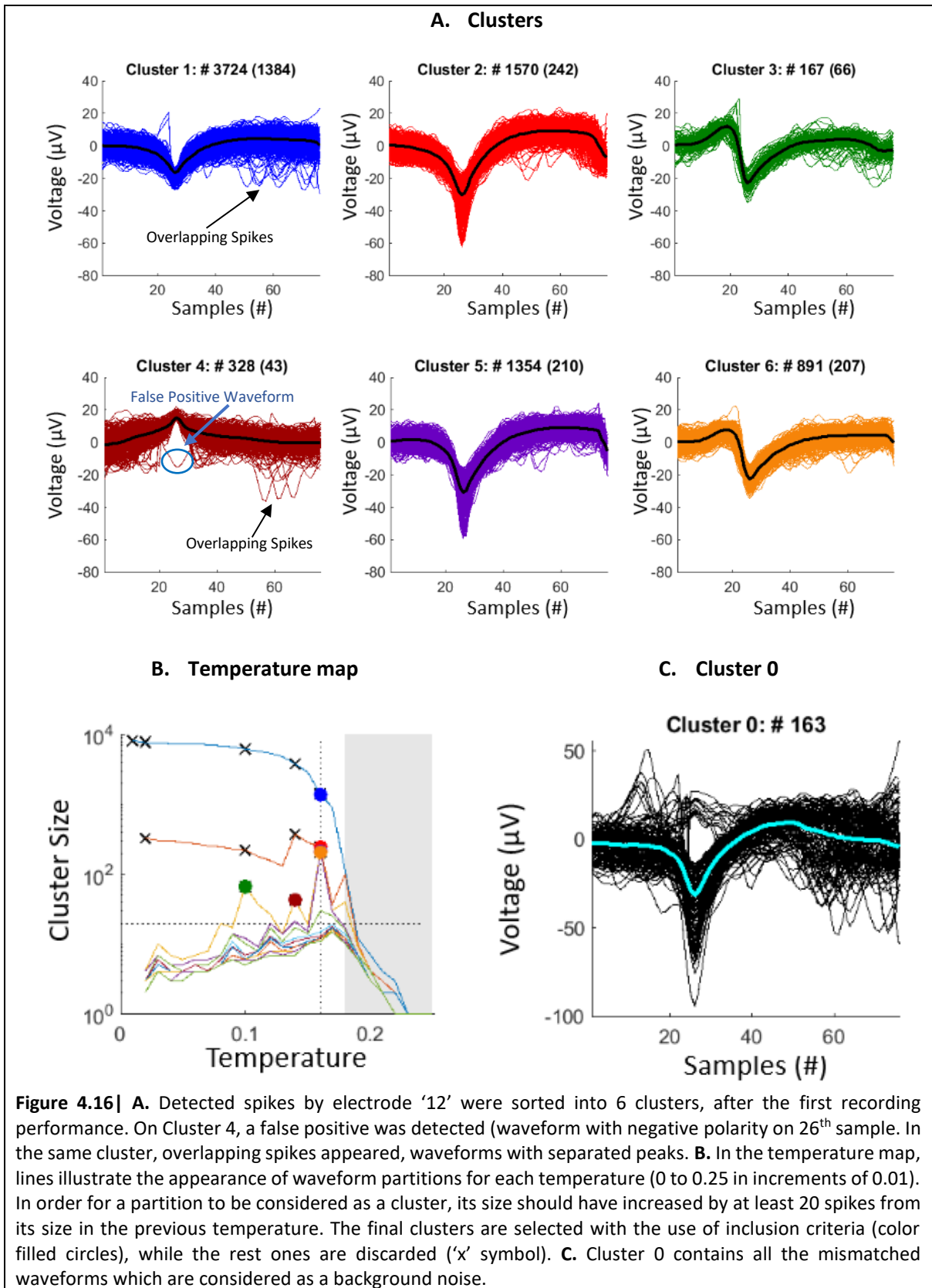
	Electrodes												Number of Clusters
	"21"	"31"	"12"	"22"	"32"	"42"	"13"	"23"	"33"	"43"	"24"	"34"	
1 st Rec.	3	5	6	3	2	2	3	2	3	3	2	2	
2 nd Rec.	3	2	3	2	2	2	2	2	-	2	2	2	
3 rd Rec.	3	2	2	2	2	4	2	2	2	2	2	2	

Table 4.6 | Number of unclassified waveforms per electrode for the three recording performances

	Electrodes												Unclassified Waveforms
	"21"	"31"	"12"	"22"	"32"	"42"	"13"	"23"	"33"	"43"	"24"	"34"	
1 st Rec.	0	29	163	0	0	0	5	0	0	2	0	0	
2 nd Rec.	1	0	6	0	0	0	0	0	-	0	0	0	
3 rd Rec.	11	3	0	0	0	167	0	0	0	0	0	0	

A result of spike clustering is depicted in the following Figure 4.16. Detected spikes from one electrode were classified into 6 clusters. Clusters 1 to 6 display the sorting spikes and the total number of spikes belonging to the cluster is written on the top of the cluster plots. The principal number of spikes assigned to each cluster before template matching is written into a parenthesis, next to the total number of spikes of each cluster. 163 spikes out of 8197 were assigned to Cluster 0 as unclassified waveforms. Additionally, a false positive waveform was observed in Cluster 4 (a waveform with negative amplitude instead of positive was detected). Some overlapping was also detected in the same clusters, high peaks appeared after the 26th sample, which was supposed to be the sample with the highest amplitude. Clusters 1 and 4 demonstrated representative examples of overlapping spikes. Remarkable was the fact that the spike shapes of Clusters 3 and 6 were not identified again on the same or another electrode in the following two recording performances, during experimental days 58 and 65.

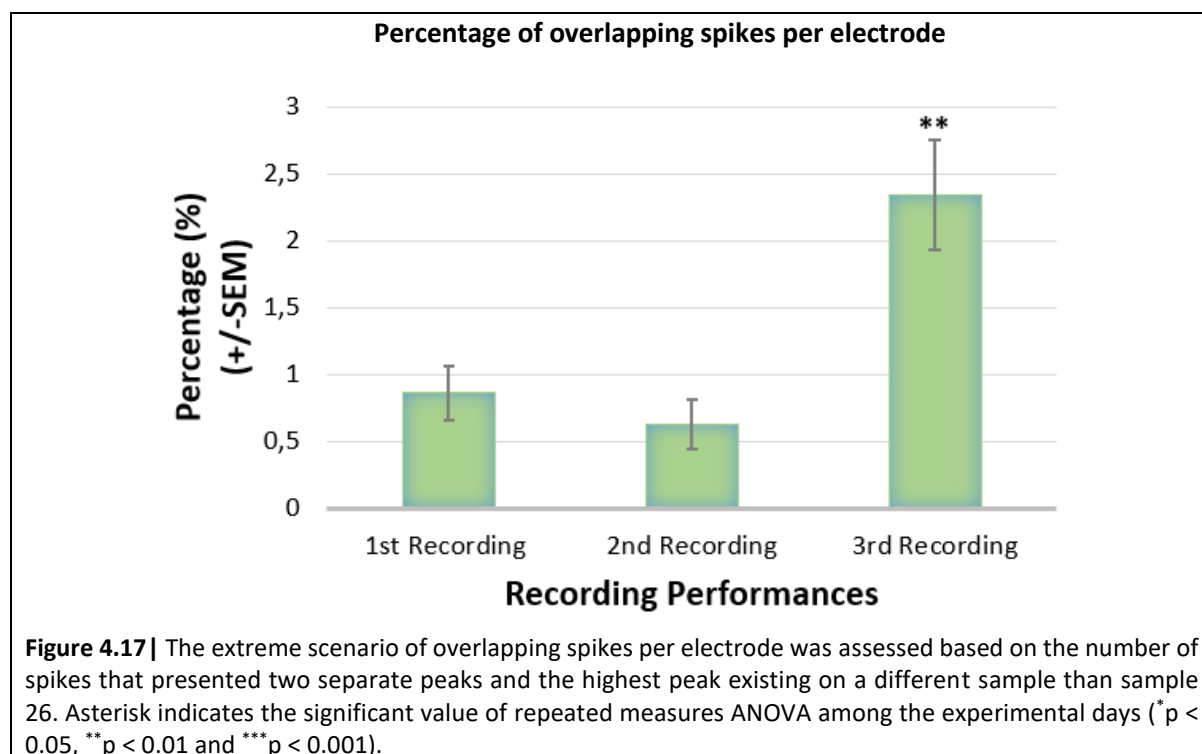
In the temperature map, 12 putative clusters (clusters marked with 'x' or color filled circles) were detected during the Wave_clus performance. As mentioned in Section 3.4, in order to consider a partition of spike waveforms as a cluster, its size should have increased by at least 20 spikes compared to the size in the previous temperature. At the end of the clustering, 6 clusters were selected (color filled circles) while the others were discarded ('x' symbols) (refer to Section 3.4 about inclusion criterion). The grey area in the temperature map illustrated the paramagnetic regime which indicated an abrupt decrease of the principal cluster (blue line) and the appearance of several small clusters (overclustering). In this grey area, the clustering process started being inefficient, as very small differences on spike waveforms were taken into account.



The overlapping spikes appeared as a general phenomenon in all clusters identified on each electrode. The overlapping issue was distinguished on spikes with separated peaks. Overlapping spikes hampered the detection performance because they were detected as single events when they appeared too close in time. As mentioned in Chapter 3, when a spike event was detected (voltage

signal overpassed a pre-defined threshold), in the following 3ms any activity was considered as a part of the detected event. Therefore, if another spike appeared during this dead time (3 ms), the MEA system did not distinguish it as another spike event, but as a consecutive part of the first spike event.

In order to determine the scale of spike overlapping, the percentage of spikes that presented two separate peaks and the highest peak existing on a different sample than the 26th, was estimated. This estimation was considered as an extreme scenario of overlapping, as there were also spikes that presented peaks apart from the first one on 26th sample, but the peak had a lower value than the 26th. As shown in Figure 4.17, the extreme scenario of overlapping spikes per electrode ranged at a low level, less than 2.5%.

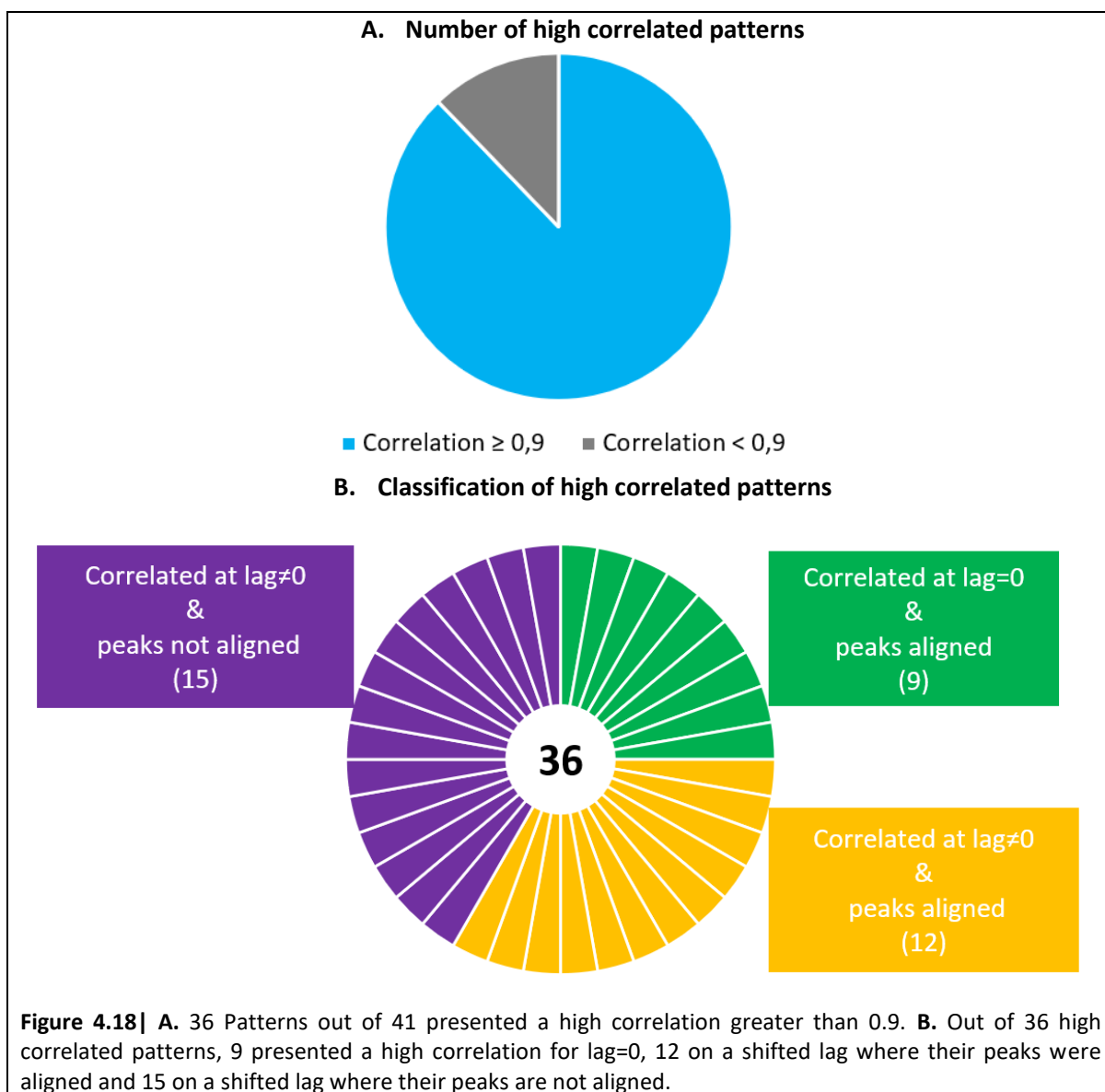


4.4.2 Assessment of mean waveform patterns

After the extraction of the clusters per electrode and their corresponding mean waveforms, a total number of 41 patterns were derived from the extracted clusters and their corresponding means. As depicted in Figure 4.18 A, by applying the correlation function on the mean waveforms of each pattern, 36 of these patterns presented a correlation greater than 0.9 among their waveforms. These 36 highly correlated patterns constituted the first positive sign over the experimental period of two weeks, that electrodes constantly detected firing activity from the same units of neurons. Examining every pattern individually, the amplitudes and the widths of the waveforms were not equal, and this was justified as the cross-correlation function compares the shapes of the waveforms. Additionally, as the neurons were growing over time, the detection of spikes with higher or lower amplitude over the recording days was expected, as a sign of cell maturity or cell death.

Subsequently, patterns were separated based on whether the waveforms presented a high correlation at a time lag equal to zero or at a shifted time point, Figure 4.18 B. In 9 patterns, the waveforms presented high correlation at a time lag equal to zero, while in the rest 27 patterns, at least one waveform presented high correlation at an earlier or later time. Out of the 27 patterns with high correlated waveforms on a time delay, 15 patterns presented a mismatch between the time point of

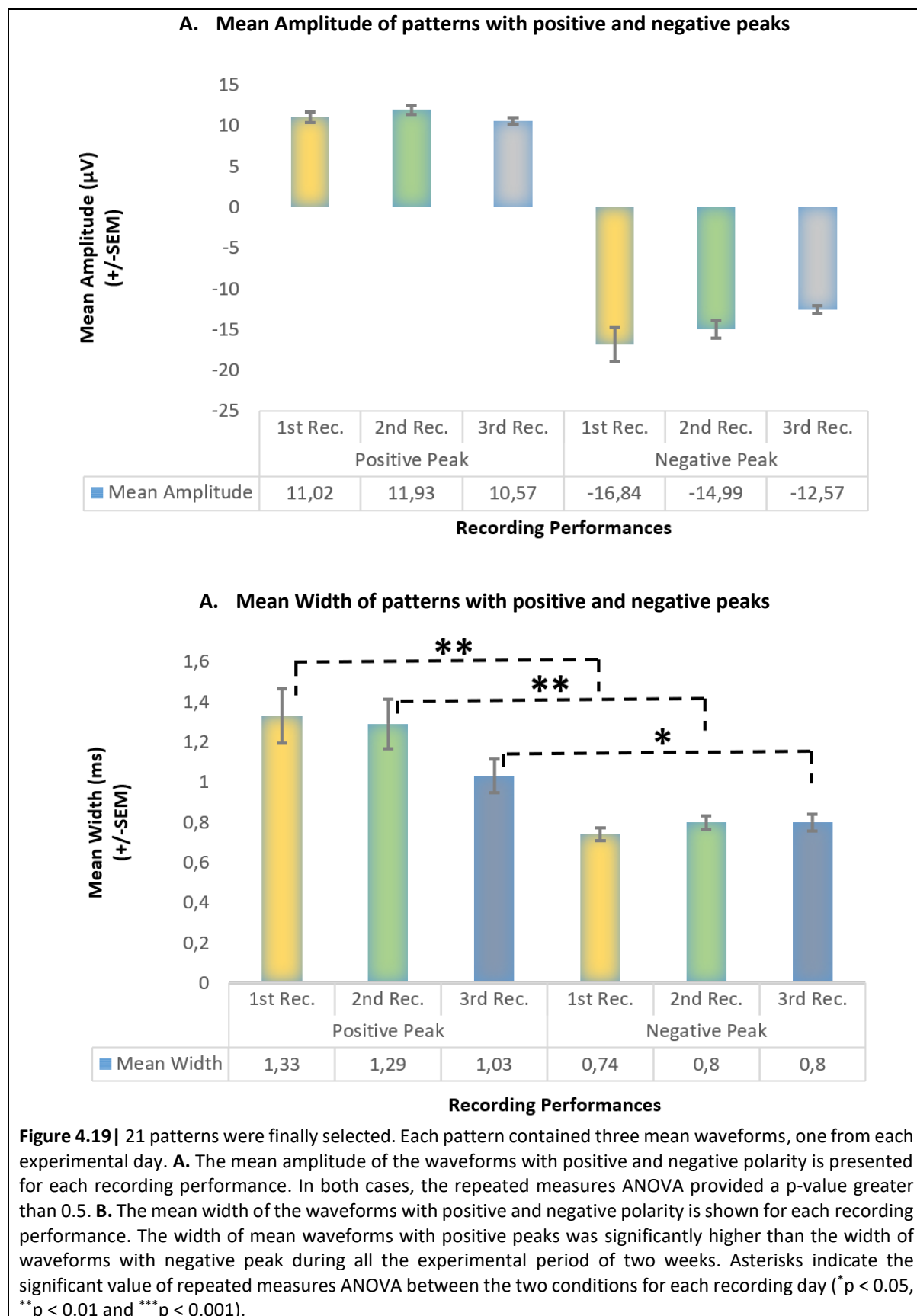
the waveforms' peaks and the lag that the waveforms presented high correlation. Specifically, the peaks of the waveforms on the 15 patterns were not aligned at the same time point where the waveforms presented a high correlation. In the rest 12 patterns, their peaks were aligned on their time point where they presented high correlation.



These 15 patterns were omitted from the final number of high correlated patterns as it probably needed a higher sampling frequency in order to assess whether the misalignment of the peaks was an indication of a significant difference between waveforms or not. Therefore, 21 patterns remained (9 with lag=0 and 12 with lag \neq 0), 6 of them having waveforms with positive polarity and 15 waveforms with negative polarity. Consequently, the average values of amplitude and width were calculated for the mean waveforms with positive and negative polarity respectively on every recording performance.

The mean amplitude of the waveforms of the 6 patterns with positive polarity for each recording performance remained at the same level of approximately 11 μ V (Figure 4.19 A). On the other hand, the mean amplitude of the waveforms of the 15 patterns with negative polarity decreased over the three experimental days, starting from -16.84 μ V and reaching -12.57 μ V on the last experimental day, although this reduction was not statistically significant. The mean width of the waveforms with

positive polarity remained significant higher during these three recordings compared to mean width of the negative polarity waveforms (Figure 4.19 B).



CHAPTER 5

Discussion and Prospects

The current thesis project demonstrated that neural cultures growing on BrainPhys medium presented a robust network activity, while they remained on the MEA substrate for a long-term period, approximately 10 weeks in vitro. Additionally, a spike sorting analysis showed the successful monitoring of spike waveforms derived from the same unit of neurons in a period of 2 weeks. Although several analysis and methodologies can be suggested for future work, the developed experimental paradigm constitutes the stepstone for a next class experimental model in which successful comparison between neural cultures derived from healthy and diseased by psychiatric disorders individuals could be achieved.

5.1 Discussion

In the current thesis project, the principal hypothesis, whether the neural differentiation protocol for a long-term culture, published by N. Gunhanlar et al., could promote functional neural networks derived from a healthy individual was verified, with the use of extracellular measurement by the commercial Multiwell-MEA system. The neural cultures presented a high firing and bursting activity with the use of BrainPhys as a cultivation medium, while they achieved to remain on the MEA substrate for a long-term period, approximately 10 weeks in vitro. Additionally, a spike sorting analysis showed the successful monitoring of spike waveforms derived from the same unit of neurons in a period of 2 weeks.

The investigation of an optimal NPC density was not conclusive, as the activity of neurons presented very low, not more than 3 active electrodes per well (Figure 4.1). It is highly possible that Neurobasal deficiency did not promote the functional maturity of neural networks, therefore having a side effect on the detected activity by the electrodes and on NPC density investigation. Additionally, the intensive cell aggregations performing big clumps on the MEA plate with five different NPC densities was a sign that the low activity was not related to inappropriate cell density, but to significant cell culturing issue. The detected low activity of Multiwell-MEA plates indicated a decreased neuronal functionality characterized as electrophysiological immature.

On the other hand, BrainPhys medium appeared as a suitable cultivation medium which enhanced the functional differentiation of NPCs into neurons. It is highly possible that BrainPhys medium plays a key role on neuronal activity, due its similar osmolarity with human cerebrospinal fluid. Additionally, Neurobasal medium failed to enhance the electrophysiological functionality of neurons during the experiments. According to N. Gunhanlar et al., in order to prove that the protocol (which was also used in the current project) promotes the functional maturity of neurons, they implemented intracellular measurements in which the medium of neural cultures was changed from Neurobasal to artificial cerebrospinal fluid, as done during mouse brain slice recordings in vivo. Additionally, based on the current experimental procedure observations, Neurobasal seems as a non-appropriate medium for extracellular recordings.

BrainPhys medium had a direct impact on neural cultures either when it was inserted at the beginning or at a later stage of the neural cell culturing process. Considering its later application, neural cultures had a direct response by increasing their firing rate and reaching a peak of 110 spikes per minute, as observed in Figure 4.3 reported in Section 4.3. The neural cultures which remained with Neurobasal medium presented MFR of 20 spikes/minute. This increase of neuronal activity could be explained as a result of cell stress and not as a superior culturing environment. The following experimental procedures (BrainPhys and Neurobasal medium comparison, BrainPhys validation) proved that BrainPhys indeed was an efficient cultivation medium by providing a similar to in vivo osmotic environment. Neural cultures with BrainPhys medium depicted a higher activity compared to neurons in Neurobasal medium from the very early beginning of 10 weeks period in vitro. The CFR and MFR appeared more than 20 times higher in BrainPhys compared to Neurobasal, reaching a peak of 1800 spikes/minute/well and 210 spikes/minute/electrode (Figure 4.5).

Neural cultures growing on BrainPhys medium presented also an intense bursting activity, a clear proof that neurons also demonstrated the characteristic of connectivity in parallel with functionality. Neurons on different cell cultures reached a peak of 800 and 700 bursts on 30th and 42nd experimental day in vitro, respectively (Figure 4.8, Figure 4.14). However, the phenomenon of network bursting activity, related to the feature of synchronicity, was sporadic and unstable between consecutive recording performances. Based on these observations, it can be considered that neurons in BrainPhys reached a robust connectivity, as there were able to develop strong cellular interconnection on a local

area that an electrode can detect (maximum 150 μm), but they were incapable of establishing strong network interconnection in longer distances for a prolonged period of time.

Interestingly, the mean spike amplitude ranged at the same level in both conditions (25-30 μV), which was a clear proof that BrainPhys did not enhance stronger EAPs compared to Neurobasal (Figure 4.7, Figure 4.13). Moreover, the investigation of AZT efficiency or the deposition of different coatings (matrigel, laminin) had almost no impact on the activity of neurons. However, AZT seemed to postpone the cell clumping in the neural cultures where added (Figure 4.10) and this result suggested that AZT can be used for cell clumping reduction, while AZT is not expected to have any effect on neuronal activity. Finally, from a technical point of view, the delamination of SU-8 of the MEA substrate after 84 days of usage, was also considered as a limitation for long-term culturing. The SU-8 layer works as an insulator and consequently, its degradation can expose the tracks of electrodes which results on the increase of the recording sites.

The spike waveforms classification into clusters and the use of cross-correlation function demonstrated that the majority of mean waveforms' patterns presented a high correlation, meaning that neuronal units remained close by the electrodes and produced the same shape of waveforms for a period of two weeks. Specifically, 88% of the detected patterns presented a cross-correlation higher than 0.9 (Figure 4.18). However, the observation of peak misalignments on the time points where the waveforms of some pattern were highly correlated, might imply an issue of an overlapping spike. Additionally, the incident of a higher in amplitude spike overlapping the already detected spike, was less than 2.5% (Figure 4.17). The amplitude of the selected negative polarity patterns appeared higher compared to the positive patterns (Figure 4.19). Referring to Chapter 2.3, a large negative spike is mainly produced by the initial rapid Na^+ ion influx during APs of neurons. Therefore, it can be assumed that these patterns were the product of the depolarization event of several APs around the corresponding electrodes. On the other hand, the lower in amplitude positive polarity patterns might be related to the repolarization of APs (the slow K^+ efflux).

In summary, a plethora of firing and bursting activity detected during the experiments, showed a robust network activity of neural cultures with BrainPhys derived from the long-term neural differentiation protocol and assessed by MEA measurements. Additionally, the findings of spike sorting analysis guarantees the easy monitoring of specific neuronal units in a short time period. Further experimentation and development will shed a light on the current limitations that the neural model presents and will positively contribute to the optimization of this neural model which could be used as a reference point for comparison with cell lines derived from patients with psychiatric disorders.

5.2 Conclusions and future prospects

The current thesis project positively contributes to the creation of an optimal neural cell culture which would recapitulate the electrophysiological functionality of neurons as it is observed in vivo assessments. As a general outcome, BrainPhys presented as the optimal cultivation medium for neuronal activity detection. However, due to limited number of samples, the repetition of experiments with BrainPhys and Neurobasal medium, which would lead to valid conclusions is suggested. Additionally, experimental questions about the optimal NPC density and the reason of sporadic network bursting activity are still open. As future work, the investigation of different NPC densities with BrainPhys medium might provide a clear answer in this research question, as BrainPhys provides a better osmotic environment where differences in functionality can be detected.

Spike sorting analysis and the use of cross-correlation function provided a clear answer on successful monitoring of the same units of neurons during a short period of two weeks in vitro with the formation of waveform patterns. This might be a useful tool for pharmacological testing in the future, as the spike waveforms of the same unit of neurons can be observed before and after drug deposition. However, the observation of peak misalignments on the time points where the waveforms of some pattern were highly correlated, suggests a further investigation in order to clarify whether that is indeed an issue, or not. A higher sampling frequency could potentially allow the investigation of whether this peak misalignment was an issue of overlapping spike or another factor disrupted the waveform shape. However, it is important to guarantee the effectiveness of Wav_clus algorithm, as a higher number of samples would be inserted due to higher sampling frequency. A smart way to enhance the spike sorting efficiency is a pre-clustering analysis, where it is examined which spikes are derived from different neuronal units and which are derived due to AP propagation [63]. Therefore, spike waveforms due to signal propagation are removed from the final spike sorting analysis, while only the spikes derived from different neuronal cell types are involved in the final spike clustering. This approach demands a high number of electrodes on the MEA substrate.

From a technical perspective, the SU-8 degradation on the MEA substrates after a long-term usage appears as a warning that even if a neural differentiation protocol guarantees neural survival for a prolonged period, technical issues will limit this effort. Microfabrication technology of MEA substrate should be improved on the direction of long-term usage. Additionally, in the current MEA system, besides the temperature control, a gas sensor is needed to achieve the optimal culturing conditions, as in the incubator. The atmosphere gas (air with 5% CO₂) is manually inserted through an inlet and there is no indication whether it flows in a constant way or if the gas mixture is distributed homogeneously. The low number of electrodes per well (12) of the Multiwell-MEA plate limits the detection of neuronal activity and the use of a plate with a higher number of active electrodes per well (50-100), which could capture the activity of a significantly higher number of cell regions, would be more efficient. It has also been observed that high density MEAs allow more complex data analyses, especially for bursting pattern investigation [37].

The development of further analytical methodology is recommended which would provide additional information on the neuronal firing patterns. For instance, colormaps derived from cross-correlograms can provide the regions of high spike and bursting activity over the recording time [47]. The problem of overlapping spikes remains as one of the most challenging issues. Although the use of dead-time windows, which just define when a spike ends, seems arbitrary, it should be mentioned that there is no optimal approach to deal with it. Several approaches have been proposed on that and the use of high density MEAs stands as the most effective way to face that issue, as what appears as an overlap in one electrode might be an isolated unit in another one [41]. Additionally, an online software for

data analysis simultaneously with the data extraction would provide an efficient way of data mining, analysis and storage. It is worth to mention that for 10 minutes recording, 7.5 GB of data was stored for each MEA measurement. From that amount of data, only 30 MB were kept for spike and bursting analysis. Therefore, the online software will reduce the computing time significantly.

To summarize, the developed experimental paradigm constitutes the stepstone for a next class experimental model to study the healthy and diseased early embryonic neurodevelopmental process. The outcomes of the thesis project in parallel with the aforementioned suggestions for future work could potentially lead to the implementation of a reliable reference model for comparison with neural cultures derived from patients with psychiatric disorders.

The current thesis project has contributed to the field of Neurobiological Psychiatry and Electrophysiology in the following:

- ✚ The neural differentiation protocol promotes a robust neuronal network activity that can be measured by MEAs.
- ✚ Neural cultures can remain in the MEA substrates approximately 10 weeks in vitro.
- ✚ BrainPhys medium enhances the functional maturity of neurons.
- ✚ Spike shorting analysis with the use of cross-correlation function can allow the monitoring of the spike waveforms derived from the same unit of neurons in a period of 2 weeks.

REFERENCES

- [1] Y. S. Kim et al., "Recent challenges to the psychiatric diagnostic nosology: A focus on the genetics and genomics of neurodevelopmental disorders," *Int. J. Epidemiol.*, vol. 43, no. 2, pp. 465–475, 2014.
- [2] A. P. Mullin et al., "Neurodevelopmental disorders: Mechanisms and boundary definitions from genomes, interactomes and proteomes," *Transl. Psychiatry*, vol. 3, no. 12, pp. e329-6, 2013.
- [3] T. J. C. Polderman et al., "Meta-analysis of the heritability of human traits based on fifty years of twin studies," *Nat. Publ. Gr.*, vol. 47, no. 7, pp. 702–709, 2015.
- [4] P. F. Sullivan et al., "Genetic architectures of psychiatric disorders: The emerging picture and its implications," *Nat. Rev. Genet.*, vol. 13, no. 8, pp. 537–551, 2012.
- [5] A. Falk et al., "Modeling psychiatric disorders: from genomic findings to cellular phenotypes," *Mol. Psychiatry*, vol. 21, no. 9, pp. 1167–1179, 2016.
- [6] C. W. Habela et al., "Modeling synaptogenesis in schizophrenia and autism using human iPSC derived neurons," *Mol. Cell. Neurosci.*, vol. 73, pp. 52–62, 2016.
- [7] S. P. Paşca et al., "Generating Human Neurons In Vitro and Using Them to Understand Neuropsychiatric Disease," *Annu. Rev. Neurosci.*, vol. 37, no. 1, pp. 479–501, 2014.
- [8] K. Takahashi et al., "Induction of Pluripotent Stem Cells from Adult Human Fibroblasts by Defined Factors," *Cell*, vol. 131, no. 5, pp. 861–872, 2007.
- [9] G. Quadrato et al., "The promises and challenges of human brain organoids as models of neuropsychiatric disease," *Nat. Med.*, vol. 22, no. 11, pp. 1220–1228, 2016.
- [10] A. F. M. Johnstone et al., "Microelectrode arrays: A physiologically based neurotoxicity testing platform for the 21st century☆," *Neurotoxicology*, vol. 31, no. 4, pp. 331–350, 2010.
- [11] Z. Wen et al., "Modeling psychiatric disorders with patient-derived iPSCs," *Curr. Opin. Neurobiol.*, vol. 36, pp. 118–127, 2016.
- [12] N. Gunhanlar et al., "A simplified protocol for differentiation of electrophysiologically mature neuronal networks from human induced pluripotent stem cells," *Mol. Psychiatry*, vol. 23, no. 5, pp. 1336–1344, 2017.
- [13] I. Kelava et al., "Dishing out mini-brains: Current progress and future prospects in brain organoid research," *Dev. Biol.*, vol. 420, no. 2, pp. 199–209, 2016.
- [14] E. N. Marieb et al., *Human Anatomy & Physiology*. 2014.
- [15] M. Telias et al., "Modeling Neurodevelopmental Disorders Using Human Pluripotent Stem Cells," *Stem Cell Rev. Reports*, vol. 10, no. 4, pp. 494–511, 2014.
- [16] W. R. Earle, "Production of Malignancy in Vitro . IV . The Mouse Fibroblast Cultures and Changes Seen in the Living Cells," vol. 4, no. 2, pp 165-212, 1943.
- [17] G. A. Tocco et al., "Establishment of functional clonal lines of neurons from mouse neuroblastoma.," *Proc. Natl. Acad. Sci. U. S. A.*, vol. 64, no. 1, pp. 311–315, 1969.
- [18] Y. Shi, "Human cerebral cortex development from pluripotent stem cells to functional excitatory synapses," *Nat. Neurosci.*, vol. 15, no. 3, pp. 477–486, 2012.
- [19] S. M. Chambers et al., "Highly efficient neural conversion of human ES and iPS cells by dual

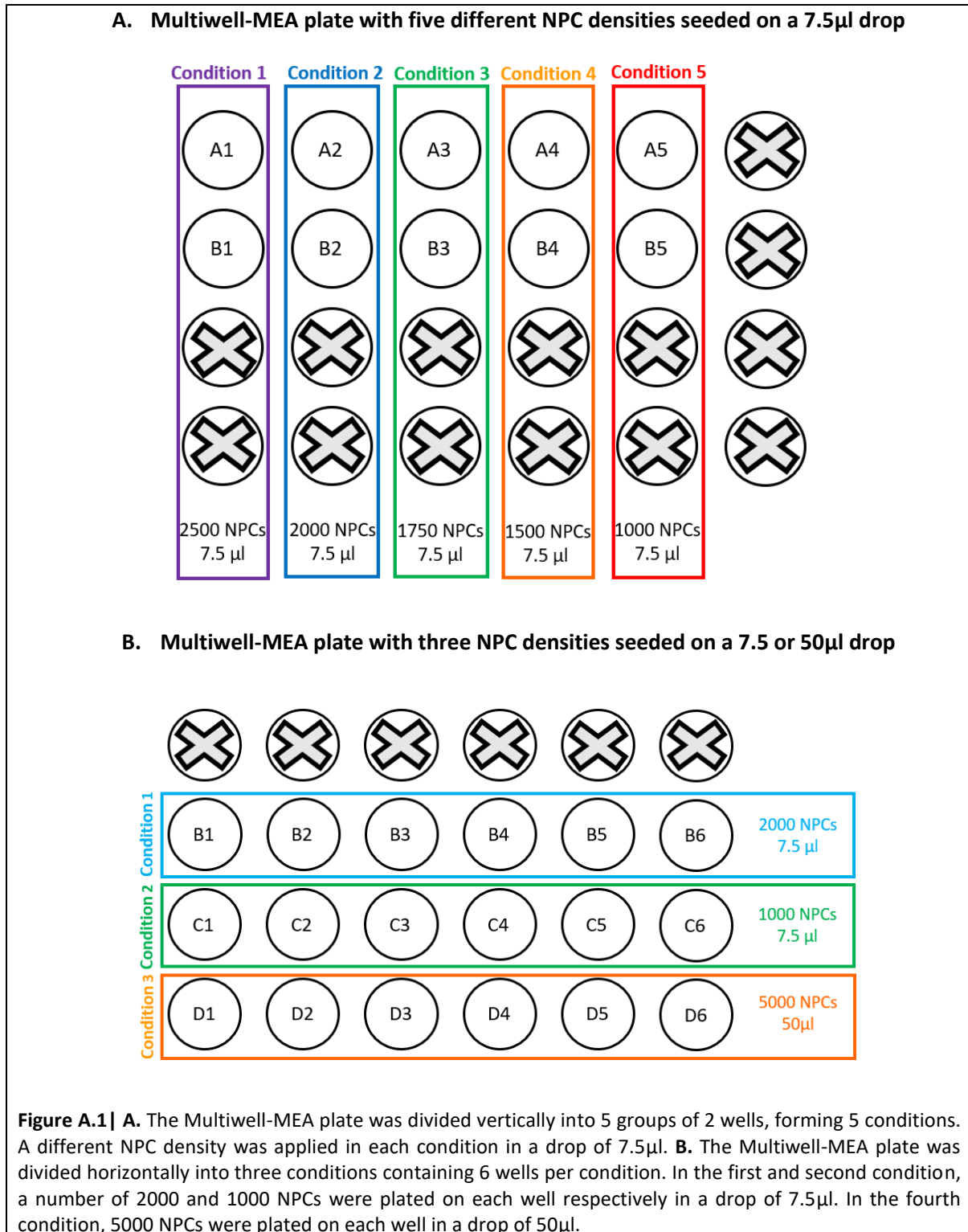
- inhibition of SMAD signaling," *Nat. Biotechnol.*, vol. 27, no. 3, pp. 275–280, 2009.
- [20] X. Qian *et al.*, "Brain-Region-Specific Organoids Using Mini-bioreactors for Modeling ZIKV Exposure," *Cell*, vol. 165, no. 5, pp. 1238–1254, 2016.
- [21] T. Otani *et al.*, "2D and 3D Stem Cell Models of Primate Cortical Development Identify Species-Specific Differences in Progenitor Behavior Contributing to Brain Size," *Cell Stem Cell*, vol. 18, no. 4, pp. 467–480, 2016.
- [22] A. M. Paşca *et al.*, "Functional cortical neurons and astrocytes from human pluripotent stem cells in 3D culture," vol. 12, no. 7, 2015.
- [23] Y. Shi *et al.*, "Directed differentiation of human pluripotent stem cells to cerebral cortex neurons and neural networks," 2012.
- [24] M. A. Johnson *et al.*, "Functional Neural Development from Human Embryonic Stem Cells : Accelerated Synaptic Activity via Astrocyte Coculture," vol. 27, no. 12, pp. 3069–3077, 2007.
- [25] Z. Wen *et al.* "Synaptic dysregulation in a human iPSC cell model of mental disorders," *Nature*, no. V, 2014.
- [26] F. Rouhani *et al.*, "Genetic Background Drives Transcriptional Variation in Human Induced Pluripotent Stem Cells," vol. 10, no. 6, 2014.
- [27] J. Choi *et al.*, "A comparison of genetically matched cell lines reveals the equivalence of human iPSCs and ESCs," *Nat. Biotechnol.*, vol. 33, no. 11, 2015.
- [28] T. M. Schlaeger *et al.*, "A comparison of non-integrating reprogramming methods," *Nat. Biotechnol.*, vol. 33, no. 1, 2015.
- [29] F. A. Ran *et al.*, "Genome engineering using the CRISPR-Cas9 system," *Nat. Protoc.*, vol. 8, no. 11, pp. 2281–2308, 2013.
- [30] K. J. Brennand *et al.*, "Modelling schizophrenia using human induced pluripotent stem cells," *Nature*, vol. 473, no. 7346, pp. 221–225, 2011.
- [31] J. Mertens *et al.*, "Differential responses to lithium in hyperexcitable neurons from patients with bipolar disorder," *Nature*, vol. 527, no. 7576, pp. 95–99, 2015.
- [32] D. Prilutsky *et al.*, "iPSC-derived neurons as a higher-throughput readout for autism: promises and pitfalls," *Trends Mol. Med.*, vol. 20, no. 2, pp. 91–104, 2013.
- [33] M. C. N. Marchetto *et al.*, "A Model for Neural Development and Treatment of Rett Syndrome Using Human Induced Pluripotent Stem Cells," *Cell*, vol. 143, no. 4, pp. 527–539, 2010.
- [34] R. M. Walsh *et al.*, "Previews Modeling Rett Syndrome with Stem Cells" *Cell*, vol. 143, no. 4, pp. 499–500, 2010.
- [35] L. Zeng *et al.*, "Functional Impacts of NRXN1 Knockdown on Neurodevelopment in Stem Cell Models," pp. 1–13, 2019.
- [36] J. Mariani *et al.*, "FOXP1-Dependent Dysregulation of GABA/Glutamate Neuron Differentiation in Autism Spectrum Disorders," *Cell*, vol. 162, no. 2, pp. 375–390, 2015.
- [37] M. E. J. Obien *et al.*, "Revealing neuronal function through microelectrode array recordings," vol. 8, no. January, pp. 1–30, 2015.
- [38] I. L. Jones *et al.*, "The potential of microelectrode arrays and microelectronics for biomedical research and diagnostics," pp. 2313–2329, 2010.

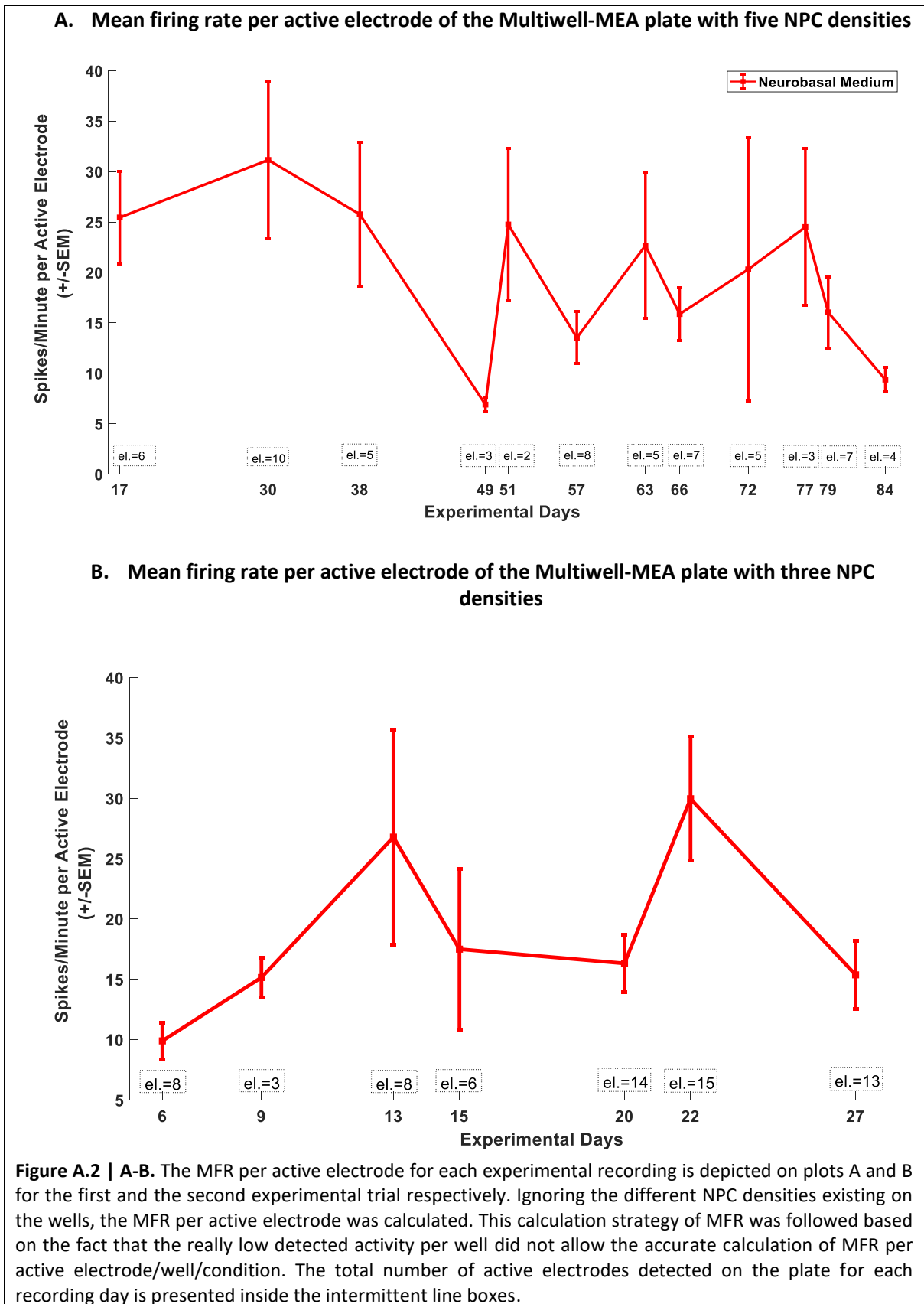
- [39] M. E. Spira et al., "Multi-electrode array technologies for neuroscience and cardiology," *Nat. Nanotechnol.*, vol. 8, no. 2, pp. 83–94, 2013.
- [40] F. O. Morin et al., "Investigating neuronal activity with planar microelectrode arrays: achievements and new perspectives," *J. Biosci. Bioeng.*, vol. 100, no. 2, pp. 131–143, 2005.
- [41] H. G. Rey, "Past, present and future of spike sorting techniques," *Brain Res. Bull.*, vol. 119, pp. 106–117, 2015.
- [42] Y. Nam et al., "In Vitro Microelectrode Array Technology and Neural Recordings," *Crit. Rev. Biomed. Eng.*, vol. 39, no. 1, pp. 45–61, 2012.
- [43] Z. Aqrave et al., "Conducting polymers for neuronal microelectrode array recording and stimulation," *Sensors Actuators, B Chem.*, vol. 257, pp. 753–765, 2018.
- [44] J. Le Feber et al., "Barbed channels enhance unidirectional connectivity between neuronal networks cultured on multi electrode arrays," *Front. Neurosci.*, vol. 9, no. NOV, pp. 1–10, 2015.
- [45] K. Shimba et al., "Long-term developmental process of the human cortex revealed in vitro by axon-targeted recording using a microtunnel-augmented microelectrode array," *IEEE Trans. Biomed. Eng.*, pp. 1–9, 2019.
- [46] F. Zeldenrust et al., "Neural Coding With Bursts—Current State and Future Perspectives," *Front. Comput. Neurosci.*, vol. 12, no. July, pp. 1–14, 2018.
- [47] M. Frega et al., "Network dynamics of 3D engineered neuronal cultures: A new experimental model for in-vitro electrophysiology," *Sci. Rep.*, vol. 4, pp. 1–14, 2014.
- [48] R. Q. Quiroga, "Concept cells: the building blocks of declarative memory functions," no. July, pp. 1–11, 2012.
- [49] H. G. Rey et al., "Single -cell recordings in the human medial temporal lobe," pp. 394–408, 2015.
- [50] C. Bardy et al., "Neuronal medium that supports basic synaptic functions and activity of human neurons in vitro.," *Proc. Natl. Acad. Sci. U. S. A.*, vol. 112, no. 20, pp. E2725-34, 2015.
- [51] Y. Hu et al., "The telomerase inhibitor AZT enhances differentiation and prevents overgrowth of human pluripotent stem cell–derived neural progenitors," *J. Biol. Chem.*, vol. 293, no. 23, pp. 8722–8733, 2018.
- [52] A. S. Pranti, A. Schander, A. Bödecker, and W. Lang, "PEDOT: PSS coating on gold microelectrodes with excellent stability and high charge injection capacity for chronic neural interfaces," *Sensors Actuators, B Chem.*, vol. 275, no. August, pp. 382–393, 2018.
- [53] Y. Zhang et al., "Application of SU-8 as the insulator toward a novel planar microelectrode array for extracellular neural recording," *2010 IEEE 5th Int. Conf. Nano/Micro Eng. Mol. Syst. NEMS 2010*, pp. 395–398, 2010.
- [54] E. Noce, "Spike detection: The first step towards an ENG-based neuroprosheses," *J. Neurosci. Methods*, vol. 308, no. July, pp. 294–308, 2018.
- [55] J. Izsak et al., "Robust Generation of Person-Specific, Synchronously Active Neuronal Networks Using Purely Isogenic Human iPSC-3D Neural Aggregate Cultures," *Front. Neurosci.*, vol. 13, no. April, 2019.
- [56] M. Frega et al., "Rapid Neuronal Differentiation of Induced Pluripotent Stem Cells for Measuring Network Activity on Micro-electrode Arrays," *J. Vis. Exp.*, no. 119, pp. 1–9, 2017.

- [57] C. R. Legendy et al., "Bursts and recurrences of bursts in the spike trains of spontaneously active striate cortex neurons," *J. Neurophysiol.*, vol. 53, no. 4, pp. 926–939, 1985.
- [58] D. Wagenaar et al. , "MeaBench: A toolset for multi-electrode data acquisition and on-line analysis," *2nd Int. IEEE EMBS Conf. Neural Eng.*, vol. 2005, pp. 518–521, 2005.
- [59] G. D. C. Mendis et al. , "Use of adaptive network burst detection methods for multielectrode array data and the generation of artificial spike patterns for method evaluation," *J. Neural Eng.*, vol. 13, no. 2, p. 26009, 2016.
- [60] F. J. Chaure et al., "A novel and fully automatic spike-sorting implementation with variable number of features," *J. Neurophysiol.*, vol. 120, no. 4, pp. 1859–1871, 2018.
- [61] R. Quian Quiroga et al., "Communicated by Maneesh Sahani Unsupervised Spike Detection and Sorting with Wavelets and Superparamagnetic Clustering," vol. 1687, pp. 1661–1687, 2004.
- [62] E. Domany et al., "Superparamagnetic clustering of data: Application to computer vision," *Comput. Phys. Commun.*, vol. 121, pp. 5–12, 1999.
- [63] K. R. Tovar et al., "Action potential propagation recorded from single axonal arbors using multielectrode arrays," *J. Neurophysiol.*, vol. 120, no. 1, pp. 306–320, 2018.

APPENDIX A

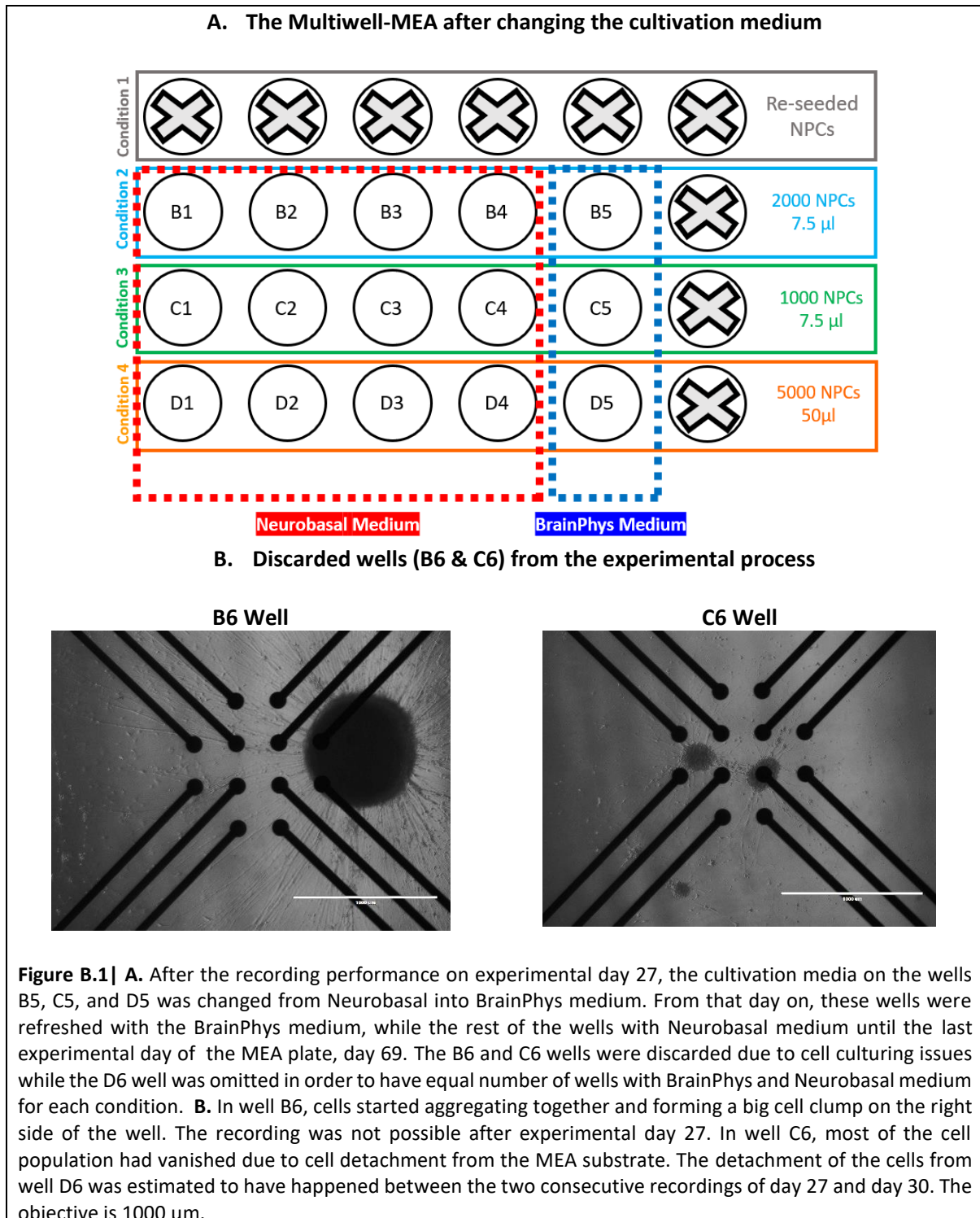
In Appendix A, additional information about the first experimental phase, investigation of an optimal NPC density, is presented. On this experiment, different NPC densities were seeded into the wells of two Multiwell-MEA plates.



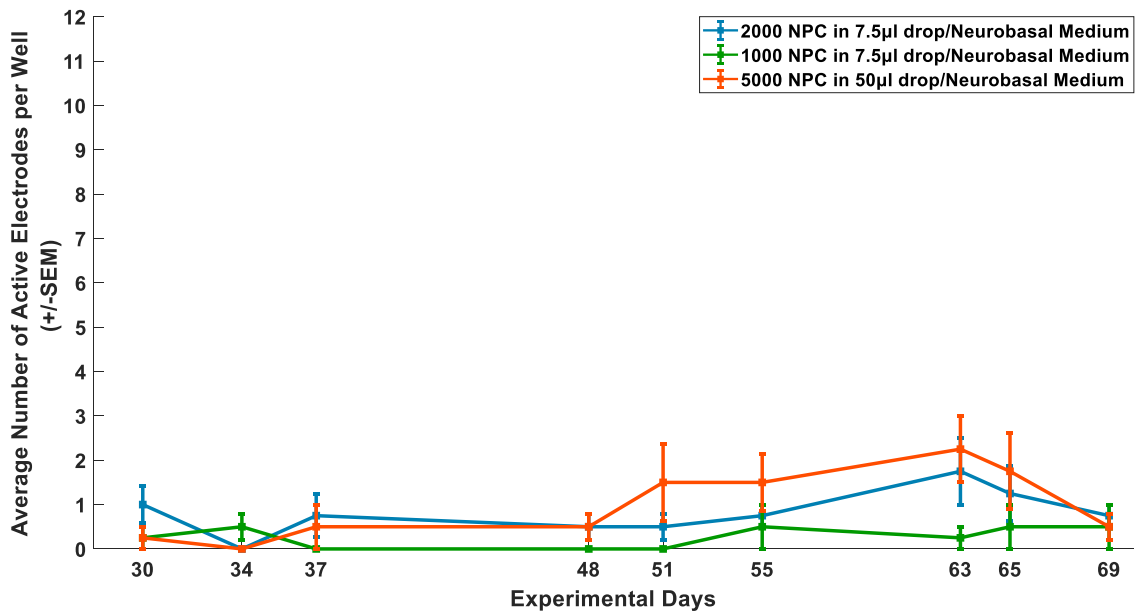


APPENDIX B

In Appendix B, additional information about the second experimental phase, evaluation of BrainPhys and Neurobasal on neural cultures, is presented. On this experiment, as it is mentioned in Chapter 4.2, three experimental concepts were implemented: the effect of the later insertion of BrainPhys medium in neural cultures growing on Neurobasal medium; the effect of Neurobasal and BrainPhys medium when both applied at the beginning of NPCs seeded on MEA plate; the functional development of neural culture when only BrainPhys is applied. For this reason, three different Multiwell-MEA plates were used, one for each concept.



A. Average number of active electrodes with Neurobasal Medium



B. Average number of active electrodes with BrainPhys Medium

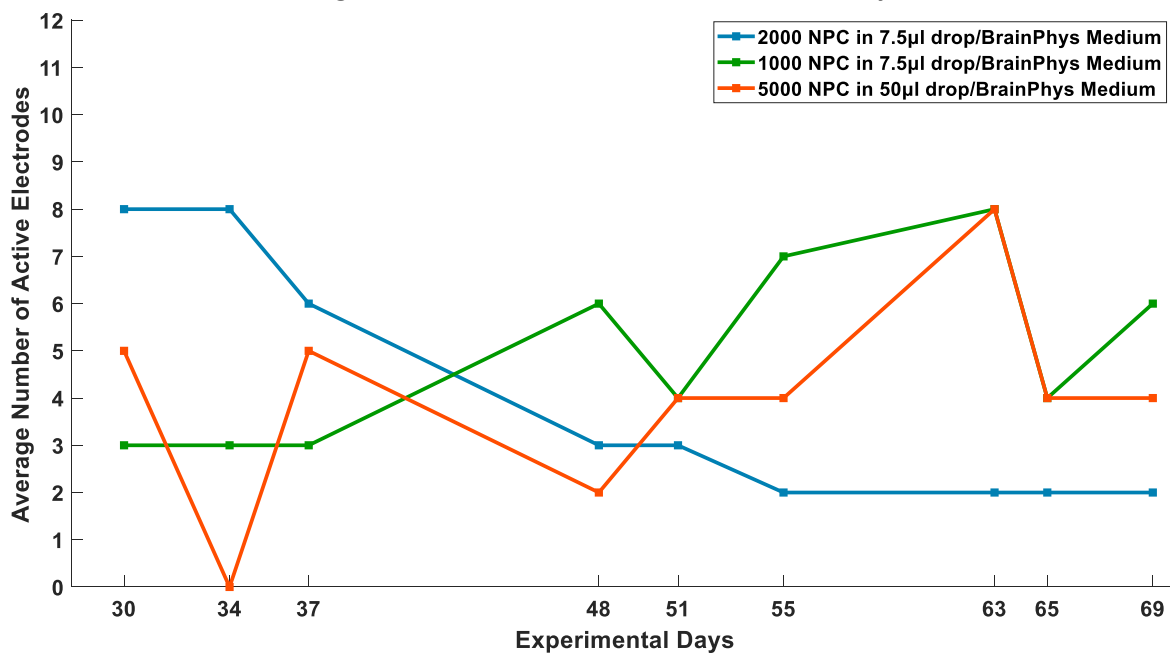
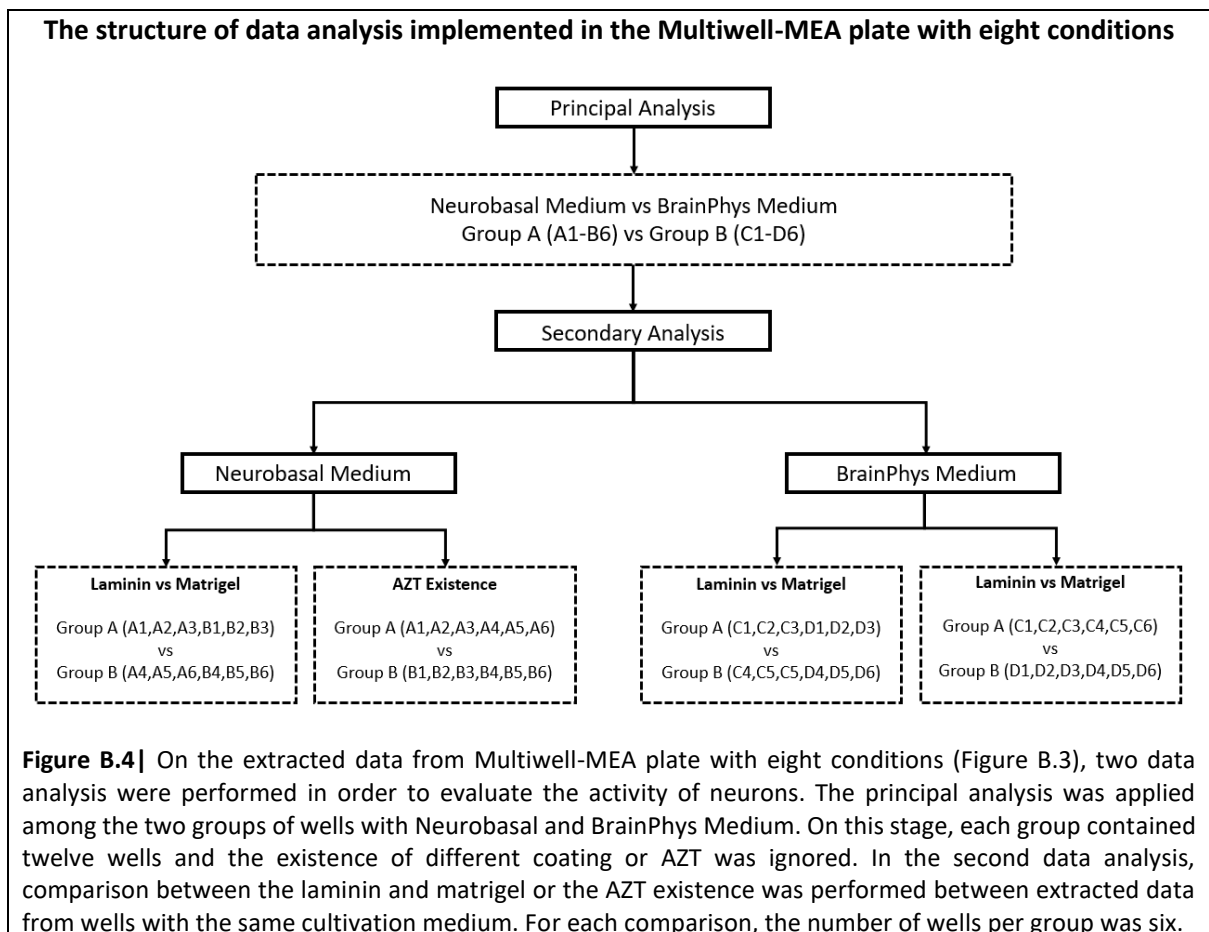
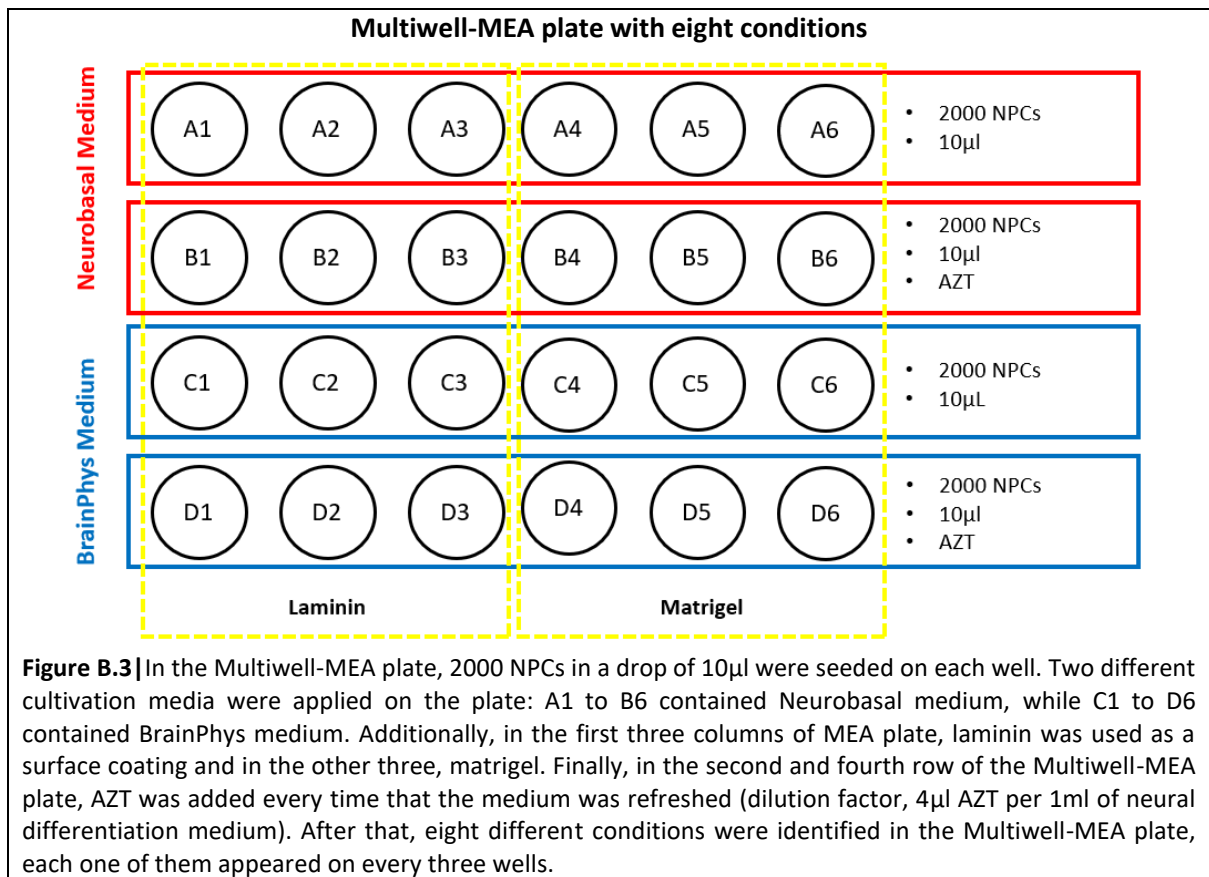
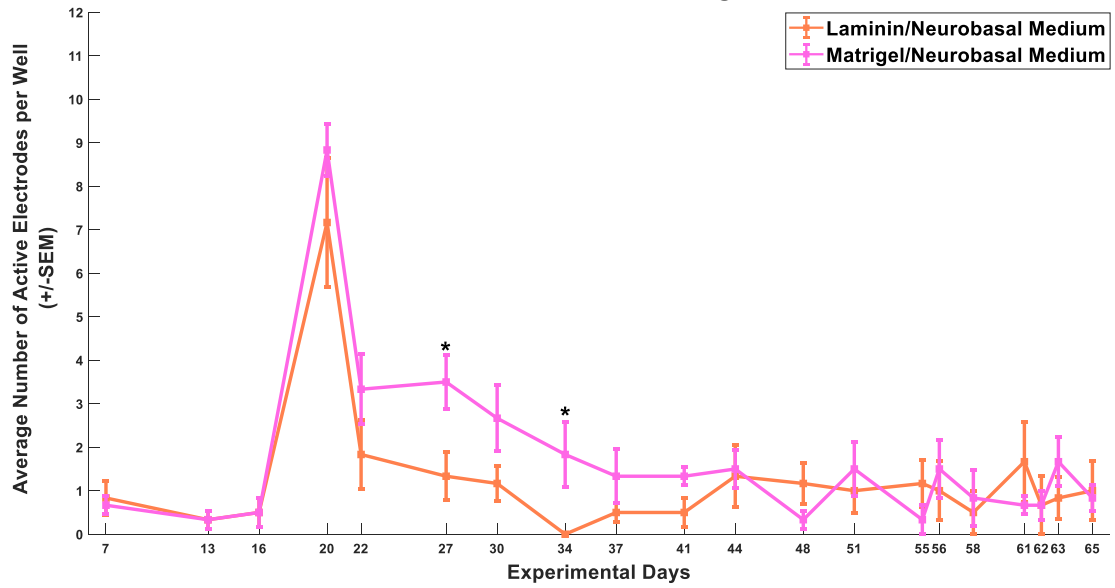


Figure B.2] A. The average number of active electrodes per well for each condition. The number of wells participating on each condition was four. **B.** The number of active electrodes per recording day for each well with BrainPhys medium for the three experimental conditions.



Sub-conditions of wells with Neurobasal Medium
Average number of active electrodes per well
A. Laminin versus Matrigel



B. With and Without AZT

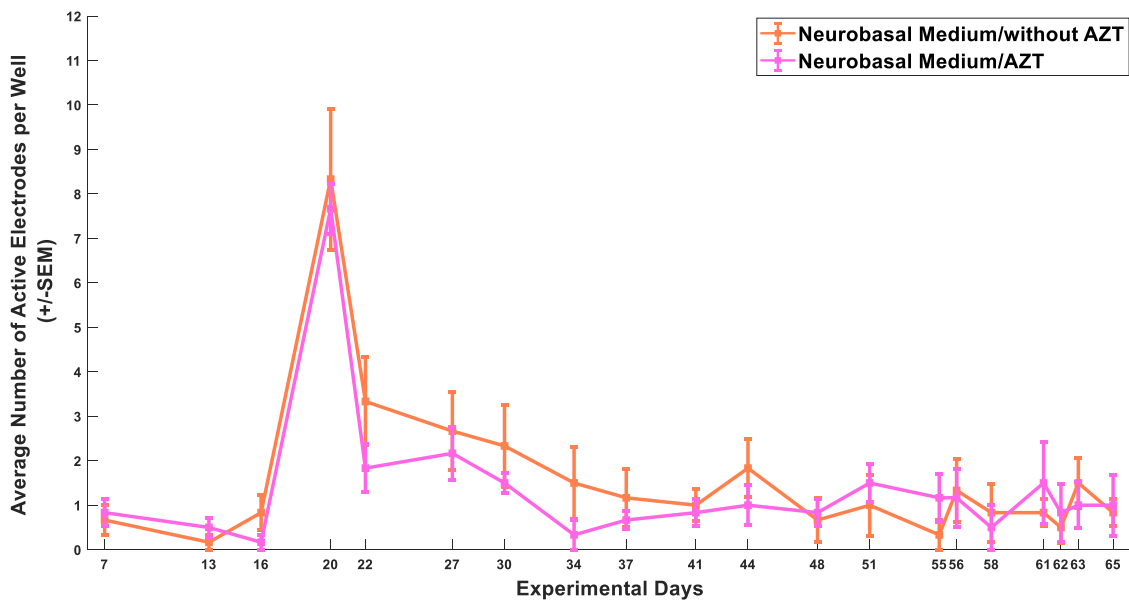
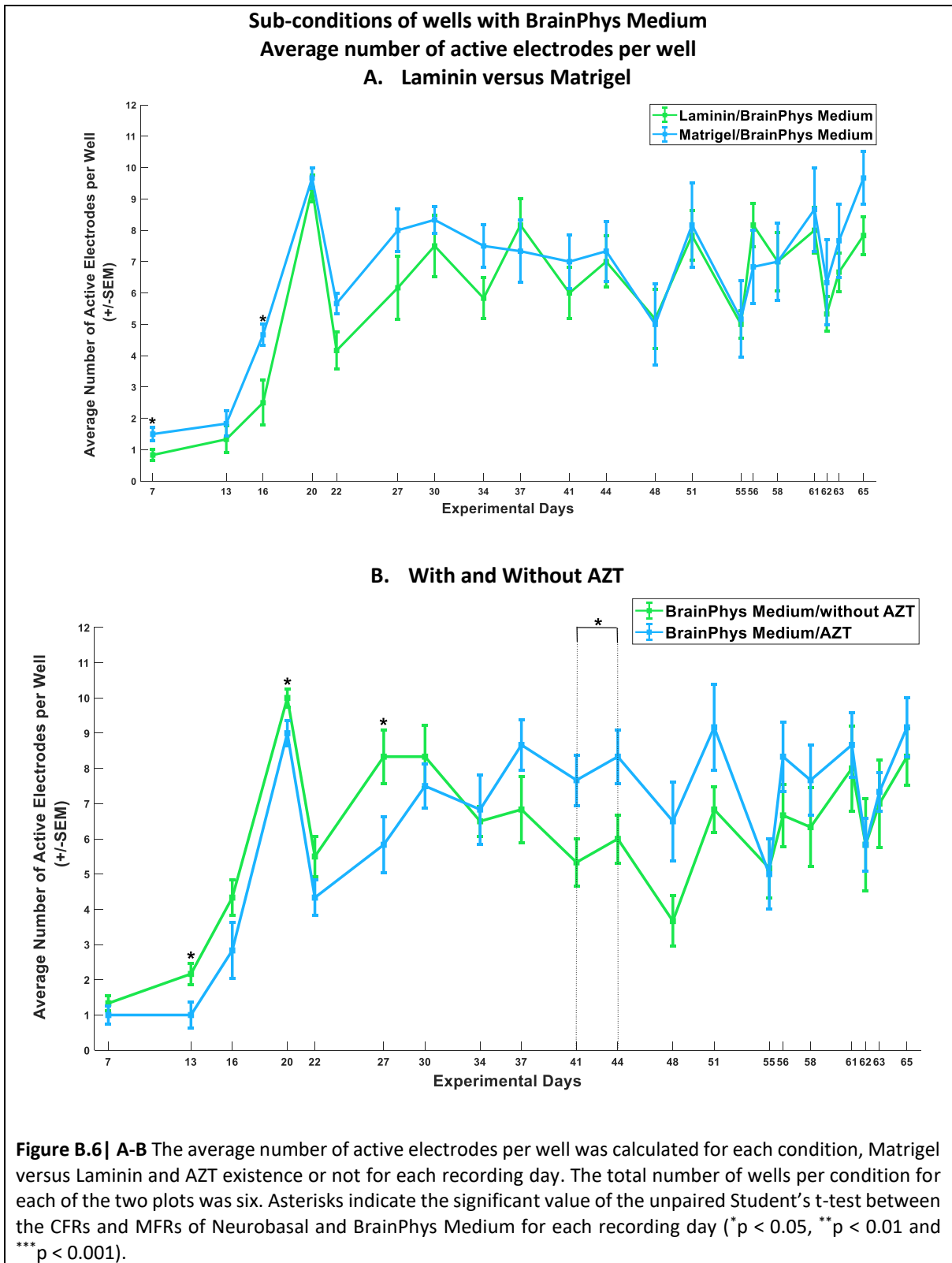
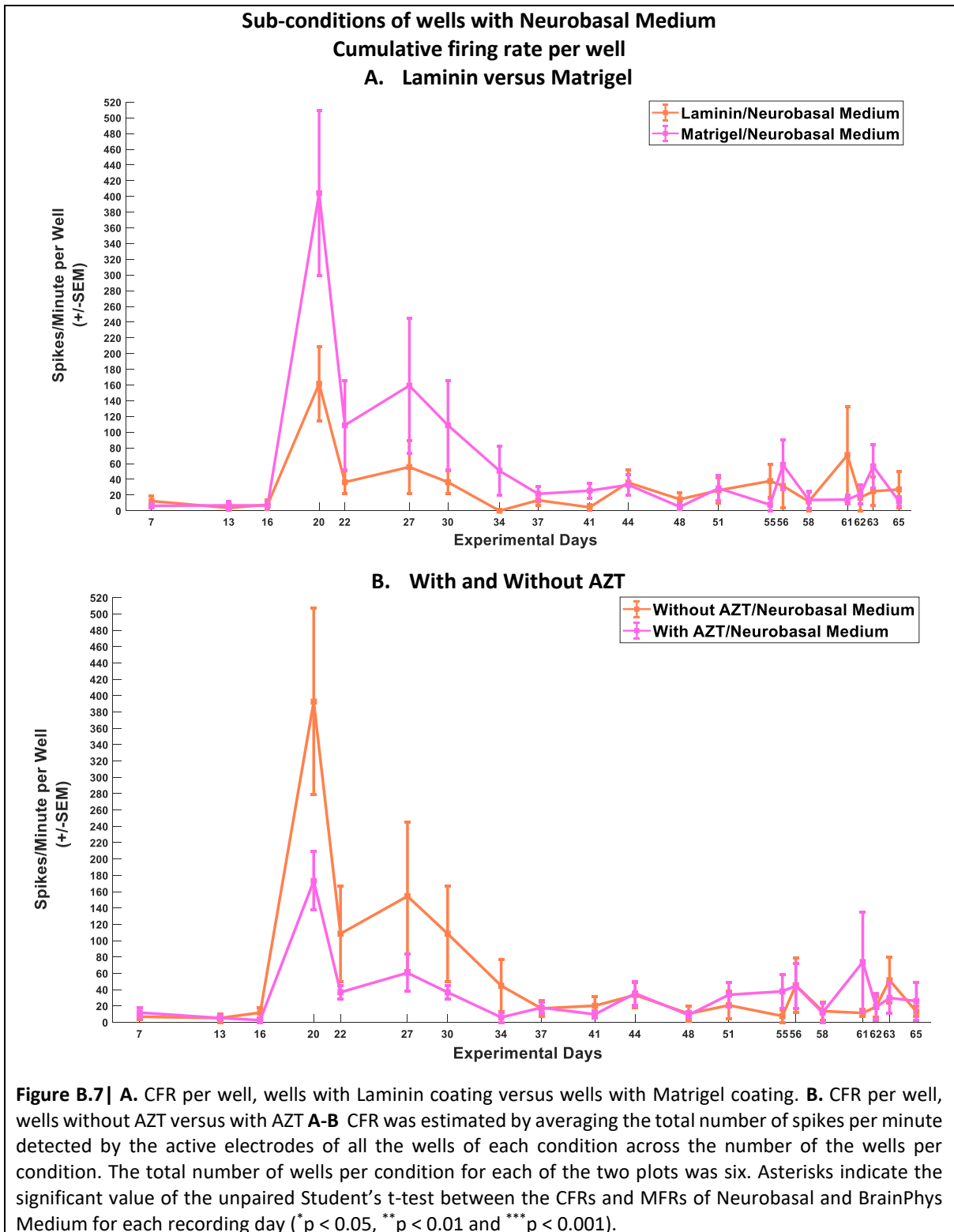
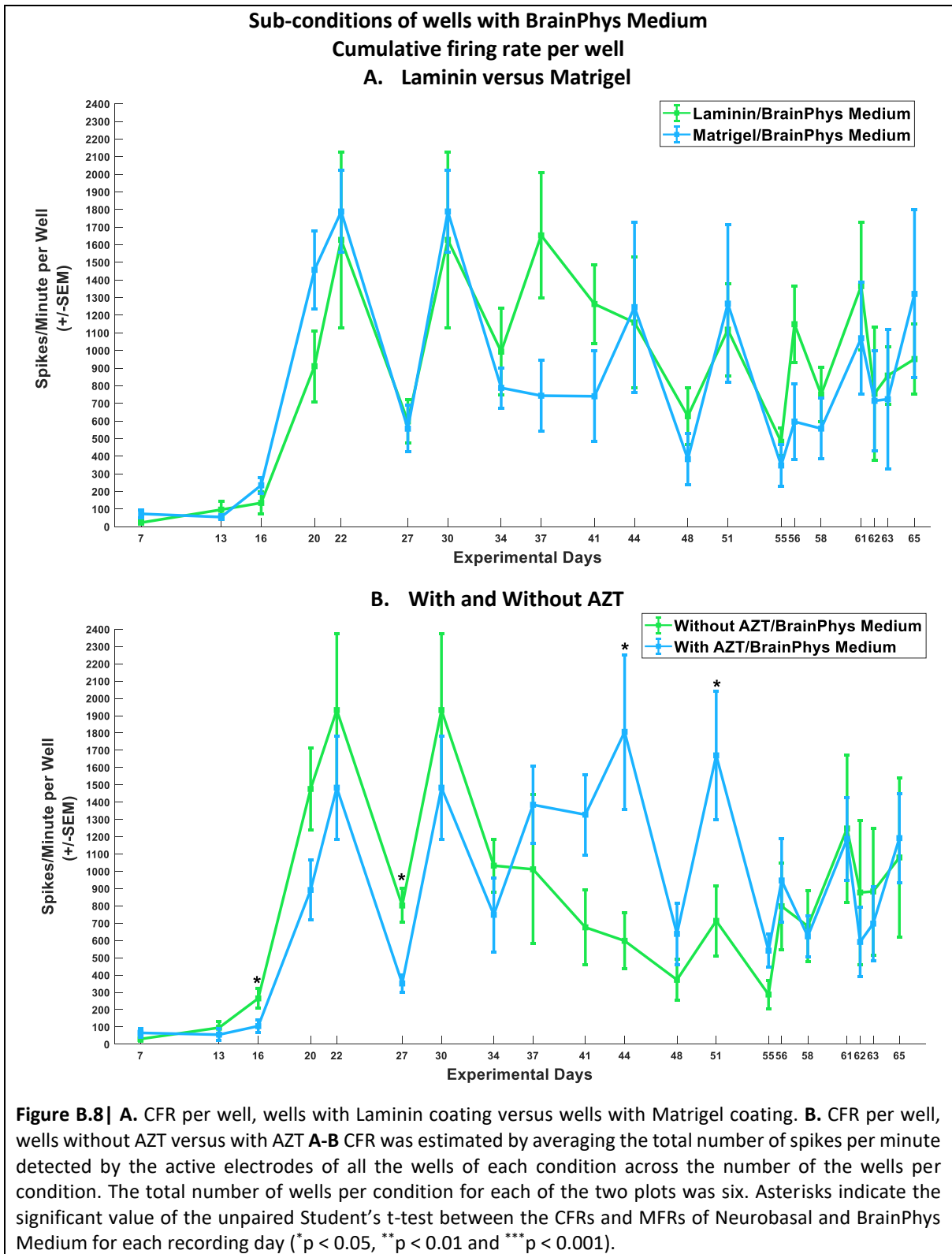
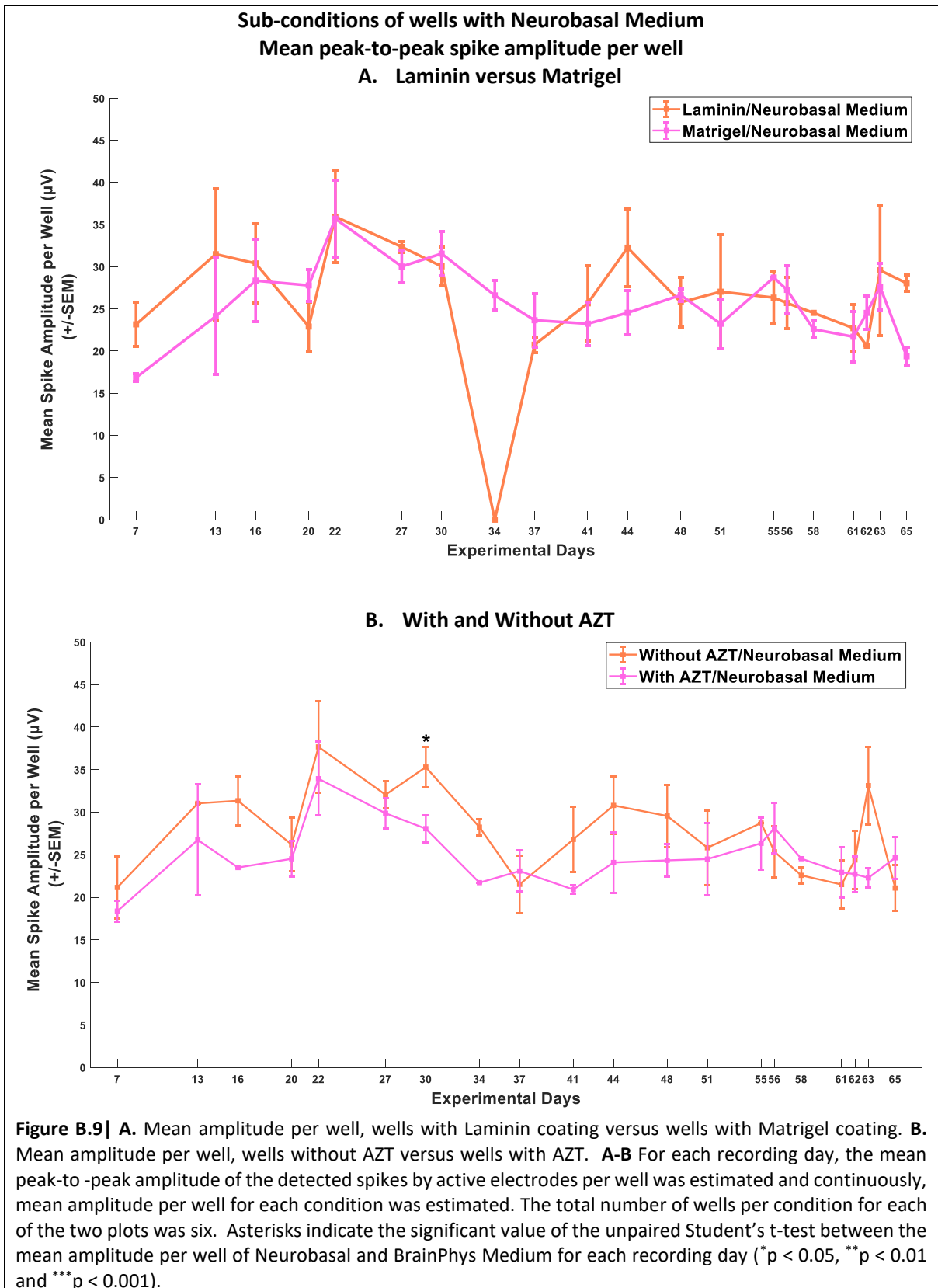


Figure B.5] A-B The average number of active electrodes per well was calculated for each condition, Matrigel versus Laminin and AZT existence or not for each recording day. The total number of wells per condition for each of the two plots was six. Asterisks indicate the significant value of the unpaired Student's t-test between the CFRs and MFRs of Neurobasal and BrainPhys Medium for each recording day (*p < 0.05, **p < 0.01 and *** p < 0.001).









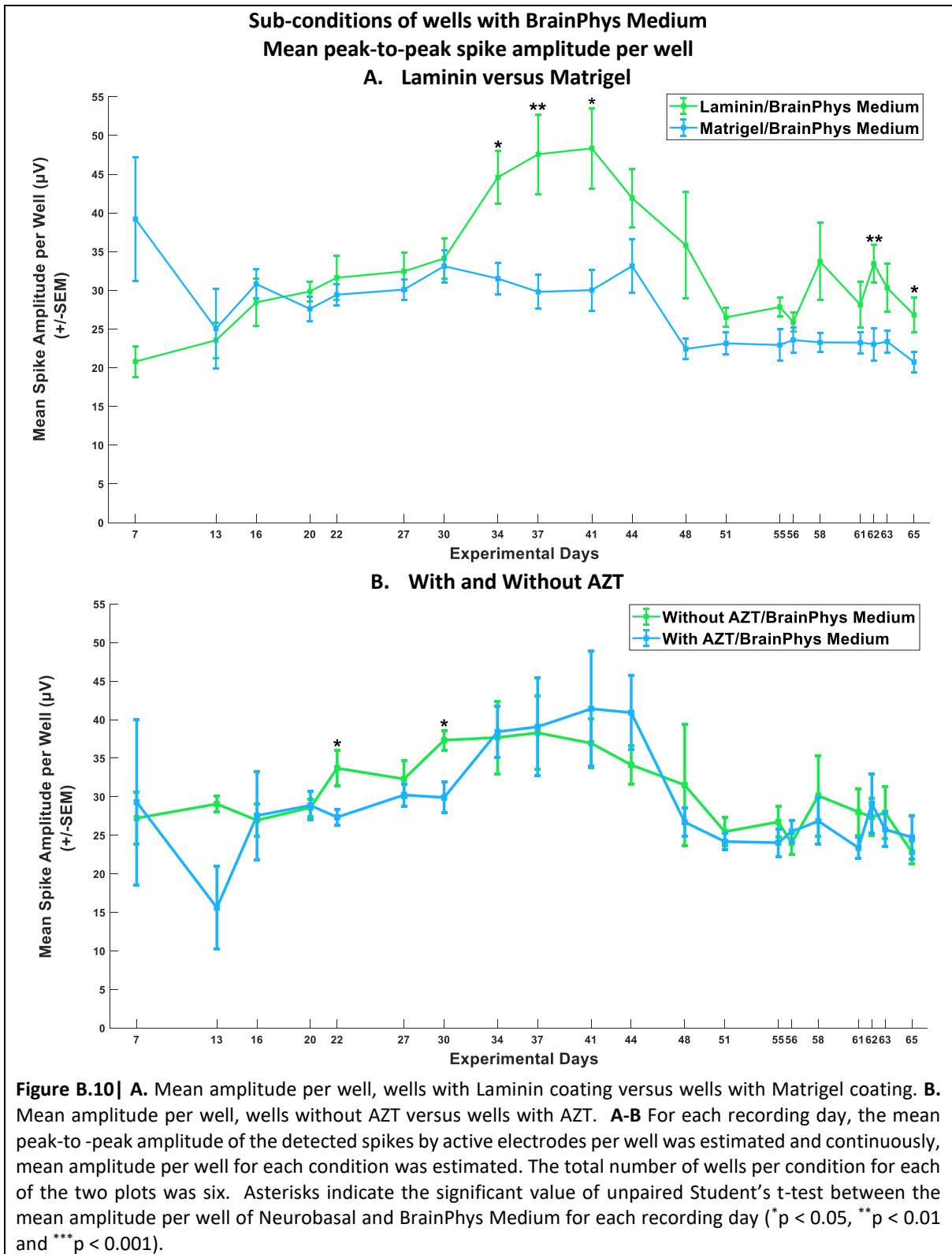
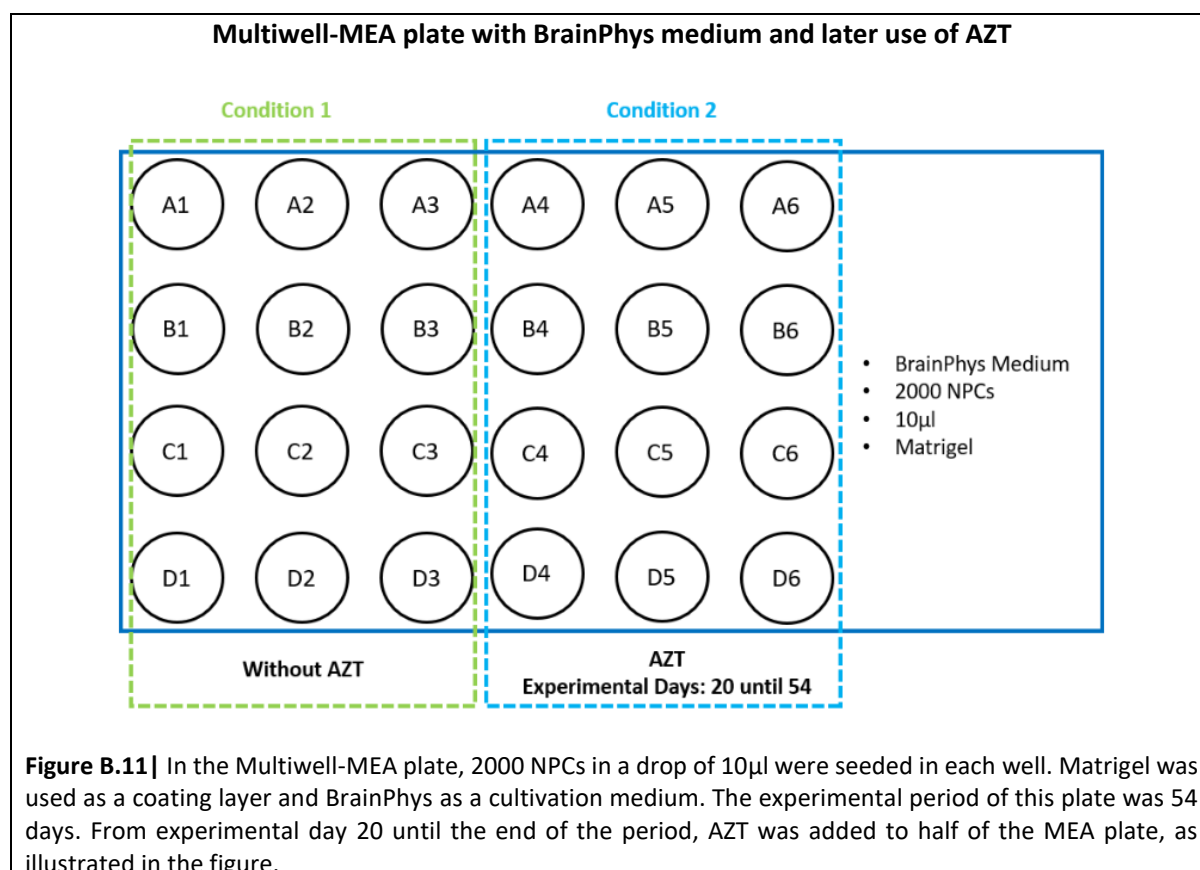


Table B.1 | Number of network bursts per well of each recording performance

	Wells											
	C1	C2	C3	C4	C5	C6	D1	D2	D3	D4	D5	D6
Day 37	1	-	-	-	-	-	-	-	-	-	1	-
Day 41	-	-	-	-	-	-	-	-	-	-	-	-
Day 44	-	-	-	-	-	-	-	-	3	-	69	-
Day 48	-	-	-	-	-	-	-	-	-	-	-	-
Day 51	-	-	-	-	1	-	1	-	8	6	52	-
Day 55	-	-	-	-	-	-	-	-	-	-	-	-
Day 56	1	-	-	-	-	-	-	-	13	-	6	-
Day 58	-	-	1	-	2	-	-	-	-	-	6	1
Day 61	31	14	-	-	26	-	-	-	24	30	40	1
Day 62	-	-	-	-	-	-	-	-	-	-	-	-
Day 63	-	-	-	-	78	-	-	-	17	-	-	-
Day 65	-	-	-	-	80	-	-	-	27	17	54	10



APPENDIX C

In Appendix C, the results of spike sorting analysis of each electrode are presented. The selected neural cultures was in the D5 well of the Multiwell-MEA plate with eight different conditions (Figure B.3). The exact experimental days where the recordings were performed were 51, 58 and 65. On each experimental day, three figures appear, the first one presents the plots of clusters detected per electrode, the second the Cluster 0 per electrode and the last one the temperature plots for each electrode.

The Wave_clus algorithm was used for every electrode separately and the waveforms of detected spikes were classified into clusters. The clusters were numbered from 0 until n. Cluster 0 depicts the spikes that were not assigned into any cluster neither during the first round of nonparametric clustering nor during the second round process of template-matching, where unclassified waveforms were assigned to the estimated clusters (Figure C.2, C.5, C.8). The spike waveforms of Cluster_0 were considered as a background noise. Cluster 1 until n display the sorting spikes (Figure C.1, C.4, C.7). The total number of spikes belonging to the cluster is written on the top of the cluster plots. The principal number of spikes assigned to each cluster before template matching was written into parenthesis next to the total number of spikes of each cluster. The waveforms of spikes on each cluster are illustrated with a different color, while the black waveform on each cluster indicates the mean waveform. Finally, the temperature maps are also depicted for each electrode (Figure C.3, C.6, C.9). All the different waveforms' partitions generated by the Wave_clus for each temperature (temperature values: 0 to 0.25 in increments of 0.01) are displayed on temperatures' plots. Each line of the temperature map is associated with the size of k^{th} cluster ranked by size at each temperature. The color filled circles represents the retained clusters and the symbol 'x' indicates putative clusters which discarded at the final cluster selection process (refer to Chapter 3 about nonparametric clustering, peak selection in the temperature plot and inclusion criterion).

Experimental Day 51

First Recording

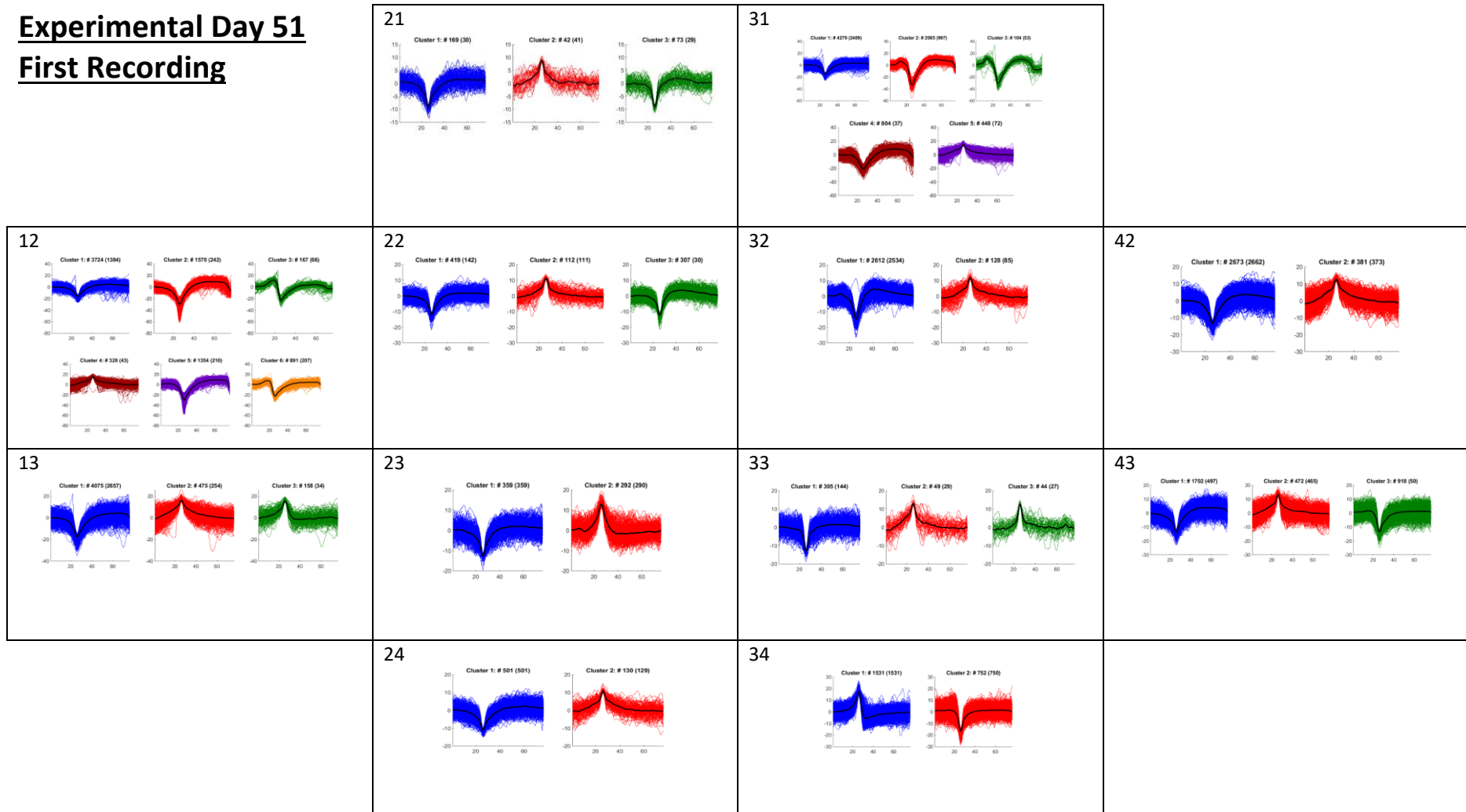


Figure C.1 | The identified clusters per electrode on the experimental day 51. The number of each electrode is written on the left up corner of each cell. The shape of the table represents the layout of the electrodes in the MEA-substrate.

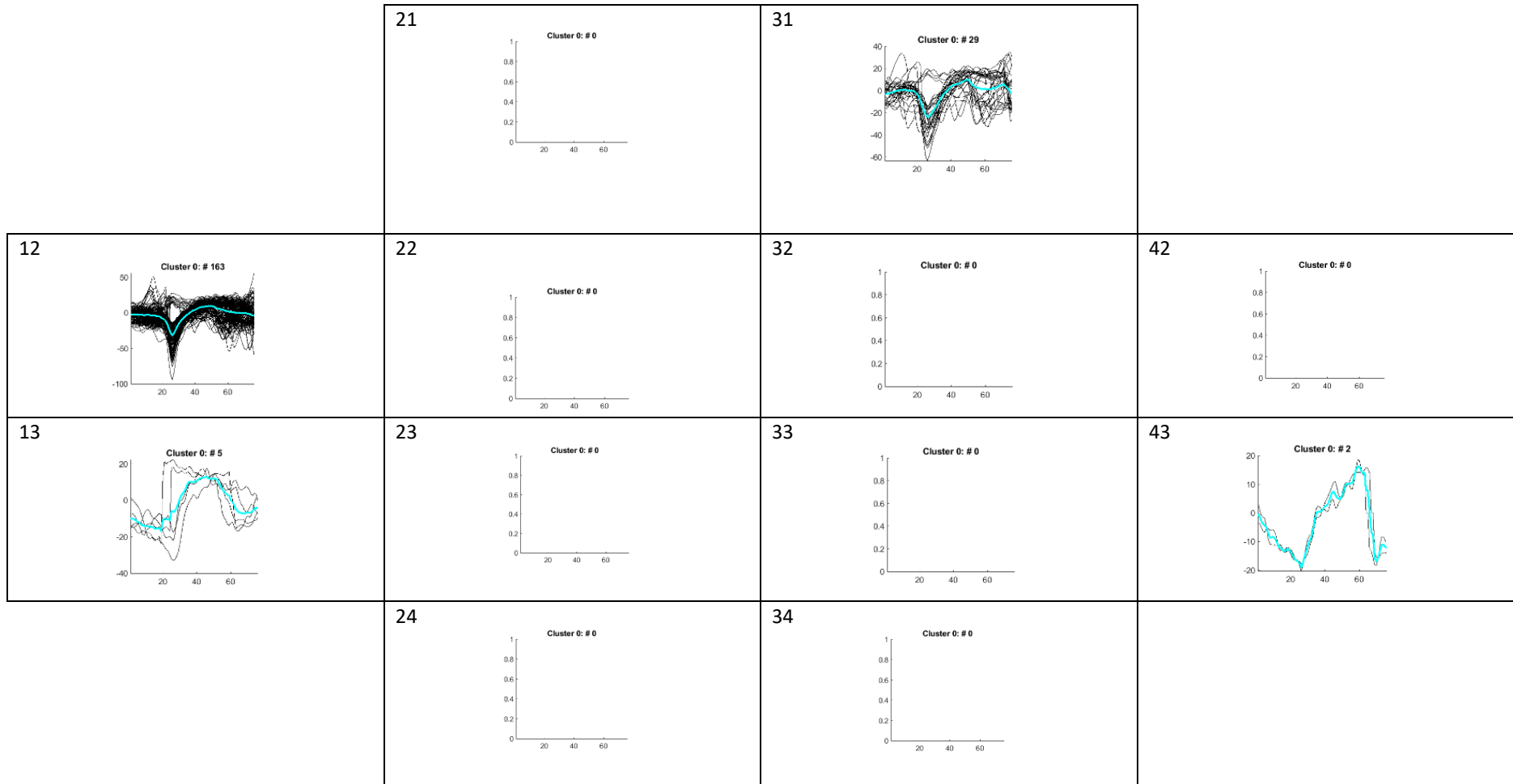


Figure C.2 | The Clusters 0 per electrode containing the mismatched waveforms, on the experimental day 51. The number of each electrode is written on the left up corner of each cell. The shape of the table represents the layout of the electrodes in the MEA-substrate.

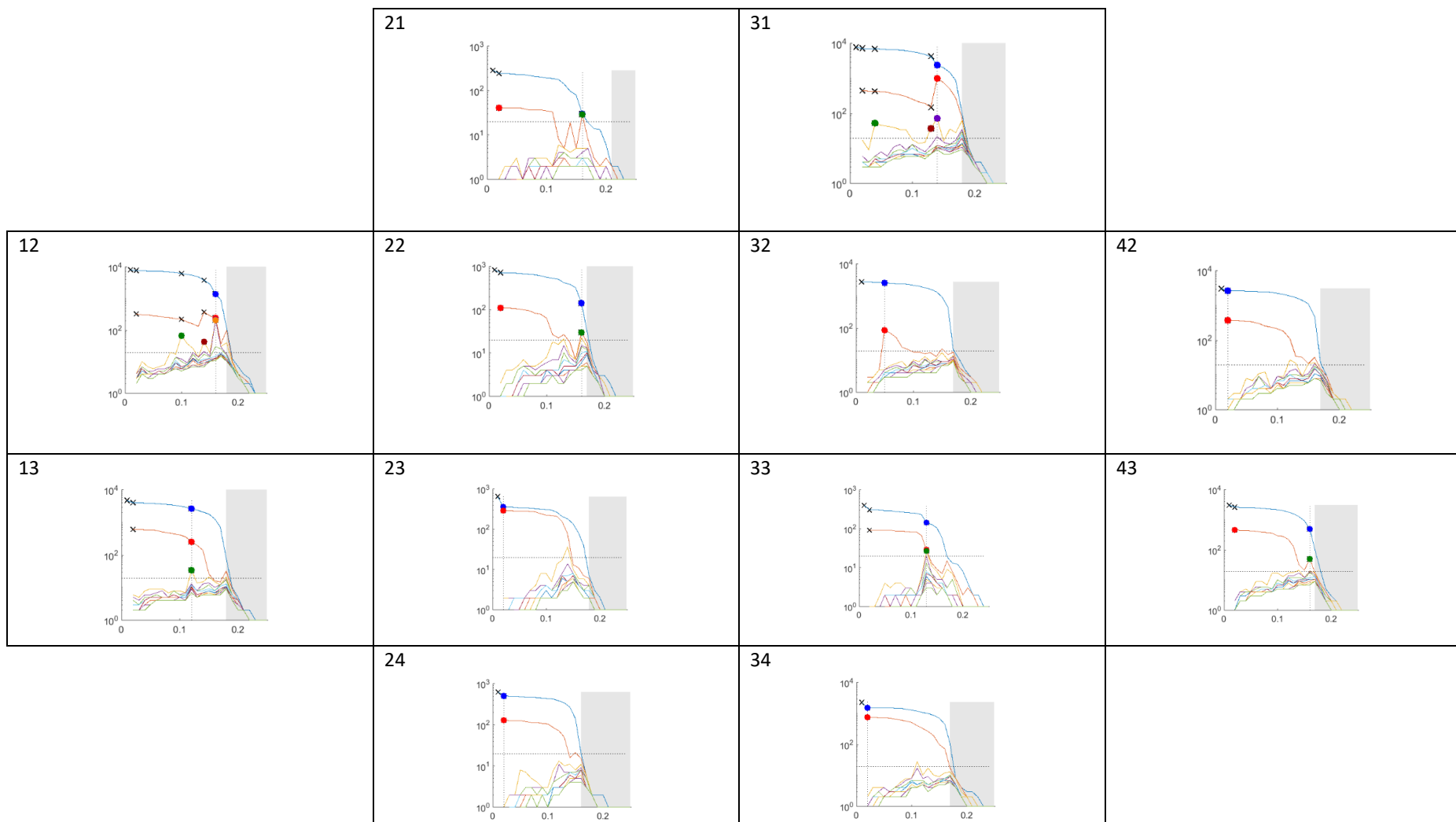


Figure C.3 | Temperature map per electrode on the experimental day 51. The number of each electrode is written on the left up corner of each cell. The shape of the table represents the layout of the electrodes in the MEA-substrate.

Experimental Day 58

Second Recording

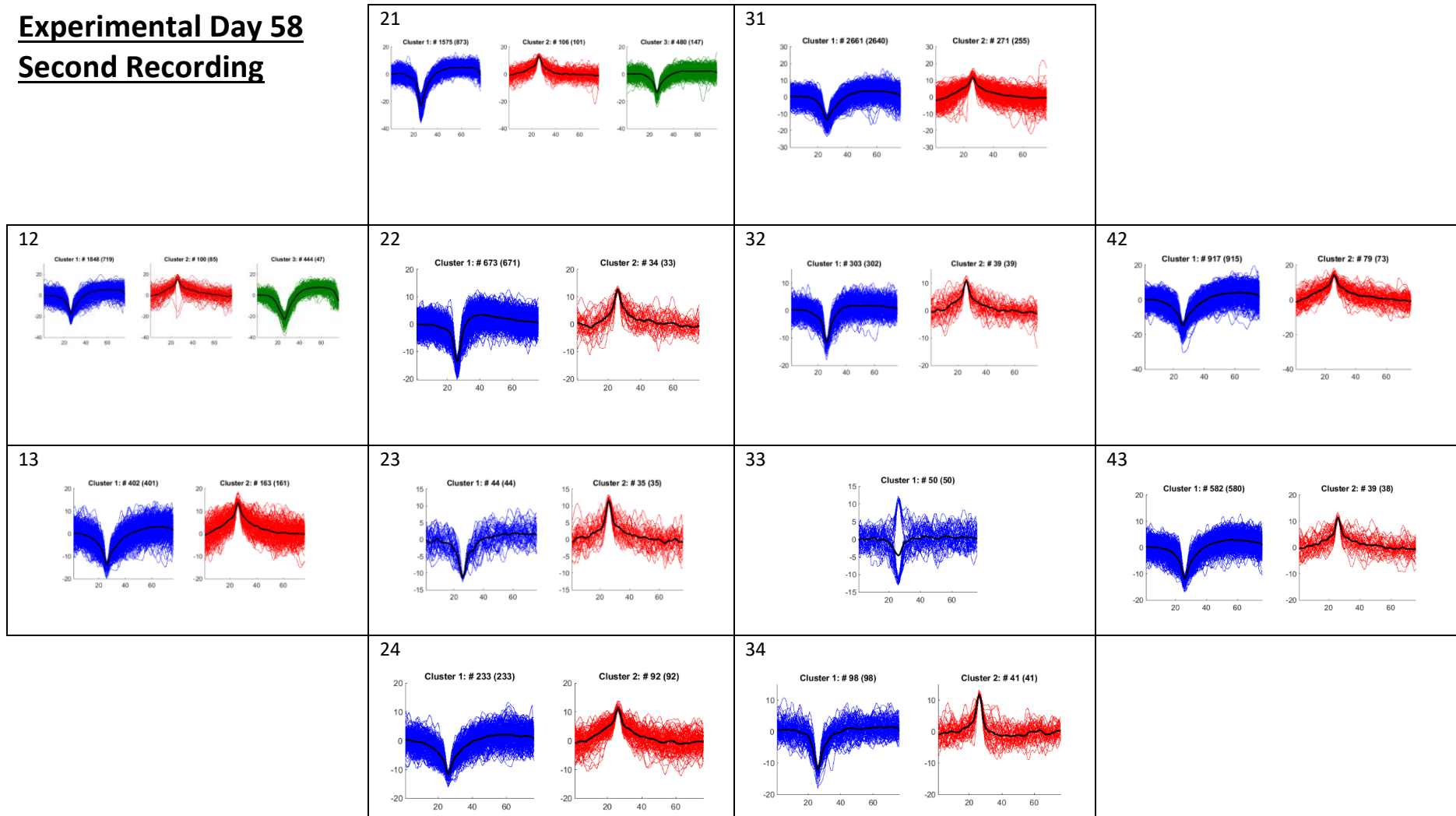


Figure C.4 | The identified clusters per electrode on the experimental day 58. The number of each electrode is written on the left up corner of each cell. The shape of the table represents the layout of the electrodes in the MEA-substrate.

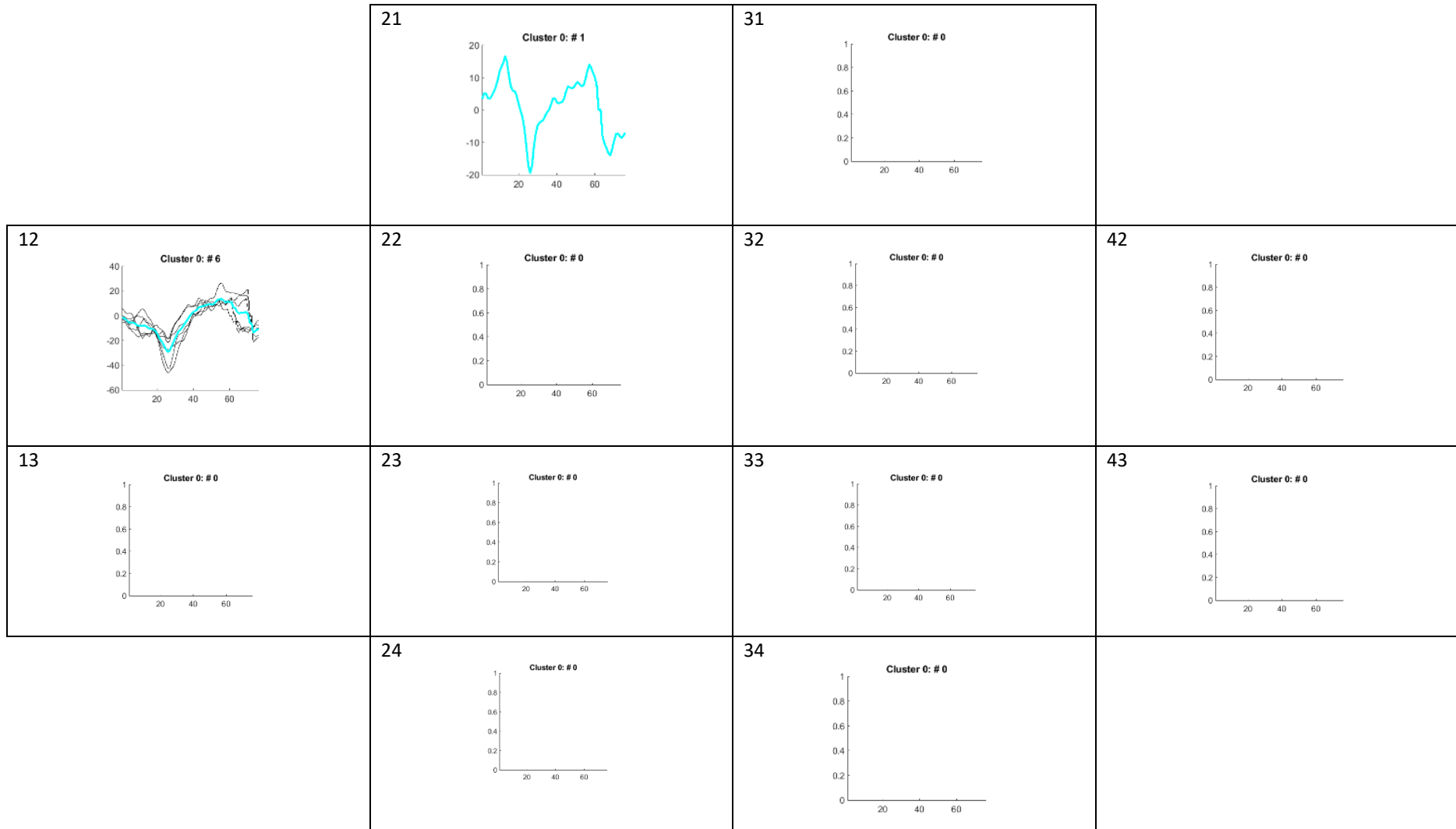


Figure C.5 | The Clusters 0 per electrode containing the mismatched waveforms, on the experimental day 58. The number of each electrode is written on the left up corner of each cell. The shape of the table represents the layout of the electrodes in the MEA-substrate.

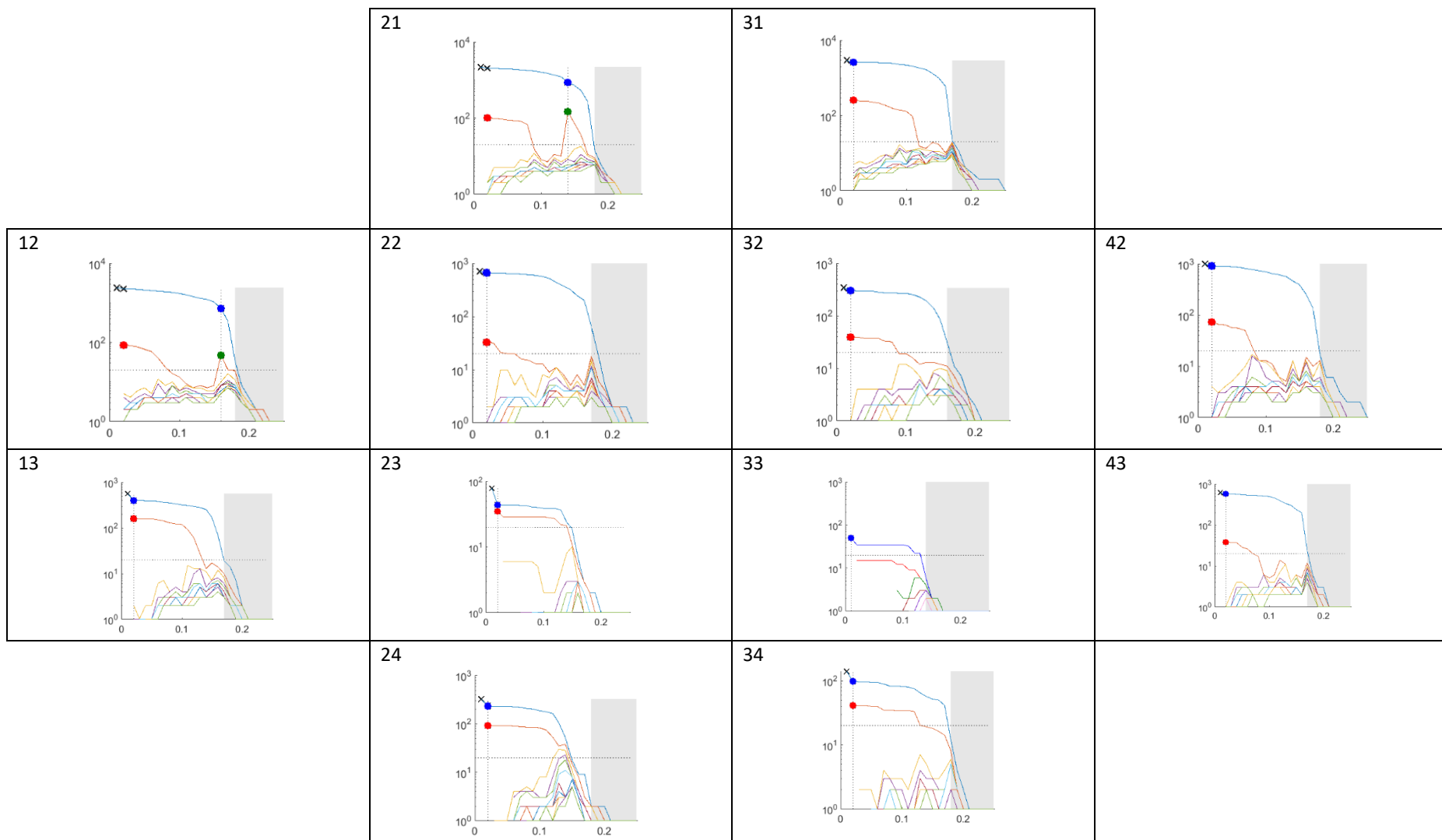


Figure C.6 | Temperature map per electrode on the experimental day 58. The number of each electrode is written on the left up corner of each cell. The shape of the table represents the layout of the electrodes in the MEA-substrate.

Experimental Day 65

Third Recording

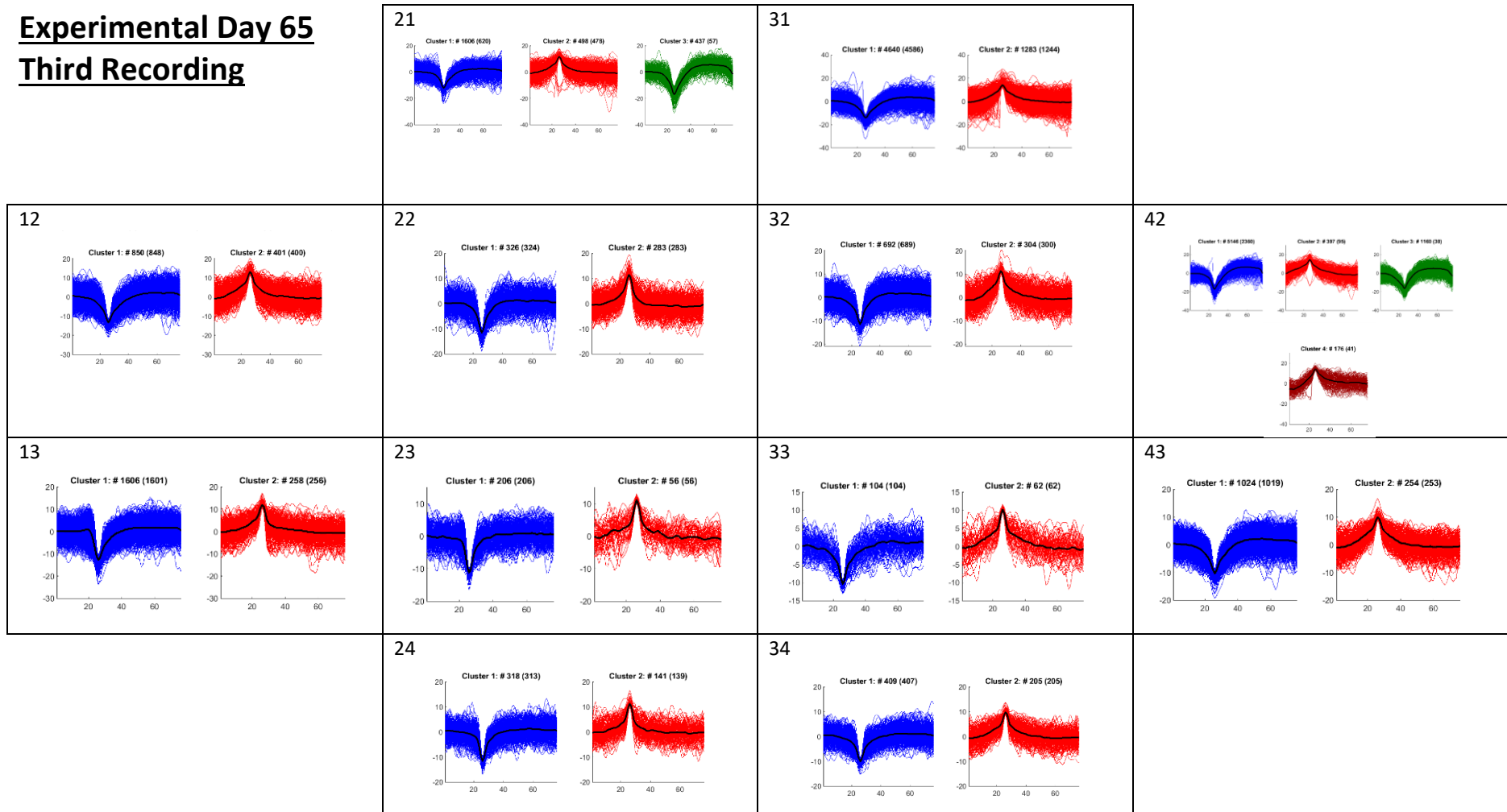


Figure C.7 | The identified clusters per electrode on the experimental day 65. The number of each electrode is written on the left up corner of each cell. The shape of the table represents the layout of the electrodes in the MEA-substrate.

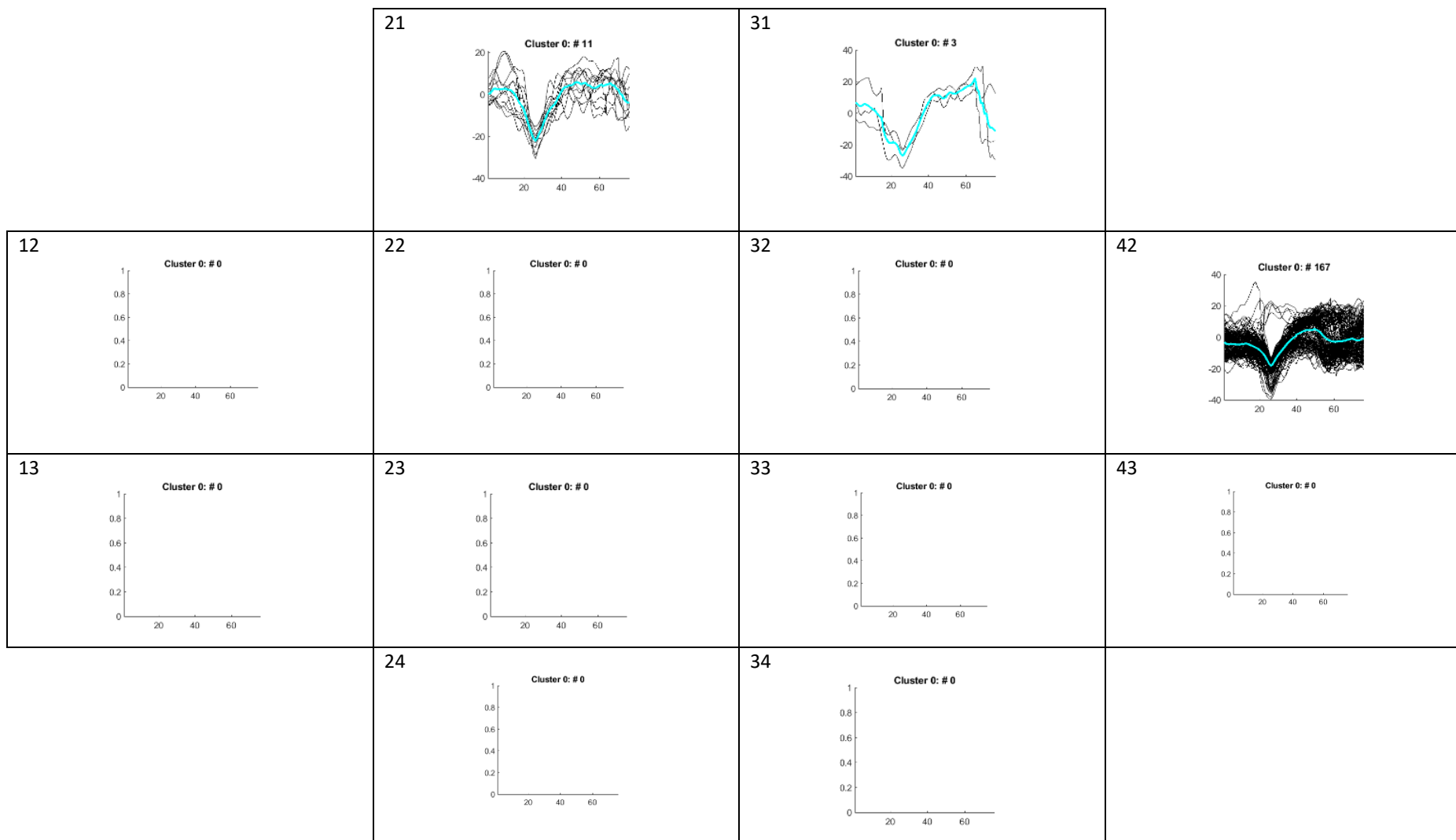


Figure C.8] The Clusters 0 per electrode containing the mismatched waveforms, on the experimental day 60. The number of each electrode is written on the left up corner of each cell. The shape of the table represents the layout of the electrodes in the MEA-substrate.

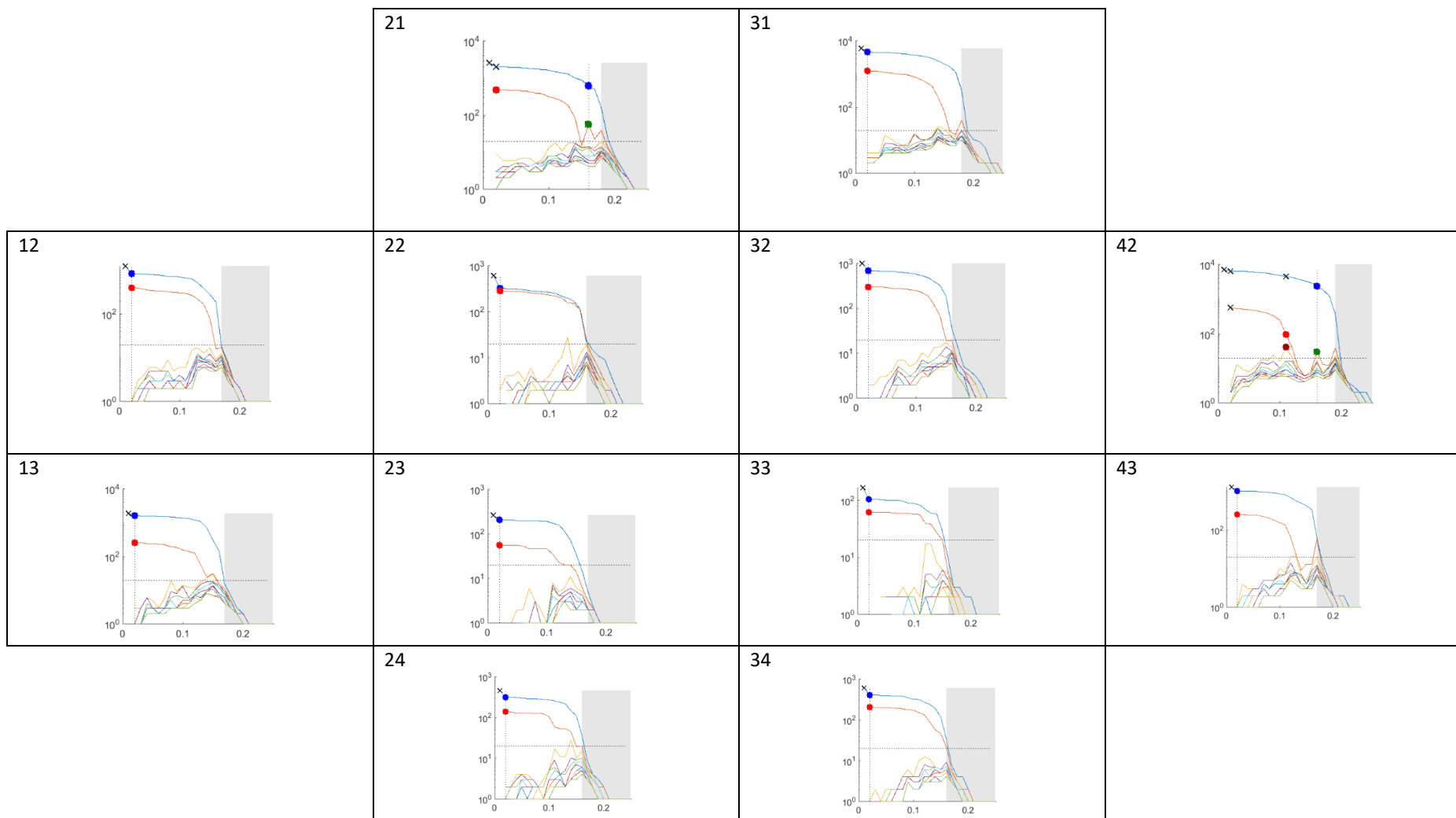


Figure C.9] Temperature map per electrode on the experimental day 65. The number of each electrode is written on the left up corner of each cell. The shape of the table represents the layout of the electrodes in the MEA-substrate

